# Conformance Control in Heterogeneous Oil Reservoirs with Polymer Gels and Nano-Spheres

Lenchenkov, Nik

**DOI**
10.4233/uuid:1686e932-2df7-41df-80af-643d5a34fb2f

**Publication date**
2017

**Document Version**
Final published version

**Citation (APA)**
Lenchenkov, N. (2017). *Conformance Control in Heterogeneous Oil Reservoirs with Polymer Gels and Nano-Spheres*. [Dissertation (TU Delft), Delft University of Technology].
https://doi.org/10.4233/uuid:1686e932-2df7-41df-80af-643d5a34fb2f

**Important note**
To cite this publication, please use the final published version (if applicable).
Please check the document version above.

# Conformance Control in Heterogeneous Oil Reservoirs with Polymer Gels and Nano-Spheres

Proefschrift

ter verkrijging van de graad van doctor
aan de Technische Universiteit Delft,
op gezag van de Rector Magnificus prof. ir. K.C.A.M. Luyben,
voorzitter van het College voor Promoties,
in het openbaar te verdedigen op dinsdag 20 juni 2017 om 12:30 uur

door

Nikita Sergeevich Lenchenkov

Candidate of Technical Sciences in Petroleum engineering,
Saint-Petersburg Mining University, Saint-Petersburg, Russia
geboren te Ufa, Russia

This dissertation has been approved by

promotor : Prof. Ir. C.P.J.W. van Kruijsdijk, Delft University of Technology

supervisor: Drs. G. Glasbergen, Shell Global Solutions Intern. B.V.

Composition of the doctoral committee:

Rector Magnificus, chairman

Prof. Ir. C.P.J.W. van Kruijsdijk, promotor

Independent members:

Prof. dr. K.S. Sorbie, Heriot-Watt University

Prof. dr. M. Golombok, Eindhoven University of Technology

Prof. dr. ir. P.L.J. Zitha , Delft University of Technology

Prof. dr. ir. T.J. Heimovaara, Delft University of Technology

Dr. ir. J.T. Padding, Delft University of Technology


*Key words:* polymers, conformance control, improved oil recovery, nano-spheres, cross-linked polymers, flow in porous media, electron microscopy, and dynamic light scattering.

*Author's email* lenchenkovn@gmail.com

ISBN: 978-94-6233-668-1

*To my beloved parents*

*Я посвящую эту работу моим дорогим родителям, которые всегда поддерживают меня*

# Table of Contents

# List of figures

# List of tables

# Summary

## Conformance control in heterogeneous oil reservoirs with polymer gels and nano-spheres

In many oil fields, water is injected into a reservoir to displace oil to the production wells. During the injection process, oil is pushed by water towards production wells which have a lower pressure than the rest of the reservoir. If the reservoir is homogeneous, then a good sweep efficiency of the water flood process is expected. However, most oil reservoirs are stratified and that creates a permeability contrast along the whole height. High permeable layers take most of the injected water resulting in lower sweep efficiency of the other layers. The water breaks through the high permeable zones, significantly increasing the water cut of the produced fluid. Excessive produced water has to be treated in surface facilities which increase the costs of the extraction process. Another disadvantage of the low sweep of a reservoir is a significant amount of remaining oil behind the displacement front.

The improvement of water flood sweep efficiency can be achieved via flow diversion in the reservoir by one of the following methods: chemical methods (polymer flooding, in-depth diversion, the continuous injection of particle based fluids), water flood optimization by adjusting the production and injection flow rates, infill drilling, or manipulating with mechanical devices in wells (e.g. downhole valves). In this work we focus on the chemical conformance control methods which regulate permeability contrast between higher and less permeable layers of the reservoir. The ideal treatment reduces the permeability of the higher permeable layers and leaves unaffected the permeability of the lower permeable layers. If successful, the treatment reduces the water cut in produced fluid for the same injection rates.

Although the idea of conformance control is simple, its implementation in practise is challenging. One of the biggest difficulties is a design of the fluid which would propagate deep into a reservoir with a resistance factor build-up over time. In our study, the resistance factor is equal to the ratio between the pressure drop during the injection of the chemically active fluid (e.g. polymer,

nano-particles) to the pressure drop during the injection of brine. This parameter depends on the volume of the injected chemical.

Two different fluids are studied in this work: organically cross-linked hydrolysed polyacrylamide and copolymer nano-spheres. These fluids have a different chemical structure which explains the differences in their propagation and the resistance factor build-up. Low initial resistance factor and the ability of these fluids to build up a resistance factor in porous media after some time make them attractive for the conformance control in heterogeneous oil reservoirs.

*The first chapter* of the thesis introduces different methods for conformance control in oil reservoirs with the main focus on the chemical methods for the improvement of sweep efficiency. It is explained that polymer flood, continuous injection of particles based fluids, and in-depth diversion are the most common chemical methods. A literature review of different chemically active fluids suitable for the conformance control was done in this chapter. That helped to define the criteria of successful fluids for the application in practice. Next, a crosslinking polymer and nano-spheres were chosen for the study.

*In the second chapter* the behaviour of the cross-linking polymer was studied in bulk, at the core scale (1 m length), as well as on the pore scale. A series of bulk experiments was carried out to select the recipe of the cross-linking polymer for in-depth diversion. The main requirement was the delay of the gelation time for at least 8 days in 5 g/l brine at 45 ºC. This time is expected to be enough to place the gel deep in the reservoir. However, the polymer starts to interact with a cross-linker after the mixing of the components together. Therefore, the question here is whether a substantial delay in cross-linking can be achieved at the conditions of the reservoir. A Poly- Electrolyte Complex (PEC) was used to (temporarily) hide the cross-linker from the polymer molecules. A series of rheology tests was carried out to represent the kinetics of gelation.

The gelation time in bulk suggested that the PEC could effectively delay the time of the cross-linking even at high brine salinity. However, the delay experienced in the core flood experiment was much shorter. Tracer tests demonstrated that the XL polymer, which is a mixture of PEC and partially hydrolyzed polyacrylamide, reduced the core pore volume by roughly 6.2 % (in absolute terms). The micro-CT images showed that most of the XL polymer was retained in the smaller pores of the core. The large increase in the dispersion coefficient suggests that this must have resulted in the creation of a

few dominant flow paths isolated from each other by closure of the smaller pores.

An alternative to the cross-linking polymer for the conformance control can be a continuous injection of nano-spheres suspension. The spheres have a small initial size ~ 200 nm and are supposed to easily propagate through porous media with an average size of pore throats ~10 μm. It is believed that the particles swell over time and that causes their accumulation deep in the reservoir. In order to understand this mechanism better, a series of bulk and core-flood experiments was carried out.

*The third chapter* focuses on the characterisation of nano-spheres by means of dynamic light scattering and transmission electron microscopy. The spheres are synthesised via an inverse emulsion polymerisation method. Therefore, they are distributed in an emulsion media. To study the increase in the size of particles and their interaction over time, the particles were separated from the emulsion media according to a specially designed procedure. As a result of the experiments, it was shown that particles swell and agglomerate over time. These results can be used for the explanation of nano-spheres flow in porous media.

*Next (chapter 4)*, a series of core flood experiments in Berea, Bentheimer and Boise outcrop cores was carried out to experimentally study the flow of nano-spheres in porous media with different mineralogy and oil saturation. Complementary to that, the dynamic of the pressure drop over cores and organic carbon concentration in effluent were analysed. Dynamic light scattering tests revealed the size of nano-spheres for different types of brine and helped to understand better its influence on the propagation in porous media.

The results of the work show that the propagation of nano-spheres in porous media is highly dependent on the brine salinity at cores with different oil saturation. For the same experimental conditions, the residual resistance factor of nano-spheres in porous media depends on the flow rate. Residual resistance factor is defined as the ratio between the pressure drop during the brine injection after a chemical was injected into porous media to the pressure drop during the brine injection before the chemical was injected.

*Finally*, conclusions were made and recommendations for the development of new conformance control fluids were given.

# Samenvatting

## Overeenstemmingscontrole in heterogene oliereservoirs met polymeergels en nano-bolletjes

In veel olievelden wordt water geïnjecteerd in het reservoir om de olie naar boven te verplaatsen. Tijdens het injectieproces, duwt het water de olie richting de productieputten die een lagere druk hebben dan de rest van het reservoir. Als het reservoir homogeen is, dan verwacht men een hoge verdringingsefficiëntie van het waterinjectieproces. Echter, de meeste oliereservoirs zijn gelaagd, resulterend in een injectiecontrast over de hele hoogte. De zeer doordringbare lagen nemen het meest van het geïnjecteerde water en dat leidt tot een lage verdringingsefficiëntie van de andere lagen. Het water breekt door naar de productieput via de hoge permeabiliteitslagen, resulterend in een hoge waterfractie in de productievloeistof. Het geproduceerde water moet behandeld worden in de bovengrondse installaties en dat verhoogt de kost van het extractieproces. Een ander nadeel van de inefficiënte verdringing is de aanzienlijke hoeveelheid achtergebleven olie.

Een verbetering van de verdringing efficiëntie van het waterinjectie proces kan bereikt worden door middel van stromingsomleiding binnen het reservoir door een van de volgende methoden: scheikundige methoden (polymeerinjectie, diepgaande omleiding, voortdurend injecteren van nano-deeltjes), injectie-optimalisatie door middel van het aanpassen van de stroomsnelheden van de productie en injectie, boren van additionele putten, of manipuleren met mechanische elementen in de putten (bijvoorbeeld ondergrondse kleppen). In dit werk focussen we ons op scheikundige verdringingscontrolemethoden die het injectiviteits-contrast tussen de meer en de minder doordringbare lagen van het reservoir vermindert. De ideale behandeling vermindert de doordringbaarheid van de sterk doordringbare lagen en verandert de doordringbaarheid van de zwak doordringbare lagen niet. Als de behandeling lukt, vermindert hij de waterfractie in de productieputten voor dezelfde productiesnelheden.

De praktische implementatie van verdringingscontrole is vaak uitdagend. Een van de grootste moeilijkheden is het ontwerp van de vloeistof die diep

binnen het reservoir doordringt met een groeiende weerstand factor in de loop van de tijd.

Dit werk bestudeert twee verschillende vloeistoffen: organisch cross-linked gehydrolyseerd polyacrylamide en nano-bolletjes van copolymeer. Deze vloeistoffen hebben verschillende scheikundige structuren, en dat is de reden voor de verschillen in hun verspreiding en de weerstand factor groei. De lage oorspronkelijke weerstand factor en het vermogen die deze vloeistoffen hebben om de weerstand factor te laten groeien in poreuze media na een bepaalde tijd maken deze vloeistoffen aantrekkelijk voor de verdringingscontrole in heterogene oliereservoirs.

*Het eerste hoofdstuk* van dit proefschrift introduceert verschillende methoden voor verdringingscontrole in oliereservoirs met de nadruk op de scheikundige methoden voor de verhoging van de verdringingsefficiëntie. We leggen uit dat polymeerinjectie, voortdurende injectie van nano-deeltjes, en diepgaande omleiding de meest voorkomende scheikundige methoden zijn. We ondernemen een literatuuronderzoek van de verschillende chemisch actieve vloeistoffen die bij de overeenstemmingscontrole passen. Dat helpt om de criteria van vloeistoffen te definiëren die succesvol zouden zijn voor de praktische toepassingen. Daarna, kiezen we cross-linked polymeren en nano-bolletjes om verder te bestuderen.

*In het tweede hoofdstuk*, bestuderen we het gedrag van cross-linked polymeren op bulkschaal, zowel als op de kernschaal (1 m lengte) en op de porieschaal. We doen een reeks bulkschaal experimenten om het recept te kiezen voor het cross-linked polymeer voor diepgaande omleiding. Het belangrijkste experiment is de vertraging van de gelatietijd tot ten minste 8 dagen in 5 g/l zoutoplossing op 5 ºC. Deze tijd is volgens verwachting genoeg om de gel in de diepte van het reservoir in te zetten. Echter, zonder ingrijpen begint het polymeer met de cross-linker te interageren onmiddellijk na het mengen van de componenten. Om dit proces te vertragen gebruiken we een Poly-Electrolyte Complex (PEC) om de cross-linker (tijdelijk) te verbergen voor de polymeermoleculen. Een reeks reologie-testen is uitgevoerd om de kinetiek van de gelatie te bestuderen.

De gelatie-experimenten in bulk laten zien dat de PEC de tijd van de cross-linking effectief kan vertragen, zelfs bij een hoog zoutgehalte van de oplossing. Echter, de echte vertraging in de kernstromingexperimenten is veel korter. Tracer experimenten hebben aangetoond dat het XL polymeer, een

samenstelling van PEC en gedeeltelijk gehydrolyseerd polyacrylamide, de kern poriënvolume met ongeveer 6.2 % (in absolute termen) heeft verminderd. De micro-CT afbeeldingen hebben aangetoond dat het meeste van het XL polymeer werd behouden in de kleinere poriën van de kern. De grote groei van de dispersiecoëfficiënt suggereert dat dit heeft geleid tot de creatie van een aantal dominante stromingspaden die geïsoleerd van elkaar zijn door het sluiten van de kleinere poriën.

Voortdurende injectie van de nano-bolletjes suspensie is een alternatief voor het cross-linked polymeer voor de verdringingscontrole. De bolletjes hebben een kleine oorspronkelijke grootte ~ 200 nm en ze zouden gemakkelijk moeten kunnen verspreiden door poreuze media met de gemiddelde grootte van de porienek ~ 10 µm. Echter de deeltjes kunnen zwellen in de loop van de tijd en daardoor verstopt raken diep binnen het reservoir. Om dit mechanisme beter te kunnen begrijpen, is een reeks bulk en kernstroming experimenten uitgevoerd.

*Het derde hoofdstuk* richt zich op de nano-bolletjes en hun karakterisatie d.m.v. dynamische lichtverstrooiing en transmissie-elektronenmicroscopie. De bolletjes worden gesynthetiseerd door een omgekeerde emulsiepolymerisatie werkwijze. Daarom worden zij verspreid in een emulsiemedium. Om de verhoging in de grootte van de deeltjes en hun interactie in de loop van de tijd te bestuderen, werden de deeltjes gescheiden van het emulsiemedium door middel van een speciaal ontworpen procedure. De experimenten tonen aan dat de deeltjes zwellen en zich agglomereren in de loop van de tijd. Deze resultaten kunnen worden gebruikt om de (afnemende) doorstroming van nano-bolletjes in poreuze media te verklaren.

*Daarna* (*Hoofdstuk* 4), is een reeks experimenten met kernen die voorkomen in Berea, Bentheimer and Boise aardlagen uitgevoerd. De experimenten bestuderen hoe nano-bolletjes stromen in poreuze media met verschillende mineralogie en olieverzadiging. Aanvullend daarop, is de dynamiek van de drukval van de kernen en de organische koolstofconcentratie in het produktiewater bestudeerd. Dynamische licht verstrooiing experimenten hebben de grootte van de nano-bolletjes voor verschillende soorten zoutoplossingen blootgelegd en geholpen om hun invloed op de verspreiding in poreuze media beter te begrijpen.

De resultaten van dit werk laten zien dat de verspreiding van nano-bolletjes in poreuze media zeer afhankelijk is van het zoutgehalte van het water

in de kernen met verschillende olieverzadiging. Onder dezelfde experimentele voorwaarden, hangt de resterende weerstandsfactor van de nano-bolletjes in poreuze media af van de stroomsnelheid.

*Tenslotte*, hebben wij conclusies gemaakt en aanbevelingen over de ontwikkeling van nieuwe verdringingscontrole vloeistoffen gegeven.

# Preface

This work was done in a collaboration between Shell Global Solutions International and Delft University of Technology. It mostly tackles reservoir engineering problems associated with the improvement of oil recovery in heterogeneous oil reservoirs during a water flood. Chemically active fluids, such as crosslinking polymer and copolymer nano-spheres, were studied for the improvement of water flood sweep efficiency. These fluids can potentially propagate deep into a reservoir with a subsequent increase of the resistance factor. If the operation is successful, then the remaining oil is displaced towards producing wells and the water cut is reduced.

It was shown that the studied fluids represent a wide class of chemical agents which can be used for the improvement of sweep efficiency in heterogeneous reservoirs. Hence, the developed procedures for core flood and bulk experiments can be used for the screening of fluids for practical applications in specific characteristics.

The results of this work can also be used for the development of new chemical systems for conformance control in heterogeneous oil reservoirs.

# Chapter 1

## Introduction

In this chapter we discuss the problem of improved oil recovery in water flooded heterogeneous oil reservoirs. It is shown that early breakthrough of the injected fluid is likely to happen in heterogeneous reservoirs along highly conductive and permeable layers from injectors towards producers. That results in low sweep efficiency and a high water cut which makes the process of oil extraction inefficient.

The improvement of sweep efficiency can be achieved by applying one of the conformance control methods (e.g. infill drilling, choking in producing wells, and the injection of chemically active fluids into a reservoir). In this work we focus on the injection of chemical fluids which propagate deep into the reservoir and regulate permeability contrast between the layers with different permeability. It can be achieved with in-depth diversion and continuous injection of particle based fluids.

Next, the overview of different fluids for the conformance control is given. Based on the literature review, important parameters for the selection of successful fluids are highlighted.

Finally, research questions of the study are given. The following chapters of the thesis will be linked to the outlined research questions.

## 1.1 The improvement of sweep efficiency in heterogeneous oil reservoirs with chemical agents

Water flooding of oil reservoirs is a common operation that maintains the formation pressure and displaces oil towards production wells. Many oil reservoirs with natural heterogeneity have a low sweep efficiency of water flooding. As the result, water breaks through the formation along high permeable layers and a significant volume of oil is left behind the displacing front (Figure 1.1). This problem often happens in mature fields with the active water flooding systems.

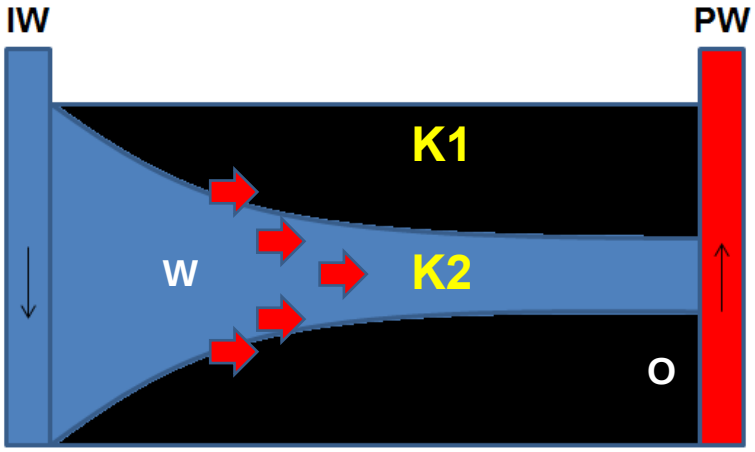


**Figure 1.1-** An element of a heterogeneous reservoir which is penetrated by two wells (K1-low permeable and K2-high permeable layers; IW-injection and PW-production wells; W-water; O-oil)

The improvement of sweep efficiency can be achieved with one of the conformance control methods (e.g. infill drilling, choking in producing wells, and the injection of chemically active fluids into the reservoir). In this work we study chemical methods for the improvement of water flood sweep efficiency which can be implemented by adding chemically active agents to the injected water. The most common methods are polymer flooding, the continuous injection of particle based fluids and in-depth diversion.

***Polymer flooding*** is usually implemented by adding a water soluble polymer (e.g. hydrolysed polyacrylamide) to the injected water. It increases the viscosity of the water and improves the mobility ratio between displacing and

displaced fluids. Depending on the target mobility ratio, the concentration of polymers can be selected accordingly. Results of experiments conducted by Seright et al., 2011 revealed that during the injection of a polymer solution into the reservoir, the displacing front becomes more stable in comparison to water injection and it penetrates into less-permeable zones as well (Figure 1.2). That improves the sweep efficiency of the flood and results in incremental oil recovery. Polymer flooding is a robust operation and can potentially mitigate mistakes during the planning of the operation. However, the propagation of the front is slow and the benefits from the polymer injection are obtained a long time after the beginning of the operation (Seright et al., 2011).

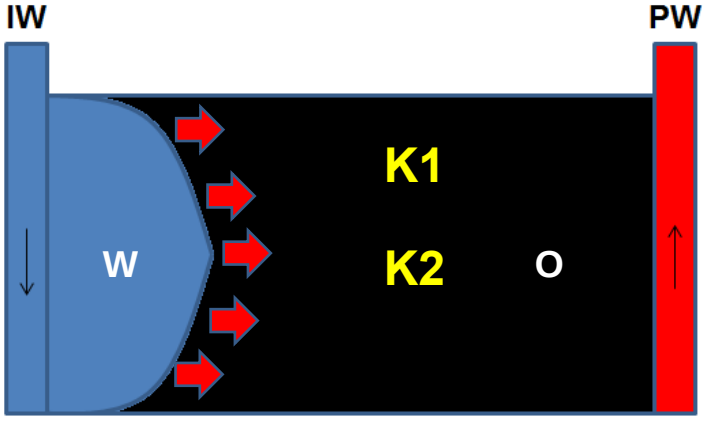


**Figure 1.2-** Application of the polymer flood in the heterogeneous reservoir

***Continuous injection of particle based fluids*** (e.g. colloidal dispersion gels, micro gels, and nano-spheres) is recommended when the permeability between layers in a heterogeneous reservoir changes significantly (Figure 1.3). Therefore, a full reservoir coverage with the injected fluid is required (Glasbergen et al., 2014). That is only possible if a significant depth of penetration happens and adsorption of the fluid on a rock surface is overcome.

The injected fluids can cause potential penetration into low and high permeability layers of the reservoir. If the injected particles mostly reduce the permeability for water and not oil, then the mobility ratio is changed after the treatment. According to Liang et al. (1995), polymers, polymer gelants and monomer gels mostly reduce the permeability to water rather than to oil or gas . That determines the selectivity of these fluids to build up a residual resistance factor in water saturated layers. The same is possible for polymer particles as

well. Residual resistance factor is defined as the ratio between the pressure drop during the brine injection after a chemical was injected into porous media to the pressure drop during the brine injection before the chemical was injected.

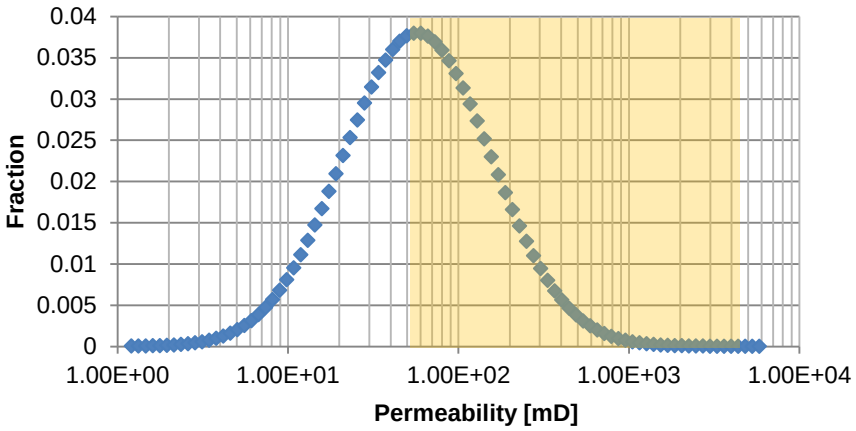


**Figure 1.3**- A heterogeneous reservoir with a log-normal permeability distribution

If a significant reduction in permeability happens for both oil and water in less permeable layers, then that situation is unfavourable (Seright et al., 2006). According to Seright et al., 2006, the improvement of particles placement in the heterogeneous reservoirs can be achieved by tailoring the size of particles according the average radius of pore throats. His analysis showed that if the particles have a normal size distribution then there is a critical standard deviation which determines the selectivity of the propagation in layers with different permeability. It is stated by Seright et al., 2006 that the lower the permeability contrast between layers, the smaller the standard deviation of the size distribution of particles has to be. In our point of view, this approach is oversimplified because many polymer particles can be squeezed and still be able to propagate into less permeable layers as well. Hence, the standard deviation of the distribution can be also influenced by the elasticity of the particles. In addition, it is always important to isolate less permeable and oil saturated zones from the treatment. That approach has to be taken into account when field operations are planned. If the operation is successful, then macro diversion in the reservoir is expected.

Particles and "weak" polymer gels can also improve the micro sweep efficiency of porous media by blocking pore throats which connect water saturated zones. In that case, preferential water flow paths change and trapped

oil can be displaced from the rock (Figure 1.4). The micro-diversion in porous media can be achieved only if the adsorption level is overcome and the subsequently injected fluid is enough to fill the water saturated zones.

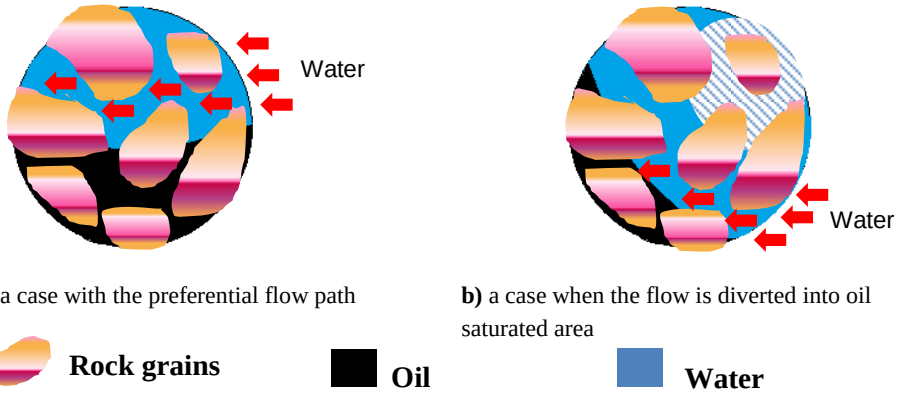


**a)** a case with the preferential flow path

**b)** a case when the flow is diverted into oil saturated area

**Figure 1.4-** Micro- diversion in porous media with particles (microscopic scale)

In contrast to the polymer flood and the continuous injection of particles, ***in –depth diversion*** aims to block high permeable layers deep in the reservoir. This treatment is recommended when a shortcut (a high permeable layer) between an injection and a production well exists (Figure 1.5). Therefore, an additional peak on the permeability distribution diagram appears representing high permeable layers (Figure 1.6).

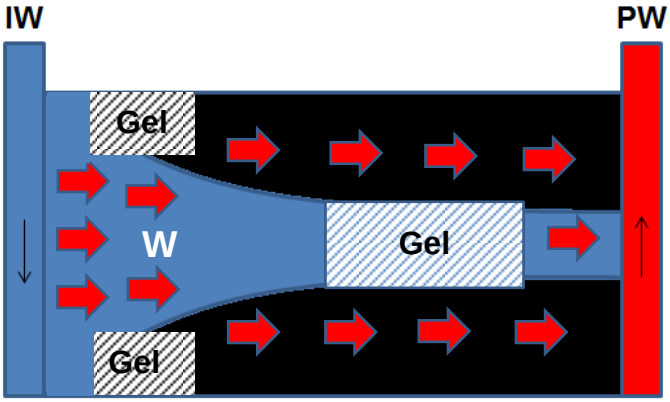


**Figure 1.5**- In-depth diversion in the heterogeneous reservoir

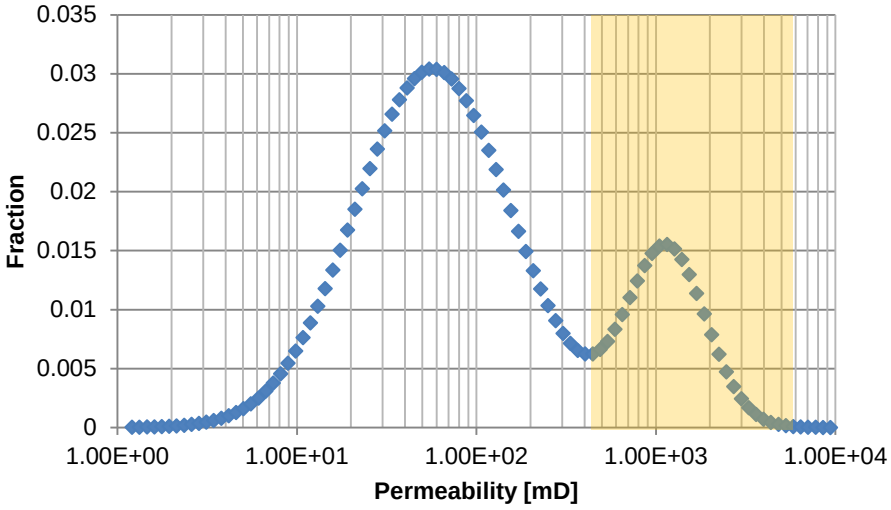


**Figure 1.6**- A heterogeneous reservoir with a bi-modal permeability distribution

The required radius of penetration R in this case is at least one third of the distance (Figure 1.7). Initially, a blocking fluid has to have a low resistance factor (viscosity) in porous media. That allows for the deep propagation into the reservoir. The following increase in the resistance factor (viscosity) causes the reduction in the permeability of high permeable layers and the diversion of the flow of subsequently injected water into low permeable layers with higher oil saturation (Seright et al., 2011). The resistance factor is defined as the ratio between the pressure drop during the injection of the chemically active fluid (e.g. polymer, nano-particles) to the pressure drop during the injection of brine. Although low permeable layers of the reservoir might be penetrated with the blocking fluid as well, the advancement of the fluid in high permeable zones has to outrun the front of the gel in low permeable zones (Seright et al. 2011, Figure 1.5). Therefore, according to Seright et al. (2011), the successful implementation of the in-depth conformance control requires a significant permeability contrast between high and low permeable layers (~10), high thickness ratios (low permeable zone is 10 times thicker than a high permeable zone), and low oil viscosities. *Particle based fluids*, as well as *cross-linking polymers* can be used for this treatment.

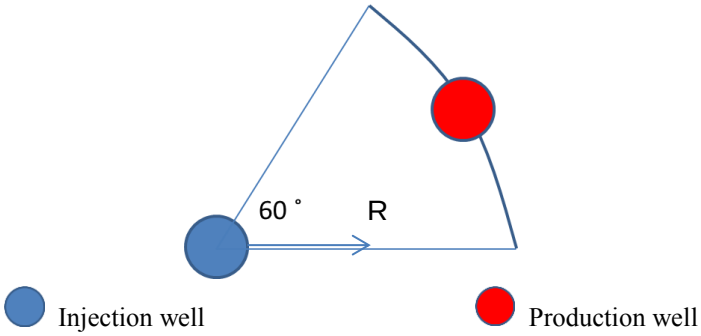


**Figure 1.7**- A sector of a water flood pattern: R- radius of penetration

Indeed, one third of the distance between an injection and a production well should be covered during the injection. However, a significant amount of the fluid is adsorbed on the rock surface during the propagation. The amount of adsorbed fluid can be calculated according to equation 1.1 for a sector of water flood pattern described on Figure 1.7. The results of calculations suggest that for a radius of penetration (R) 100 m into a reservoir which has a height (h) of 20 m, a porosity $\phi$ of 25 % and an adsorption ($\Gamma$) of 50 µg/g, the mass of the fluid which is lost is 10 400 kg.

$$M_{loss}=1/6 \cdot \pi \cdot R^2 \cdot h \cdot \phi \cdot \rho_{rock} \cdot \Gamma \qquad (1.1)$$

$M_{loss}$- mass of the gelant which is lost in the reservoir due to the adsorption, kg; $V_{rock}$- volume of the rock, $m^3$; $\rho_{rock}$=2650 kg/$m^3$- density of the rock; $\Gamma$- adsorption, µg/g.

The calculated adsorption can be satisfied after 50 days of injection at the concentration of 1040 ppm at the flow rate of 200 $m^3$/day.

There are several advantages of in-depth diversion in comparison with the polymer flood: short-term economic profit and high injectivity after the gelation. In contrast, the profit from polymer flood comes as soon as the oil bank reaches production wells. That can take a long time before the project starts to give a profit. Nevertheless, the ultimate recovery is higher for the polymer flood than for the in-depth diversion (Seright et al., 2011).

The advantages of the in-depth diversion are attractive for oil producing companies. However, the success of these technologies depends on a fluid for the treatment of reservoirs. In the majority of cases it is difficult to control the parameters of the technologies (viscosity, propagation in porous media, and size) which make the implementation difficult. In addition, the mechanisms

behind the complex fluid flow in porous media are poorly understood. This work is focused on the chemical methods for the in-depth diversion.

## 1.2 Overview of fluids for the improvement of sweep efficiency in heterogeneous reservoirs

A large variety of modern chemical methods for the improvement of sweep efficiency in heterogeneous reservoirs exist. These fluids usually have low initial resistance factor in porous media which allows for the deep propagation into the formation. After some time the resistance factor starts to build up. Depending on the composition of a fluid, the increase of the resistance factor can happen due to in-situ gelation and/or the accumulation of gel particles in the reservoir. The most frequently applied technologies are listed in table 1.1. From the table it is clear that the mechanisms for the triggering of the resistance factor build up are different and it depends on the composition of fluids. That gives a pool of different solutions for the treatment of reservoirs with different characteristics.

**Table 1.1**- Description of fluids for the conformance control in heterogeneous reservoirs

| Fluid | Content | Mechanism of the diversion | Advantages/Disadvantage |
|---|---|---|---|
| **Preformed particle gels (*PPG*)** (Bai and Zhang, 2011; Imqam et al. , 2014) | Copolymer particles which have the size >10 μm (Bai and Zhang, 2011). | Particles are designed to plug fractures of a reservoir. The subsequently injected water is diverted into the matrix of the reservoir. | +No chromatographic separation;<br>+Particles are elastic;<br>+Can be applied in reservoirs with mixed minerology;<br>+The size of particles is big enough to effectively plug fractured reservoirs;<br>+Can tolerate high temperatures (up to 130 ºC) and salinities ;<br>-Particles cannot propagate in a matrix.<br>-If the particles are produced they affect wells and facilities. |

| | | | |
|---|---|---|---|
| **Colloidal dispersion gels (*CDG*)** (Mack and Smith, 1994; Seright et al. 2006; Spildo et al., 2009,2010) | CDG formed by the crosslinking of a polymer (PAA) with a metal cross-linker (e.g.$Al^{3+}$). Due to the low concentration of the polymer (300- 1200 ppm, bellow the overlapping concentration C*) separate gel particles are created via intra-molecular crosslinking with $Al^{3+}$. The size of particles depends on the type of synthesis (≥100 nm) | Particles might propagate deep into a reservoir. Later they retain due to adsorption, jamming and straining in porous media. The micro diversion takes place and oil is displaced from small pores. | +No chromatographic separation;<br>+Particles are elastic;<br>+Can be applied in reservoirs with mixed minerology;<br>-If the particles are created in-situ, chromatographic separation might take place between a cross linker and a polymer;<br>-Unfavourable propagation into low permeability layers happens as well (Seright, et. al., 2006).<br>-When gel particles are formed, propagation might be difficult to achieve. |
| **Micro and nano-spheres** (Wang et al., 2010; Barari et al, 2011; Yao et al. 2016) | Particles (e.g. spheres) of micro- and nano-size are formed by the polymerisation of different monomers (e.g. acrylamide and N,N'-methylene bisacrylamide) with an organic cross linker. The size of particles depends on the synthesis (≥50 nm). | | +No chromatographic separation;<br>+Can be applied in reservoirs with mixed minerology;<br>+Particles are elastic;<br>+Can tolerate high temperatures (up to 100 ºC ) and salinities (up to 30 g/l);<br>-Can have a poor propagation. |
| **Thermally active micro gel particles (*Bright Water*)** Frampton et al., 2004 | The chemical content and a synthesis process are similar to micro-spheres. The difference is that it includes a crosslinker which reacts to the change of temperature. | At high temperatures, a partial de-crosslinking happens. It results in the reduction of the crosslinking density and a subsequent swelling of the particles occurs. | +No chromatographic separation;<br>+Can be applied in reservoirs with mixed minerology;<br>+Preformed particles;<br>-Swelling kinetics depends on pH, salinity and temperature. |
| **Cross-linking polymers** (Sorbie and Seright, 1992; Reddy et al., 2013; Glasbergen et al., 2014) | A continuous gel network is formed via the intermolecular crosslinking of a linear polymer (e.g. HPAM) with an organic/inorganic cross linker (e.g. PEI/ $Cr^{6+}$). | The crosslinking polymer has a low initial viscosity and is able to propagate in porous media. After some time, the viscosity of the gel builds up and it blocks the high permeable layers of the reservoir. | + Initial viscosity is low;<br>+The gelation time can be tailored;<br>+Can be applied in reservoirs with mixed minerology;<br>+Organically crosslinked polymers are more robust (Reddy et al., 2013);<br>-Chromatographic separation is possible;<br>-Early viscosity build up can be triggered by the influence of temperature, brine salinity and pH;<br>-Difference in behaviour between bulk and core. |

| | | | |
|---|---|---|---|
| **Thermally active polymers (*TAP*)** (Hourdet et al., 1997; Liu et al., 2012; Zhu et al., 2013; Roy et al., 2013; Al-Maamari et al., 2015) | Thermally active polymers can be synthetic (derivatives of acrylamide) and biopolymers (e.g. made from a cellulose fiber). | Initially the viscosity is equal to the polymer viscosity. Later, during the propagation in a reservoir, when the threshold temperature is overcome, the viscosity increases and gelant becomes a gel. | +Initial viscosity is equal to the polymer viscosity;<br>+Can be applied in reservoirs with mixed minerology;<br>+Single component system-no chromatographic separation;<br>-Viscosity might decrease with an increase in temperature in a dilute solution;<br>-Solubility of the polymers significantly affected with salts in brine. |
| **Inorganic gel systems** (Iler, 1979; Stavland, et al. 2011) | There is a variety of inorganic systems which form gel. The most common one is sodium silicate dissolved in brine. | Initially the viscosity of the gelant is low. That allows for the propagation into a reservoir. After some time, viscosity builds up. | +Initial viscosity is low which allows for the propagation into porous media;<br>-Might be only applied in sandstones;<br>-The gelation time might be limited (5 days).<br>-Divalent ions in brine might result in an early gelation. |
| **Foam** (Zitha et al., 2003; Rossen and Bruining, 2004; Farajzadeh et al. 2012; Hernando et al., 2016) | Dispersion of gas bubbles which are separated with liquid films and stabilised with a surfactant | Foam has a high resistance in high permeable layers and low resistance in low permeable layers. It improves the sweep efficiency. | +Selective mobility in layers with different permeability;<br>+Can be applied in reservoirs with mixed minerology;<br>-Low stability in high temperatures and in the presence of oil (Farajzadeh et al. 2012). |

According to Table 1.1, none of the fluids are perfect. All technologies have advantages and disadvantages. Therefore, every fluid has its own area of application.

**Preformed particle gels (*PPG*)** synthesised via a polymerisation reaction between acrylamide monomers, ammonium chloride and a cross-linker (N,N'-methylene bisacrylamide) in deionised water (Bai and Zhang, 2011). The obtained preformed gel particles are later cut into small pieces and dried. The final size distribution of dry particles is wide and changes within an interval between 10 μm and 1 mm.

When the PPG are in contact with water, they start to absorb it and swell. Particles might increase their diameter by ~15 times of their initial diameter. It was shown by Bai and Zhang, 2011 and Imqam et al., 2014 that the extent of swelling depends on the concentration of sodium chloride in brine. Hence, salinity has to be taken into account for the planning of field operations.

The size of the gel particles determines their application. They are mostly injected into fractures to divert flow into the matrix of a reservoir.

The residual resistance factor and the resistance factor of PPG also depend on the brine salinity. It was demonstrated (Imqam et al., 2014) that *the resistance factor and residual resistance factor are higher in higher brine salinity due to the higher swelling ratio of individual particles. If the brine salinity decreases, then the particles swell and they become more deformable. Therefore, the salinity influences the compressibility of the particles and, for example, in low brine salinity their propagation improves.* In addition to that, the higher the concentration of particles in the suspension, the higher the resistance factor.

**Colloidal dispersion gels (CDG)** are spherical gel particles which have a size in the range of 50-150 nm (Mack and Smith, 1994; Spildo, et al., 2010). According to Mack and Smith (1994), CDG are made by the cross-linking of a low concentration of polyacrylamide. Usually, the concentration of polymers is in the range from 100 to 1200 ppm (Mack and Smith, 1994). Hence, due to mostly intramolecular links, gel particles are formed. The authors also mentioned that different metals can be selected as a cross-linker. The most common one is $Al^{3+}$.

In contrast to the low concentration of the polymer, the high concentration of the polymer results in a continuous gel network which is formed with the inter-molecular crosslinking (Spildo et al., 2009).

Propagation of CDG in porous media was studied by different researchers (Mack and Smith, 1994; Seright et al., 2006; Spildo et al., 2010; Skauge et al., 2010). According to these studies, there are two ways for the gel particles to be formed: *1) in-situ; 2) preformed at the surface before the injection into porous media.* The most common approach for the injection is when the polymer and the cross linker are injected a few hours after the mixing of the components together. That results in the formation of gel particles in-situ. However, the results of experiments have demonstrated that the in-situ formation of gel particles might lead to their retention in porous media. Hence, in-depth diversion might be unrealistic. According to another approach (Spildo et al., 2010), gel particles are formed at the surface via the interaction between the polymer and the cross-linker in high salinity brine. The injection of preformed CDG particles was done by Spildo et al., 2010 into Berea cores and the

retention was studied. The results of experiments revealed that the propagation of preformed CDG is better than the CDG formed in-situ. *Nevertheless, the pressure drop during the injection of preformed CDG appeared to be significantly higher than the pressure drop during the injection of brine (*Spildo et al.,2010; Skauge et al., 2010*).* Unfortunately, there is no published data about the resistance factors during the injection of the polymer and CDG in the same core flood experiment. However, *there is an indication that some formation damage of a core occurred after the preformed CDG passed it*. In practice, it might be unrealistic to push the gel particles deep into the reservoir with such a high gradient pressure.

**Micro- and nano-spheres.** Micro- and nano-spheres are synthesised via an inverse emulsion polymerisation method where droplets of water serve as reactors for the polymerisation reaction between monomers (e.g. acrylamide and N,N'-methylene bisacrylamide) and an organic crosslinker (Wang et al., 2010; Barari et al., 2011; Yao et al., 2016). Barari (2011) explained that a significant amount of surfactant is required to effectively disperse water in oil. That makes the size of water droplets small affecting the final size of polymer particles. Micro and nano-spheres when in contact with water do not dissolve, instead they absorb water and swell over time. The kinetics of this process is slow and depends on brine salinity, temperature, and pH.

*According to Yao et al. (2016), the micro- and nano- spheres can tolerate high temperatures (up to 90 ˚C), salinities (up to 30 g/l) and pH (4-10.3) without damaging the structure*. At higher temperatures (>200 ˚C) the links between monomers break and at higher salinities (>30 g/l) the shape of the spheres loses its roundness. Yao et al. (2016) also obtained the size distribution curves of polymeric micro- spheres with a particle analyser at different temperatures and salinities. They revealed that *the higher the temperature, the bigger the size of the spheres* (below 200 ˚C); *the higher the salinity, the lower the size of spheres.*

Yao et al. (2014 and 2016) also studied the pore scale transport of nano-spheres. It was demonstrated that *four main mechanisms play a role during the flow of micro-spheres: smooth passing* (when the size of pore throats is bigger than the size of particles and the particles easily propagate without straining); *elastic plugging* (particles have a bigger size than pore throats. That results in the plugging of the throats and the resistance factor increases. The increase of a local pressure leads to the elastic deformation of the particles and the

subsequent passing through the throat); *bridge plugging* (this happens at a high concentration of particles at the entrance of pore throats when the individual size of particles is smaller than the size of pore throats; the resistance of such clogs of the spheres is higher than elastic pugging); *complete plugging* (straining of the spheres, when the size of spheres is much bigger than the size of pore throats). These mechanisms can explain the fluctuation of pressure drop along a core during the injection of spheres.

*Unfortunately, there are only a few studies which demonstrate the propagation of spheres at different salinities in core flood experiments with multiple pressure taps (Chapter 4). Oil recovery from porous media by nano-spheres is a subject of study as well (Wang, et al., 2010).*

Application of nano-spheres in a conformance control project at the Scovil reservoir (East-Centrak Alberta, Canada) are reported by Irvine et al., 2015. The average permeability of the reservoir is low ~ 90 mD and it is heterogeneous. It was reported *that during the continuous injection of the spheres (6 months), the incremental oil recovery was increased by 14 %.* At the same time, there was no increase in wellhead injection pressure which indicates a good propagation in the reservoir. Results of micro-spheres application in Dagang oilfield in China was reported by Yao et al., 2016. *Results suggest that the injection pressure increased by 2 times over 8 months of the injection. It was noted that the injection profile was improved by plugging of high permeable intervals of the reservoir.* That indicates the efficiency of the n

**Thermally active micro gel particles (*Bright water*).** As described by Frampton et al., 2004, *the chemical content and the synthesis reaction of this gel system is similar to the micro-spheres*. The obtained gel particles have a size distribution in the interval of 0.1 to 3 μm. The main difference of thermally active micro gel particles is that at high temperatures a partial de-crosslinking happens resulting in the reduction of a crosslinking density. This effect is responsible for the swelling of the particles. Depending on the target temperature, a crosslinker can be selected accordingly. The initial concertation of the crosslinker in the particles is high. Thus the size is not affected much with the change in brine salinity.

Theoretically, when the particles are injected into a reservoir in cooler water than the rest of the reservoir, then particles keep their initial size and can propagate in porous media. Later, when the temperature of the injected brine

increases, the particles swell and block pore throats diverting subsequently injected water into low permeable zones.

In the paper of Frampton et al., 2004 the results of a core flood experiment were reported. *One of the mechanisms which influences the propagation of small micro gel particles* (the reported size is smaller than the size of pore throats) *is the interaction between the particles and a carrier fluid, as well as, the particles and the rock surface*.

It was reported that the propagation of the particles in core flood experiments was difficult to study using the effluent analysis due to the possible breakthrough of mineral oil in which the particles were initially dispersed. Hence, the propagation was estimated only on the pressure drop behaviour. According to multiple pressure taps along a coreholder used in the experiments, the propagation does occur over the time of the injection. The reported resistance factor of non-activated particles in a sand pack with a permeability of 3 D was around 3. After the temperature was raised, the RF was increased by 30 times which indicates the activation and swelling of the particles. The resulting RRF increased to 100. *Unfortunately, this study does not indicate the RF during the propagation of the non-activated particles' in cores with multiple pressure taps in different brine salinities*.

**Cross-linking polymers** *are continuous gel networks* which are formed via an intermolecular interaction between negatively charged groups of a polymer and a positively charged cross linker (Reddy et al., 2013; Glasbergen et al., 2014). Literature review has showed that the variety of polymers can be used for crosslinking: polyacrylamide, 2-acrylamido-2-methyl-propane sulfonic acid (AMPS), acrylamide copolymers and biopolymers. Organic and inorganic cross-linkers can be used to form a three dimensional network with polymers. Polyvalent metals such as $Al^{3+}$ and $Cr^{6+}$ are widely used for the crosslinking of polymers in conformance control systems. The most common organic crosslinkers are polyethylenimine (PEI), polyvinyl alcohol and phenyl acetate (Reddy et al., 2013). According to Reddy et al. (2013), the *organically crosslinked polymers are more robust than inorganically crosslinked systems*. Hence, it makes the former more attractive for application in conformance control technologies.

Initially, the viscosity of a cross-linking polymer is low. The fluid in this state is called gelant (Sorbie and Seright, 1992). The gelant bank is pushed into the reservoir by the subsequently injected water (polymer) without a significant

resistance factor build up. *Due to the low viscosity of the gelant, its penetration into a low permeability layer is minimised* (Sorbie and Seright, 1992). *After some time, the viscosity of the gelant increases and it becomes a gel.* It is important that the gelation time is enough to place the gel in a target region of the reservoir. Hence, *during the post flush period, due to the crossflow between layers of the reservoir, the water is diverted from highly permeable into low permeability layers*, oil is pushed back into high permeable layers. If this operation is successful, then the sweep efficiency of the reservoir will be improved.

It is highly desirable that the gelant propagates deep into a reservoir. Thus, the efficiency of the treatment will be maximised.

One of the disadvantages of this technology is that chromatographic separation might take place during the flow of the polymer and a cross linker together. Therefore, the resulting gel might have a lower residual resistance factor. However, if the polymer is a continuous phase for the system, then the resulting cross-linking polymer is less vulnerable to the chromatographic separation.

Another disadvantage is that the cross-linked polymer is affected by reservoir characteristics (e.g. brine salinity, temperature and rock minerology), which can trigger an early gelation.

**Thermally active polymers (TAP)** can be made via copolymerisation with hydrophobic or hydrophilic co-monomers. According to Zhu et al. (2013), a majority of water-soluble thermosensitive polymers include N-isopropylacrylamide (NIPAM), poly(ethylene oxide) (PEO), or poly(propylene oxide) (PPO). At the temperatures above the critical solution temperature (CST), self-assemble micelles or physical networks are formed. Depending on the concentration of hydrophobic/hydrophilic comonomers in the polymer, CST can be different (Liu et al., 2012; Zhu et al., 2013; Roy et al., 2013). It was experimentally demonstrated that these molecular structures significantly increase the viscosity of the polymer solution (Zhu et al., 2013). The rheology of the TAP is also concentration dependent and in dilute solutions intramolecular behaviour is observed leading to the reduction of the viscosity.

Al-Maamari et al. (2015) studied a thermally active biopolymer which is produced from a cellulose fibre. The polymer contains anhydroglucose units which connect together in a spatial gel network via hydrogen bonding when the

temperature is increased. This polymer does not contain any additives (e.g. cross-linker) which makes it free of chromatographic separation. The initial viscosity of the gelant is equal to the viscosity of the polymer. Later, when the *threshold temperature is exceeded, the fluid becomes a gel*. The gelation reaction is reversible.

It was experimentally demonstrated (Al-Maamari et al., 2015) that the increase in brine salinity leads to the decrease of the threshold temperature. Thus, the salinity of a makeup brine has to be adjusted accordingly. The authors demonstrate that the threshold temperature can be within the range of 30 ºC and 90 ºC.

The reported adsorption in porous media was relatively low (Al-Maamari et al., 2015) and equal to 52 µg/g. Unfortunately, results of the propagation of the studied TAP through porous media are absent, so it is difficult to estimate the resistance factor in porous media.

**Inorganic gel systems.** There is a wide range of inorganic systems which can form strong gels over time. One of the most common is based on a sodium silicate dissolved in brine (Stavland, et al. 2011). The gelation reaction is caused by an activator resulting in the formation of silicate aggregates.

Sodium silicate is a liquid with a pH in the range of 11-13. It turns into a gel when the pH is reduced (Iler,1979). Hence, the placement of the gel bank in a reservoir can be controlled by pH.

Core flood experiments conducted by Stavland, et al., 2011 using Bentheimer cores (permeability is about 2D) demonstrated that the resistance factor gradually increase over time. That can be explained by the gelation process where silica agglomerates are being formed. *The experiments also showed that the gelation time might be limited to 5 days, which might not be enough for the in-depth placement in a reservoir.* The gelation time can be also affected by the temperature, cation exchange with rock minerals or brine salinity.

**Foam.** According to Farajzadeh et al. (2012) and Hernando et al. (2016), foam is a dispersion of gas bubbles which are separated with liquid films and stabilised with a surfactant. Foam can be generated in porous media by different approaches: 1) co-injection of gas and surfactant; 2) surfactant alternating gas (Rossen and Bruining, 2004). Both methods have been discussed in the literature.

The rheology of the foam depends on porous structure. Thus the difference of selective mobility in high and low permeable layers makes it suitable for conformance control in heterogeneous reservoirs. The main weaknesses of foam are low stability at high temperatures and in the presence of oil (Farajzadeh et al., 2012).

A broad overview of different chemical technologies for conformance control has been given in this chapter. That helped to define parameters which are crucial for the treatment. The selection of a technology for a field operation has to be done according to the following requirements: 1) initial viscosity (resistance factor) of a gelant has to be comparable to the viscosity (resistance factor) of a fluid injected before the gelant (e.g. brine or polymer); 2) the ratio between fluxes in less and higher permeable layers should be similar during the injection of a fresh gelant; 3) the propagation has to be achieved in porous media with mixed mineralogy; 4) the final residual resistance factor has to be high enough to reduce the permeability of higher permeable layers; 5) easy to mix and inject into a well (operation requirement); 6) initial components of the fluid has to be available, cheap and *environmentally friendly* (non-toxic!!!).

*According to criteria outlined above, organically cross-linking polymers and nano-spheres can be selected as candidates for the study*. Thus, these types of fluids are promising for the improvement of sweep efficiency.

Rheology, size distribution and propagation in porous media are examined. Finally, methods for the testing of fluids are designed. Recommendations for the design of the new fluids for the in-depth diversion are given.

## 1.3 Research questions of the study

Two different polymer based fluids are studied in this work. There are general research questions which can be addressed to their flow in porous media. The major ones are *how well these fluids propagate in porous media? What factors does the propagation depend on? Do these fluids effectively decrease the permeability of high permeable layers after gelation time?* There are also specific research questions which explain the mechanisms of the fluids' resistance factor build up over time.

A cross-linking polymer increases viscosity over time and after it reaches a gel point, the flow stops. The relevant questions here are *What does the*

*kinetics of the viscosity build up depend on? Are there any differences between the kinetics of viscosity build up in bulk and porous media?*

Nano-spheres, in turn, can swell and might aggregate over time and after it reaches a size which is comparable with the size of pore throats, the flow stops. *Do nano-spheres aggregate over time? What is the aggregation rate? How does salinity influence particles propagation in porous media? Is the bridging effect (jamming effect) or size exclusion due to the swelling of the spheres responsible for the resistance factor build up?*

To answer these research questions, a series of bulk and core flood experiments were carried out.

# Chapter 2

## Cross-Linking Polymer for Conformance Control

Heterogeneous oil reservoirs often have poor sweep efficiency during flooding. Although polymer flooding can be used to improve the oil recovery, in-depth diversion might provide a more economical alternative. Most of the in-depth diversion techniques are based on the propagation of a system that forms a gel in the reservoir. Premature crosslinking of the system prevents the fluid from penetrating deeply into the reservoir and as such reduces the efficiency of the treatment. We studied the effect of using a Poly-Electrolyte Complex (PEC) to (temporarily) hide the cross-linker from the polymer molecules. In addition to studying the cross-linking process in bulk, we demonstrated its behaviour at the core scale (1 m length) as well as on the pore scale. The gelation time in bulk suggested that the PEC could effectively delay the time of the crosslinking even at high brine salinity. However the delay experienced in the core flood experiment was much shorter. Tracer tests demonstrated that the cross-linking polymer (XL polymer), which is a mixture of PEC and partially hydrolyzed polyacrylamide, reduced the core pore volume by roughly 6.2 % (in absolute terms). The micro-CT images showed that most of the XL polymer was retained in the smaller pores of the core. The large increase in dispersion coefficient suggests that this must have resulted in the creation of a few dominant flow paths isolated from each other by closure of the smaller pores.

## 2.1. Introduction

In-depth profile modification is a promising technology for improving the sweep efficiency of water flooded heterogeneous reservoirs (Seright et al. 2011; Sydansk et al. 2000; Bailey and Crabtree 2000; Glasbergen et al. 2014). It can be implemented by injecting a cross-linking polymer (XL polymer) that propagates deep into the reservoir. The viscosity of the polymer has to be low for some period of time followed by a fast viscosity build up as it reaches the gel point (Winter 1987). The formed gel has a high apparent viscosity (approx. 15 000 mPa·s) which reduces the effective permeability of layers with higher conductivity. Once the target zone permeability is reduced, brine flow from injection wells will be diverted into zones with lower permeability (and higher oil saturation). As a result, the production of excessive water will be reduced and oil production will be increased. The efficiency of the process depends on the geological characteristics of the reservoir, as well as on the physical properties of the chemical agents, its concentration in the target zone and the interaction with the minerals of the rock (Seright et al. 2011; Bailey and Crabtree 2000; Glasbergen et al. 2014; Lake 1989).

The most appropriate chemical system for in-depth profile modification in a reservoir should have the following properties: tolerance to the salinity of the brine, thermal stability, low initial viscosity, deep propagation into a reservoir, and low mechanical degradation (El Karsani et al. 2014; Zhang and Zhou 2008; Zitha et al. 2002). There are a few XL polymers that can meet the desired requirements for profile modification problems in specific reservoir conditions (Crespo et al. 2014). One of the commonly applied cross-linking systems is a mixture of a hydrolysed polyacrylamide (HPAM) and polyethylenimine (PEI) (Al-Muntasheri et al. 2008; Crespo et al. 2013). Despite its frequent application, there is a lack of knowledge about the in-situ dynamic cross-linking of such systems and hence the efficiency of the XL polymer cannot be predicted from reservoir to reservoir. Therefore, it is important to study the in-situ dynamic cross-linking of polyacrylamide both from a theoretical as well as from a practical point of view. Cross-linking of HPAM often happens fast (2-4 days) (Glasbergen et al. 2014). In general this is not acceptable for the purpose of injecting a XL polymer deep into a reservoir. In order to extend the gelation time it is desired to make a cross-linker, which is a polycation, less active by mixing it with a retardant, polyanion. As a result of that reaction, a polyelectrolyte complex (PEC) is formed (Cordova et al. 2008;

Müller et al. 2011; Spruijt 2012; Jayakumar et al. 2012). Over time the chemical bonds between the polycation and the polyanion become weaker and the cross-linker becomes available for interaction with HPAM. In the current work, a PEC was employed for delaying the reaction between HPAM and PEI. The flow of this mixture in porous media was studied experimentally according to a specially developed framework. That framework includes bulk, pore scale , as well as a core flood experiment. The bulk rheology of different XL polymer recipes was tested first to select a relevant recipe with a gelation time suitable for the core flood experiment. There are different parameters which influence the kinetics of cross-linking of the polymer: temperature, different concentration of divalent ions, and cross-linker concentration. These parameters were varied during the bulk tests to meet the following requirements:1) the initial viscosity of a mixture (polymer + cross-linker) has to be low and the gelation time not less than 5 days; 2) the XL polymer has to be stable at 45 ˚C, which is the target temperature of the experiment; 3) no dramatic precipitation occurs during the gelation time.

Next, a slug of the selected XL polymer was injected into a 1 m Boise core and it was subsequently displaced by HPAM in order to study the in-situ dynamic cross-linking of the polymer. During the injection process the pressure drop over the core was recorded. To understand the reason for the pressure drop build up during the injection of the XL polymer into the core, a series of filtration tests was carried out. Filters with 3 different pore sizes were used in the test to study the size of the cross-linking particles which are formed during the cross-linking reaction. In addition to that, porosity reduction and the change of the dispersion coefficient were obtained by the injection of a tracer into the core (before and after XL polymer injection). Tracer transport in porous media was modelled by fitting an experimental breakthrough curve for a tracer with a one dimensional advection-dispersion model, where porosity and dispersion are matching parameters (Sorbie 1991; van der Hoek et al. 2001; N. Seetha et al. 2014). The two tracer tests show a porosity reduction of 6 % and an increase of the dispersion coefficient by a factor of 20 which indicates that the in-situ crosslinking took place in the porous media.

Distribution of the polymer in the porous medium was studied by micro computed tomography of core samples which were drilled out from the 1 m core after the experiment was finished (van Krevelen and te Nijenhuis 1990; Hove et al. 1990; Turner et al. 2004; Saadatfar 2004). The size of a core sample

is 4 mm to 10 mm. The results show that the polymer is concentrated mostly in the smaller pores of the samples.

## 2.2. Experimental material and procedures

### Bulk experiments

Selection of the XL polymer recipe for the core flood experiment was done via the study of the gelation time and gel stability. As mentioned before, we used the following criteria to select the recipe to be used in the core floods:

1) low initial viscosity of the mixture (polymer +cross-linker);
2) gelation time of more than 5 days;
3) stable at elevated temperatures;
4) no dramatic precipitation over time.

HPAM with PEI as a cross-linker was selected for this study. The reaction between HPAM and PEI can be explained as imine nitrogen from PEI attacking the carbonyl carbon attached to the amide group of the polymer (Figure 2.1) (Hu Jia et al. 2010). That creates covalent bonds which are much stronger than ionic bonds.

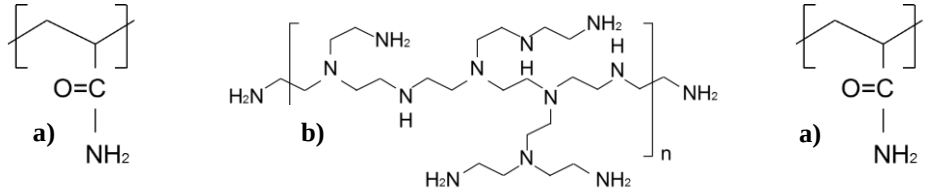


**Figure 2.1**- Chemical structures of polymers: a- carbonyl carbon group of HPAM; b- PEI.

The thermal stability of this system over a wide range of temperatures is ensured by the resulting covalent bonding (Moradi-Araghi 1991; Hutchins et al. 1996).

Activation of the XL polymer deep in the reservoir requires a delay in the reaction between the polymer and the cross-linker. Consequently the polymer needs to be (temporarily) shielded from the cross-linker. Poly Electrolyte Complexes (PEC) have shown their effectiveness for entrapping and delivering small molecules (large proteins) while maintaining colloidal stability via electrostatic repulsion (Figure 2.2).

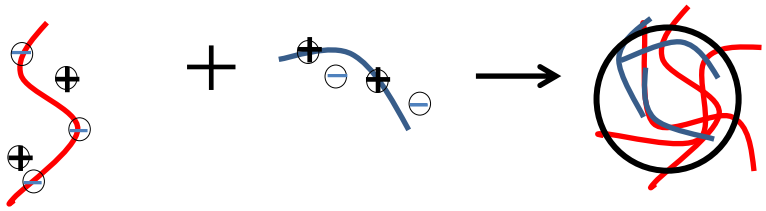

**Polyanion** **Polycation PEI** **PEC Nanoparticle**

**Figure 2.2**- Sketch of PEC formation from PEI and an appropriate polyanion

A polyanion (e.g. dextran-sulfate), together with the organic polycation cross-linker PEI can form a nano-particle polyelectrolyte complex by self-assembly through electrostatic intermolecular interactions (Müller et al. 2011). In time the PEC particle will unfold, releasing the cross-linker.

*The preparation procedure for the XL polymer samples*

We prepared a total of 16 different recipes by altering the following parameters:

1) divalent ions concentration ($Ca^{+2}$, $Mg^{+2}$) (2 different brines to validate robustness);

2) temperature of the test (30, 45, 60, 85 ˚C);

3) cross-linker concentration (754, 3077 mg/l).

Initially two HPAM stock solutions were prepared by dissolving a polyacrylamide powder (Mw = $20 \cdot 10^6$ D) in two types of brine, which differ by divalent ions concentration (Table 2.1). Brine type 2 contains a 20 times higher concentration of $Ca^{2+}$ compared to the brine type 1. The polymer solution was stirred for 48 hours to achieve a complete dissolution of the polymer. Subsequently the prepared stock solution was filtered to remove impurities using a 5 μm Millipore filter.

**Table 2.1** – Brine compositions

| Type 1 | | Type 2 | |
|---|---|---|---|
| **Ions** | **Concentration mg/l** | **Ions** | **Concentration mg/l** |
| $Na^+$ | 1656 | $Na^+$ | 1519 |
| $K^+$ | 28 | $K^+$ | 871 |
| $Mg^{+2}$ | 11 | $Mg^{+2}$ | 77 |
| $Ca^{+2}$ | 24 | $Ca^{+2}$ | 491 |
| $Cl^-$ | 2534 | $Cl^-$ | 4108 |
| $SO_4^{-2}$ | 159 | $SO_4^{-2}$ | 159 |

The components of the PEC were diluted in demineralized water separately (Table 2.2). The hydrogen-ion concentration of the PEI solution was adjusted by using concentrated HCl to a pH of 10.7. Subsequently PEI and polyanion were mixed together while stirred at 600 rpm. In order to avoid polymer degradation, the samples were prepared in a glove box maintaining an oxygen-free environment (Sorbie 1991).

**Table 2.2-** Initial concentrations of the chemicals in the selected XL polymer

| Component | Molecular weight, $10^3$ D | Concentration, mg/l |
|---|---|---|
| HPAM | 20,000 | 2500 |
| PEI (XL agent) | 25 | 754 |
| Polyanion (retardant) | 5 | 151 and 313 |

### Study of a XL polymer gelation time

The gelation time, indicative of the cross-linking kinetics, was studied using a falling ball viscometer. Although that approach is less accurate than a small amplitude oscillatory shear test, it gives a good indication of viscosity increase over time. Moreover this approach is very efficient and allows assessment of a large number of samples in a short time. The test requires a long glass tube that is completely filled with a XL polymer. The viscosity can be estimated from the time it takes for the ball to fall to the bottom according to equation 2.1 (Batchelor et al. 1967):

$$\mu = \frac{g \cdot d^2}{18l} \cdot (\rho_s - \rho_f) \cdot t \qquad (2.1)$$

where μ [Pa·s] - viscosity, t [s]-time, $\rho_{s,f}$ [kg/m$^3$]-densities of the glass ball and fluid respectively, l [m]-length of a tube, d [m]-diameter of the ball, and g [m/s$^2$]-gravitational acceleration.

## Core-flood experiment

In order to study the in-situ crosslinking of HPAM a core flood experiment was done. The core flood set-up (Figure 2.3) has a core holder (1) designed for a 1 m core with a diameter of 5.1 cm covered by a rubber sleeve to allow a confining pressure of 50 bar. The core holder is covered by a heating jacket (6), to maintain elevated temperatures during the experiment. The test was run against a back pressure of 5 bar, maintained by a back pressure

regulator (4) connected to a high pressure nitrogen vessel. The pump (5) is used to inject fluids through a bottom part of the core holder. The pressure drop over the core is measured using a pressure transducer (2) and recorded by the data acquisition system (7) together with the data from temperature sensors and the pump. The effluent collector (3) was used to take samples of the produced brine for further analysis ($K^+$, $Na^+$, $Ca^{2+}$, $Mg^{2+}$) using an Inductively coupled plasma spectrometry ICP. The experiment consisted of multiple steps as listed in Table 2.3. Brine type 1 was used for the permeability test and the XL polymer preparation.

**Table 2.3**- Procedure of the core flood experiment

| Steps | Description | Objective |
|---|---|---|
| Evacuating the set-up | The outlet of the set-up is connected to a vacuum pump. | Removing air from the set-up |
| Saturating the core with brine and heating it up | While the outlet of the set-up is connected to the vacuum pump, inject 1 PV of brine (type 1) into the core at a flow rate of 2.5 ml/min. Disconnect vacuum pump. Inject 10 PV brine. During brine injection the core's temperature was increased to 45 ºC; The concentration of $Ca^{2+}$, $Mg^{2+}$, $Na^+$, $K^+$ in the effluent was tracked via ICP analysis. | Filling the tubes of the set-up, as well as saturating the core with brine.<br>Equilibrium of the rock-fluid system is expected to be established after 10 PV of brine injection |
| Permeability test | Test at different flow rates: 0.4, 1, 1.6, 2.2, 3 ml/min. | Initial permeability of the core. |
| Initial tracer test | Injection of 2 PV brine with potassium iodide (20 ppm) into the core at 0.12 ml/min (1 ft/day). Followed by 5 PV brine injection without tracer to wash out the KI. Concentration of KI in the effluent was detected by a spectrophotometer. | Determine the original pore volume and dispersion coefficient of the core. |
| Polymer slug | 4PV of a polymer slug was injected to saturate the rock surface with polymer. The effluent ions concentration was tracked using ICP.<br>In-situ rheology of the polymer was determined as well. | Establish equilibrium with polymer. Saturating the rock surface with polymer. Determine polymer mobility. |
| Tracer test | The polymer solution, together with 1000 ppm KI tracer, was injected into the core. Followed by 2 PV polymer solution without tracer. | Assess the impact of the adsorbed polymer on pore volume and dispersion coefficient |
| XL polymer slug | The XL polymer solution was injected at the flow rate of 1 ml/min for 0.5 PV. | This step represents a XL polymer injection into a near well-bore area. |
| Small polymer slug | Displacing the XL pol. with 2500 ppm HPAM at 0.12 ml/min for 0.1 PV. | Propagation of the XL polymer in porous media. |

| | | |
|---|---|---|
| Shut-in period | The core was shut-in for 24 hours. | Crosslinking occurred over this time. |
| Multiple small polymer slugs followed by shut-in periods | Periodic displacing the XL polymer by HPAM (2500 ppm) at 0.12 ml/min. | Assessing the development of the mobility reduction |
| After flood tracer test | The polymer solution, together with 1000 ppm KI tracer, was injected into the core. | Determine post flood pore volume and dispersion coefficient |
| Micro CT scan of a core sample | A sample (4x10 mm) was drilled from the core and scanned by the Micro CT. Subsequently the sample was cleaned with NaClO (to remove the polymer) and scanned again. | Distribution of the polymer in porous media. |

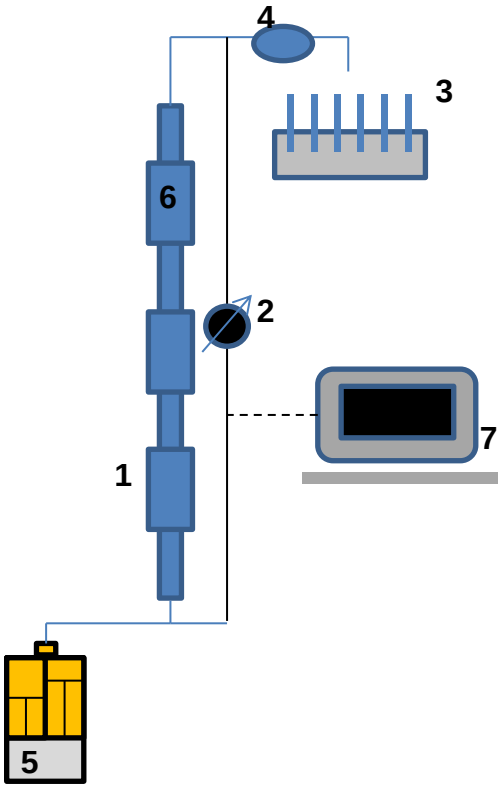


**Figure 2.3-** Core flood set up:

1- core holder with 1m core;
2-pressure transducer;
3-effluent collector;
4-back pressure regulator;
5-pump;
6- heating jacket;
7-data acquisition system.

## 2.3. Results and analysis

The bulk viscosity for the different recipes of the XL polymer are presented in Figures 2.4 and 2.5.

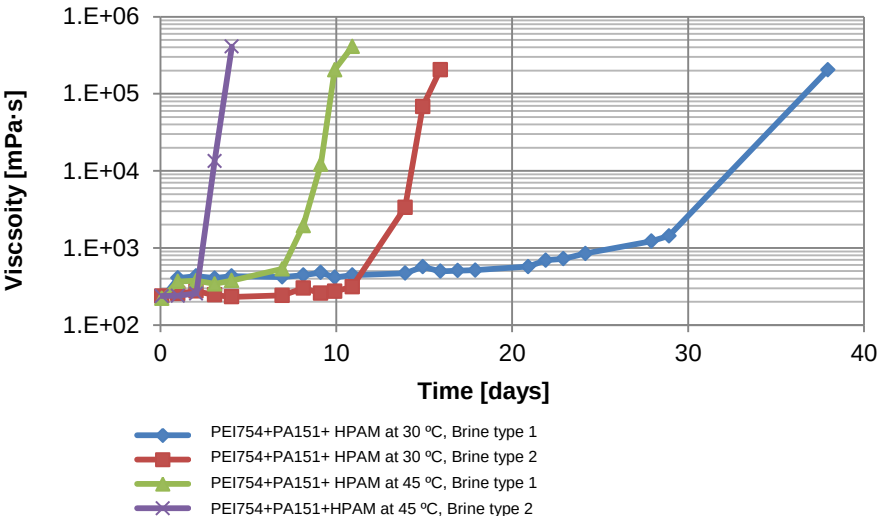


**Figure 2.4**- The viscosity of the HPAM / PEC solutions at different brine compositions (Type 1 and 2) and temperatures (30 and 45˚C)

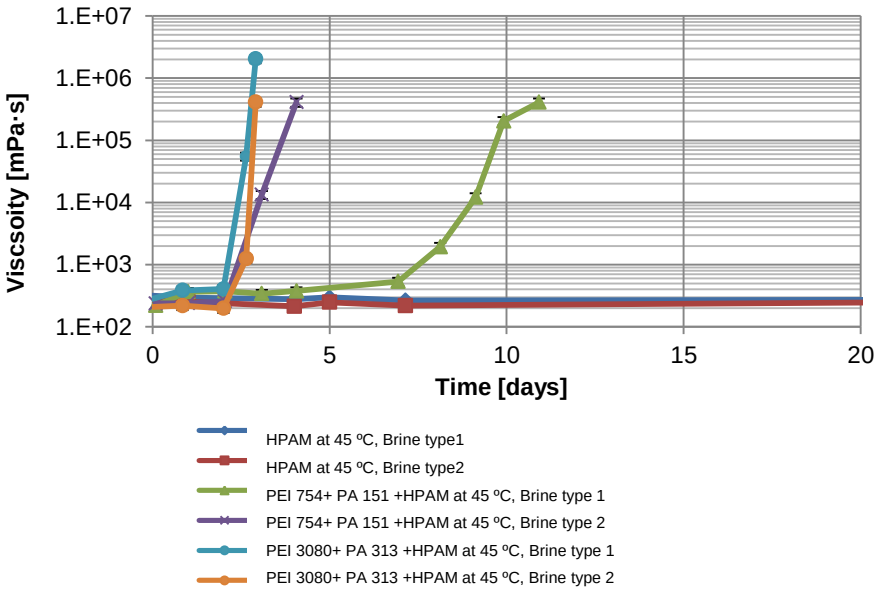


**Figure 2.5**- The viscosity of the HPAM / PEC solutions at different brine compositions (Type 1 and 2) at 45˚C

It appears from Figures 2.4 and 2.5 that faster cross-linking of HPAM occurs at higher concentrations of divalent ions. However, the faster crosslinking at higher brine salinities is unexpected because the higher ionic strength results in a smaller radius of gyration (Sorbie 1991; Hu Jia 2010; Glasbergen et al. 2014). That makes negative sites of the polymer less accessible to the cross-linking molecules. Nevertheless, two possible explanations of the faster cross-linking are given in literature:

1) weaker links between PEI and the retardant at high salt concentrations, which makes PEI available for crosslinking with HPAM
2) the interaction of divalent ions and carboxylic groups is more complex- an interconnection of multivalent cations ($Ca^{2+}$, $Mg^{2+}$) with HPAM chains occurs (Zhang, 2008).

Additional experiments are required to better understand the chemistry / physics of the reaction.

Faster crosslinking is also observed in the case of a higher weight ratio of the PEI to retardant. The mechanism of a faster gelation at lower concentrations of the retardant can be explained by the availability of free PEI in the beginning of the chemical reaction. Higher temperatures result in faster crosslinking as well.

Based on these results the fluids selected for the core flood experiment contain the following components: HPAM (2500 ppm), PEI (754 ppm) and polyanion (151 ppm).

As stated earlier, the falling ball viscometer is a quick screening method to determine the gelation time of the XL polymer. To obtain a more accurate estimate of the viscosity (including its shear-rate dependence), a rotation viscometer was used (Figure 2.6).

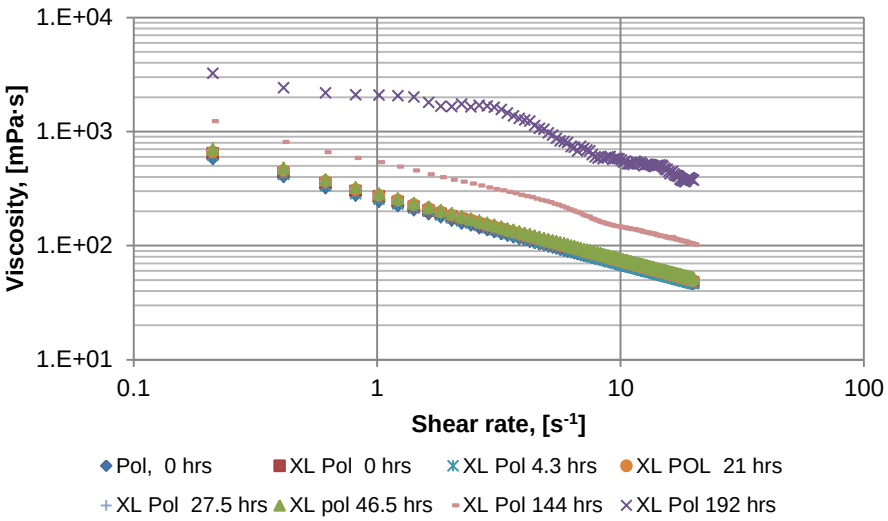


**Figure 2.6-** Viscosity as a function of shear rate for different time steps of the selected XL polymer at 45˚C (HPAM (2500 ppm), PEI (754 ppm), polyanion (151 ppm) and brine Type 1)

Results of the rheology experiments carried out at 45 ºC show that the initial viscosity of the XL polymer is 88 ± 3 mPa·s at 7 $s^{-1}$ and it is equal to the viscosity of polymer (Figure 2.6). Due to the crosslinking of the polymer, the increase of the bulk viscosity happens over time. However, due to the presence of the polyanion in the fluid, the active crosslinking in the bulk is delayed. From the figure it can be seen that the increase of the viscosity is observed after 144 hrs of the reaction. The result is in agreement with the results obtained from the falling viscometer method (Figure 2.5).

The rheology of the XL polymer can be affected by polymer degradation leading to a reduction in viscosity. To validate the polymer stability, separate rheology tests of the polymer (2500 ppm) were carried out at different aging times (Figure 2.7). Results of the tests show that the polymer maintains its viscosity 83 ± 3 mPa·s at 7 $s^{-1}$ for the 165 hrs.

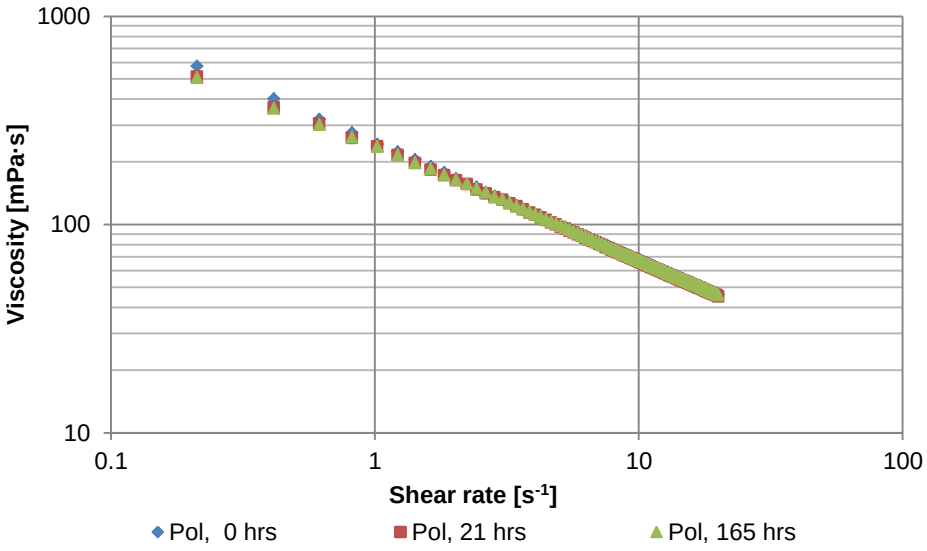


**Figure 2.7-** Viscosity as a function of shear rate at different aging times ( HPAM 2500 ppm) at 45˚C

## Brine injection into the core

After evacuating the core, 10 PV of brine was injected to ensure equilibrium between rock and injection brine. The concentrations of various ions ($Ca^{+2}$, $Mg^{+2}$, $Na^{+}$, $K^{+}$) in the effluent were measured using the ICP (Figure 2.8). During brine injection, after 5.2 PV was injected, the temperature of the core was raised to the target temperature of 45 $^{o}$C. Note that as the temperature is increased the equilibrium is disturbed. At the end of this phase $Na^{+}$ and $Mg^{+2}$ are at the injectant concentration level. The $K^{+}$ and $Ca^{+2}$ are still somewhat above their injected concertation indicating the dissolution of the cations from the rock minerals.

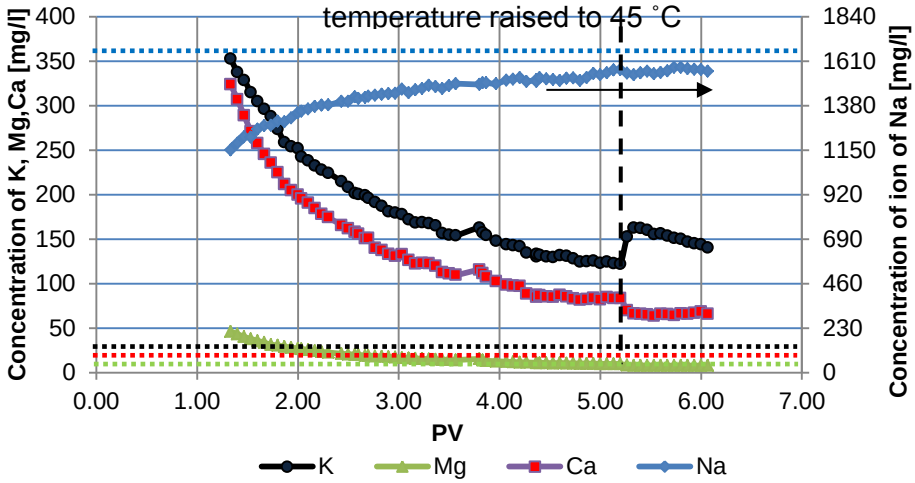


**Figure 2.8** – ICP analysis of the effluent during the brine injection. The dashed lines indicate the concentration of the various ions in the injectant

For the permeability test 6 different flow rates were employed yielding an estimate of $2.15 \cdot 10^{-12}$ $m^2$.

### Initial tracer test

In order to determine the effective pore volume of the core as well as the dispersion coefficient, 20 ppm of potassium iodide was dissolved in the brine, and injected at 0.12 ml/min (~1 ft/day). The tracer concentration in the effluent was determined using a DR 6000™ UV-VIS Spectrophotometer set at a wavelength of 226 nm. The results are plotted in Figure 2.9. The tracer test was interpreted by fitting the analytical 1D convection-dispersion solution (equation 2.2) through the data points (Marle 1981; Lake 1996) using an $L_2$-norm.

$$C_D = \frac{1}{2}\operatorname{erfc}\left(\frac{1-t_D}{2\sqrt{\frac{t_D}{N_{Pe}}}}\right) + \frac{1}{2}\exp(N_{Pe})\operatorname{erfc}\left(\frac{1+t_D}{2\sqrt{\frac{t_D}{N_{Pe}}}}\right) \qquad (2.2)$$

where $C_D = \frac{C-C_I}{C_J-C_I}$ [-]- dimensionless concentration, $C_I$ [-]- initial concentration, $C_J$ [-]- injection concentration, $L$ [m]-core length, $N_{Pe} = \frac{uL}{\phi D}$ [-] - Peclet number, $D$[$m^2$/s]- dispersion coefficient, $t_D = \int_0^t \frac{q\,dt}{V_p}$ [-]- dimensionless time of PV injected, $u$ [m/s]-

Darcy velocity, q[$m^3$/s]- flow rate, t [s]-time, $V_p$ [$m^3$] - accessible pore volume, $x_D = \frac{x}{L}$ [-] - dimensionless distance, $\phi$ [-] - porosity.

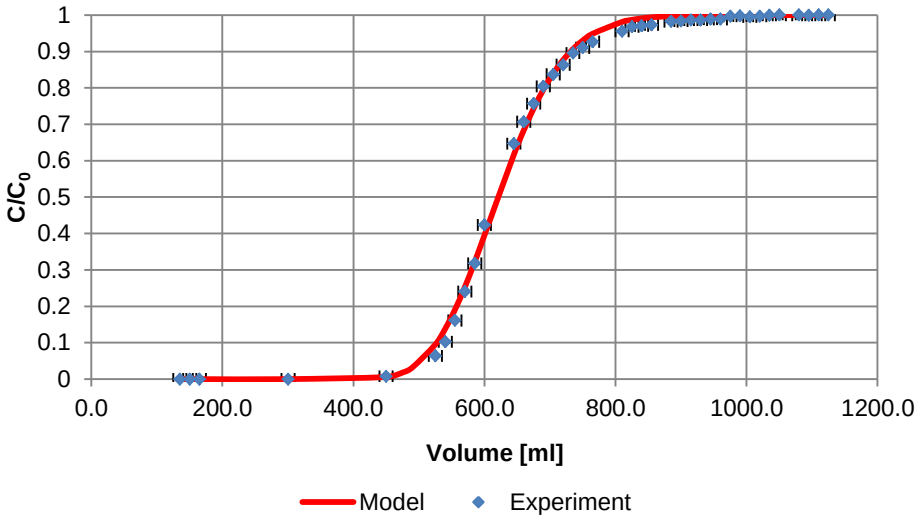


**Figure 2.9**- Initial tracer profile with model fit

The data match yielded an effective pore volume of 636 $\pm$ 20 [ml] (porosity 31.8±1 %) and a dispersion coefficient of 2.5 ± 0.6 •$10^{-4}$ [$cm^2$/s] ($N_{Pe}$= 127$\pm$40).

### Injection of the polymer into the core

After 17.6 PV of brine was injected, we switched to the polymer solution and started to saturate the rock surface. ICP analysis of the effluent showed that the $Ca^{+2}$ and $Mg^{+2}$ concentrations did not change significantly during this phase of the experiments (Figure 2.10). That might be explained by the interaction of the injectant with the rock surface which can favor the dissolution of $Ca^{+2}$ and $Mg^{+2}$. This may lead to the high concentration of the ions in the produced fluid. The $Na^+$ concentration dropped to the injection value after 2 PV injected. The $K^+$ concentration reduced to the value which is slightly above the injectant concentration after 2 PV.

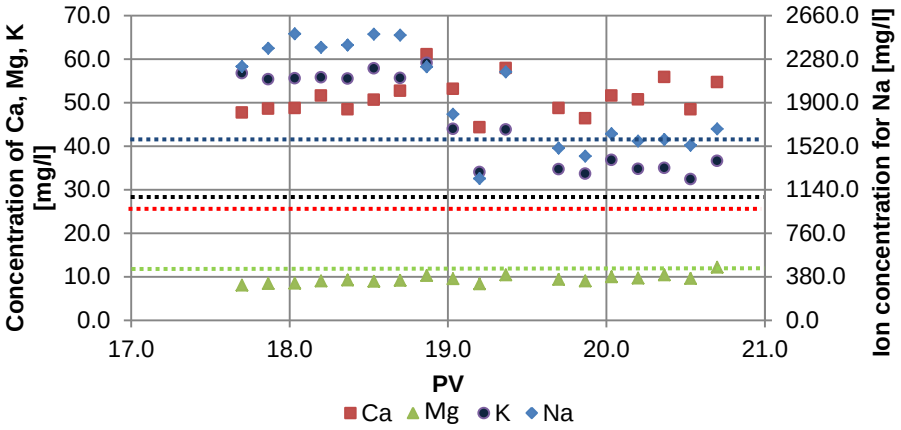


**Figure 2.10** – ICP analysis of the effluent during the polymer injection. The dashed lines indicate the injectant values

Subsequently the tracer test was repeated. The fluid collected during this step contains the polymer and the tracer in the same testing tubes. In order to avoid interference of the polymer with the tracer analysis, the effluent was diluted by a factor of more than 50. Consequently a significantly higher injected KI concentration (1000 ppm) was required. Figure 2.11 shows the results of the tracer test together with the initial tracer test as well as both model fits. The analysis shows an effective pore volume of 660 $\pm$ 30 [ml] (porosity = 33$\pm$3 %) and a dispersion coefficient of 2.7 $\pm$ 1.8 $\bullet 10^{-4}$ [cm$^2$/s] ($N_{Pe}$= 133$\pm$46). The results are statistically not very different from the initial tracer test, indicating that the pore morphology has not been significantly altered.

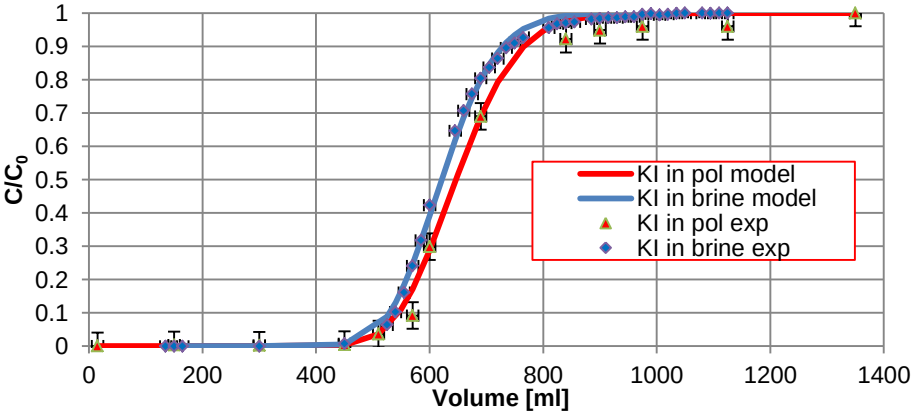


**Figure 2.11**- Tracer concentration in the effluent during brine and polymer injection, including the model fits

**XL polymer injection into the core**

With the core now fully prepared we injected a 0.5 PV slug of the XL polymer at a flow rate of 1 ml/min (reproducing the conditions in the near well bore region). The XL polymer slug was pushed further into the core by a 0.1 PV polymer only slug (Figure 2.12).

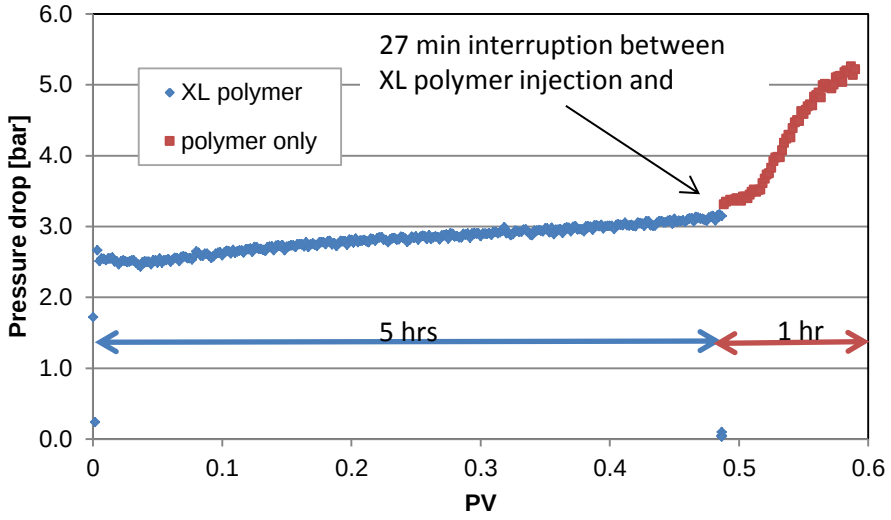


**Figure 2.12** – The pressure drop recorded during XL polymer injection and the polymer follow-up at 1 ml/min.

During the XL polymer injection, only a modest pressure increase took place. However during the short polymer chase the pressure drop built up quickly, indicating that cross-linking started to have an effect. This happened much faster than expected from the bulk results. Subsequently we shut the core in to allow the cross-linker to do its work. The absence of the shear stimulates the growth of cross-linked agglomerates which block the core. At various intervals we briefly flow the polymer solution through the core at a rate of 0.12 ml/min to assess the change in mobility (Figure 2.13). The mobility reduction increases almost linearly the first 400 hours to roughly a factor of 7.5[1] measured over the core compared to the XL-free polymer. After this it appears to stabilize suggesting that no more cross linker is available.

[1] For XL-free polymer injection at a 0.12 mL/min flow rate, a pressure drop of 0.56 [bar] was measured, corresponding with an in situ viscosity of 1.2 *$10^2$ [mPa·s].

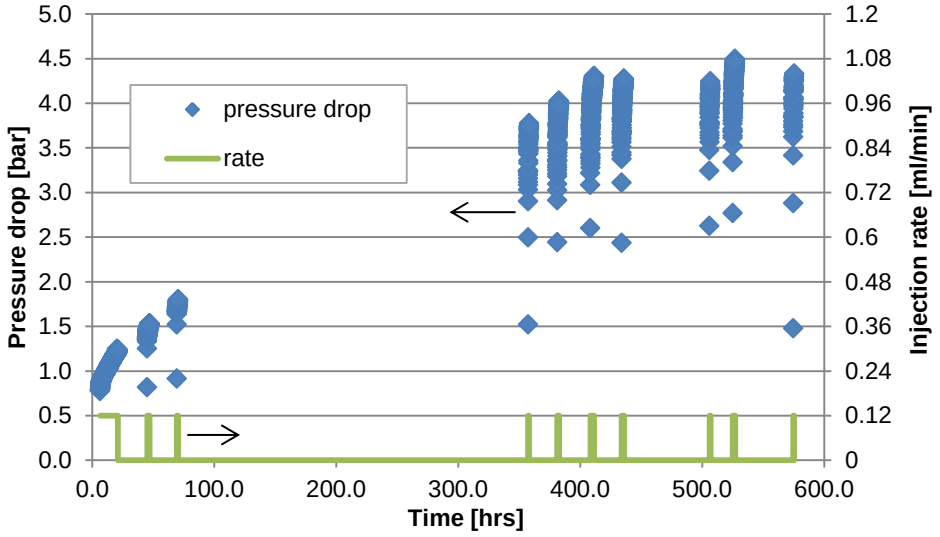


**Figure 2.13** – Several brief intervals of polymer injection probe the changing mobility reduction in the core

## Effect of cross-linking in porous media

Despite the effective delay of the crosslinking in bulk, the results of the core flood experiment show that the increase in the pressure drop is observed within hours from the beginning of the XL polymer injection (Figures 2.12 and 2.13). The overall bulk viscosity initially is not considerably affected by the creation of small aggregates. However as they grow over time interactions between the aggregates start to sharply increase the viscosity (McCool et al. 1991; Todd et al. 1993). In order to connect this to the porous media viscosity, a series of filtration tests was carried out using isopore filters with an average pore size of 1.2 µm, 5 µm and 10 µm respectively. The size of the pores in a filter influences the resistivity towards the flow of the Xl polymer. The smaller the size of the pores, the higher the resistivity and the time it takes to filter the fluid. During the cross-linking process, the size of colloid particles increases and they block the pores of the filter. For example, it took 5.3 hrs to filter 50 g of the crosslinking polymer through a 1.2 µm filter after 22.5 hrs of aging, whereas it took 19 min to filter 80 g of the crosslinking polymer through a 5 µm filter. Thus, to optimize the time of the filtration ratio tests, we adjusted the volumes of the fluids. In our study, the filtration tests were carried out to filter 180 g of the fluid through a 10 µm filter; 80 g through 5 µm and 50 g through

1.2 µm. After the aging of the cross-linking polymer, an injection of the polymer through different filters is repeated again. Eventually, a set of tests was collected to plot a graph which represents the time of the filtration tests at different aging times.

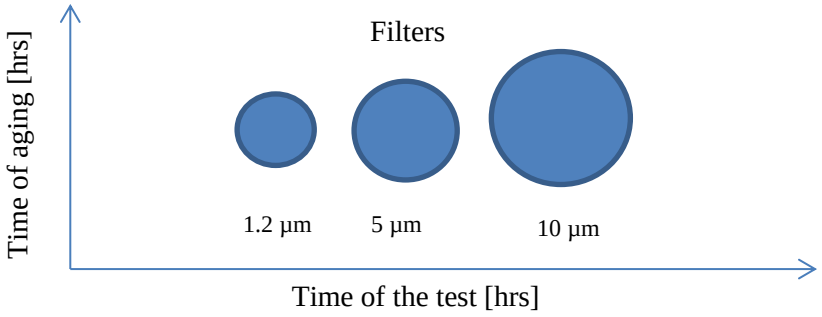


**Figure 2.14**- Workflow of the filtration test

The filtration test experiments show that filters get plugged earlier than gelation is observed in bulk (Figure 2.15). The smaller the size of the filter, the earlier it gets plugged by the cross-linked agglomerates. As an example, after 46.5 hours of aging, the XL polymer hardly flows through the 1.2 µm filter. The test was aborted after 10 hours and the results extrapolated. To obtain a conservative estimate we used linear extrapolation of the data resulting in 17.5 hours. Using a power law extrapolation instead would have yielded 55 hours.

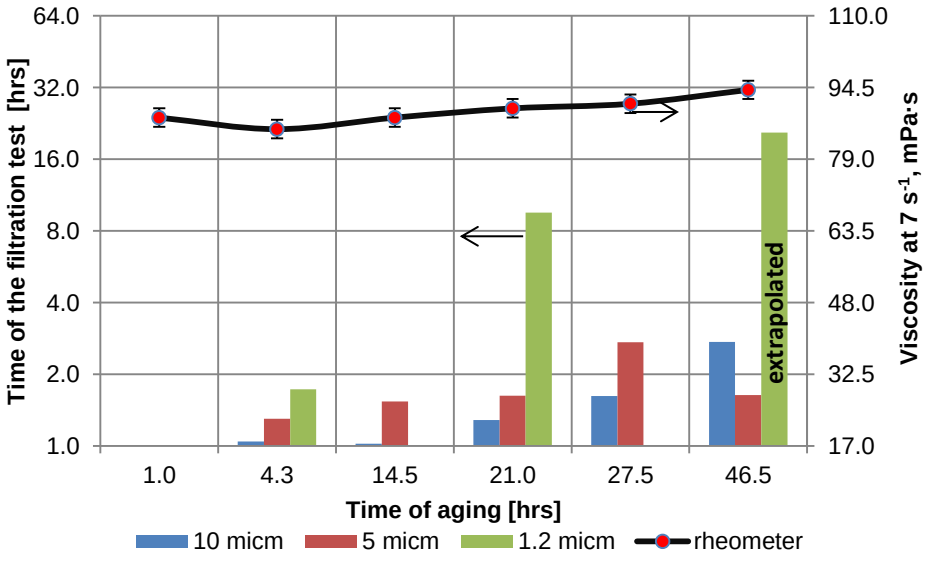


**Figure 2.15**- Combined filtration and rheology tests for the XL polymer

Figure 2.15 shows that the increase of the time of the filtration test within the period of aging from 5 hrs to 22.5 hrs is 5.5 times for 1.2 μm filter and 1.25 times for 5 μm. However, the increase of the bulk viscosity (Figure 2.6) for that period of the experiment is negligible and is within the error margin. It is indicated that the time of filtration ratio tests does not have a steady increase over the aging time. That can be explained by the stochastic nature of the particles formation. Therefore, every time when a sample of the cross-linking polymer is taken for the analysis, different size distributions of the particles is presented in the sample. Despite the possible differences in the size distribution of the cross-linked particles, the general trend of the filtration time increase over aging time is observed. This indicates that particles grow steadily over time.

From the presented results it is clear that cross-linked agglomerates affect the viscosity earlier in a porous media as size exclusion occurs. The absence of the shear stimulates the growth of agglomerates which block the core.

The modest increase in pressure during the initial stage of the XL polymer injection can be explained by the formation of gel aggregates as well. The evidence for this hypothesis is illustrated in the filtration test. Indeed, according to Figure 2.15, after 5 hours of aging, the time of the filtration test increased by 1.7 times (1.2 μm filter).

### Tracer test after XL polymer injection

The pressure drop displayed above confirms that crosslinking occurred in the core. To assess the associated changes in pore morphology we again ran a tracer test. This time we injected brine with HPAM and KI (1000 ppm) for 0.95 PV followed by 1 PV without the tracer (Figure 2.16, red squares). As is clearly evident from Figure 2.16 (compared to Figure 2.11), breakthrough happens significantly faster. The model match (blue line) yields the following estimates: effective pore volume of 534 ± 12 [ml] (porosity = 26.8±1.3) and a dispersion coefficient of 56 ± 11 $\bullet 10^{-4}$ [$cm^2/s$] ($N_{Pe}$= 6.3±1.6). Because the tracer-slug size was too small to approach the injection concentration in the effluent, the analytical model was extended by superposition.

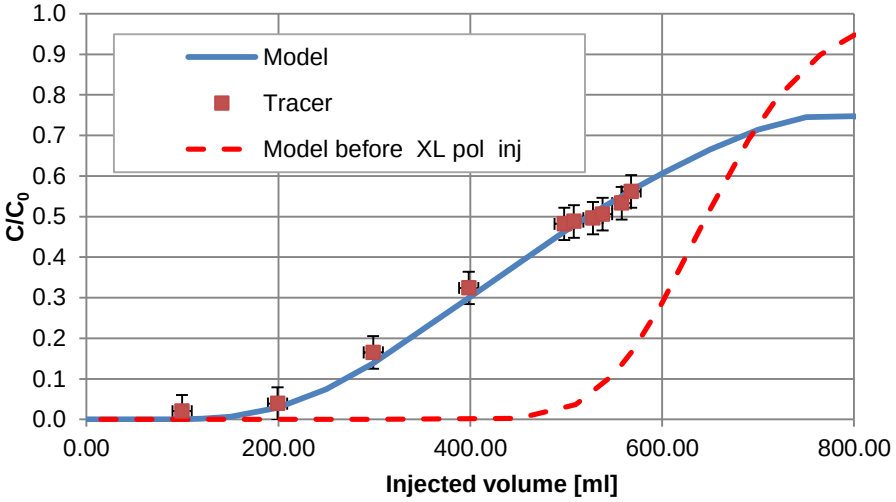


**Figure 2.16 -** Tracer data after XL polymer injection

The tracer test indicates a 6.2 % reduction of effective porosity and a 20 times larger dispersion coefficient.

## Distribution of the polymer in the core

As shown by the tracer test, the flow characteristics of the core are significantly altered by the cross-linked polymer. In order to determine its in situ distribution several small plugs were drilled from the outlet section of the 1m core (40 x 10 mm) and scanned using a micro-CT. Subsequently we immersed the plugs in NaClO for 7 days, in an attempt to remove the cross-linked polymer, and scanned them again. Figure 2.17 shows the grey value histogram before (A) (with XL polymer), after (B) (without XL polymer) and the clean sample of the Boise outcrop (C) respectively. The high density peak (normalised grey value ≥4500) indicates rock whereas the low density peak represents pore space. There is a clear expression of a medium density area indicated by the yellow band in Figure 2.17A that is noticeably absent after the NaClO flush (Figure 2.17B). This suggests that it corresponds to the XL polymer. It is also important to notice that the histogram of grey value distribution for the clean sample (C) is similar to the histogram for the sample treated with NaClO (B).

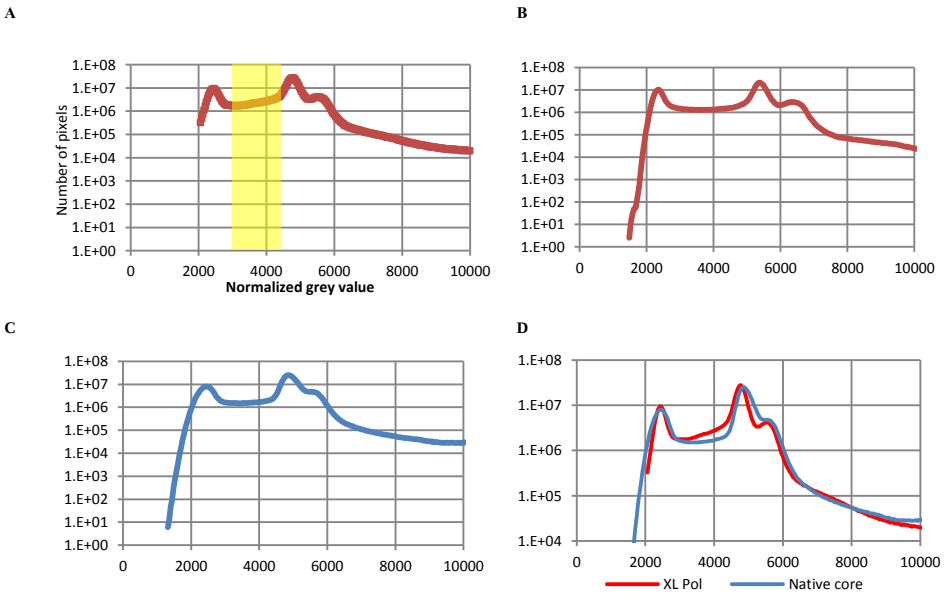


**Figure 2.17-** Grey value histograms of core plugs: A- sample containing XL polymer; B - the same sample treated with NaClO; C- native Boise core; D-Combined histograms of A and C

Reconstruction of the initial micro-CT scan with the segmentation (high – rock, medium – XL polymer and low density – porosity) suggested above yields a 3D image of the plug (Figure 2.18).

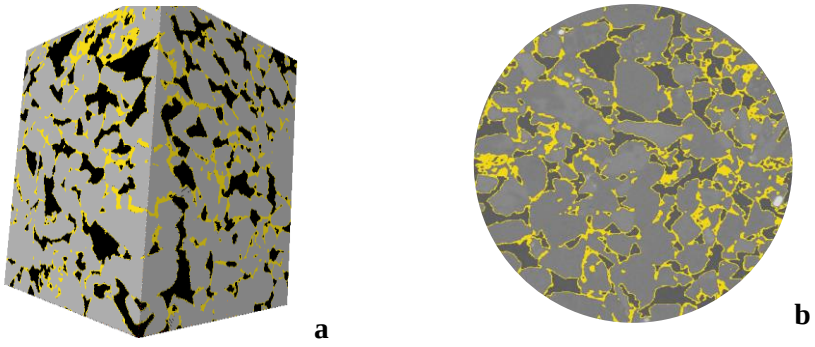


**Figure 2.18-** a) 3D reconstruction and b) 2D slice of the plug showing the pore space as black and XL polymer in yellow

As can be seen from these images, many of the smaller pores are filled with XL polymer. Calculation of the volumes corresponding to different grey

intensities was done using the Multi-Tresholding and Label analysis modules of Avizo (Avizo User's Guide 2015) (Table 2.4).

**Table 2.4-** Results of the image analysis

| | |
|---|---|
| Absolute porosity,% | 31.9 |
| Fraction of the XL polymer,% | 6.1 |
| Porosity alteration after the treatment with the XL polymer,% | 25.8 |

From the calculated data (Table 2.4) we can see that due to the treatment of the core with the XL polymer, porosity was reduced from 32 % to 25.8 % which is in reasonable agreement with the tracer data from the full core experiment. This lends credence to the segmentation choices outlined above.

The blockage of the smaller pores by the XL polymer is also confirmed with pore size distribution in the Boise core before and after the injection of the XL polymer (Figure 21). From the analysis of the pore size distribution it is clear that the XL polymer blocks mostly pores within the range from 0 to 25 µm, whereas bigger pores from 25 to 30 µm stays unaffected.

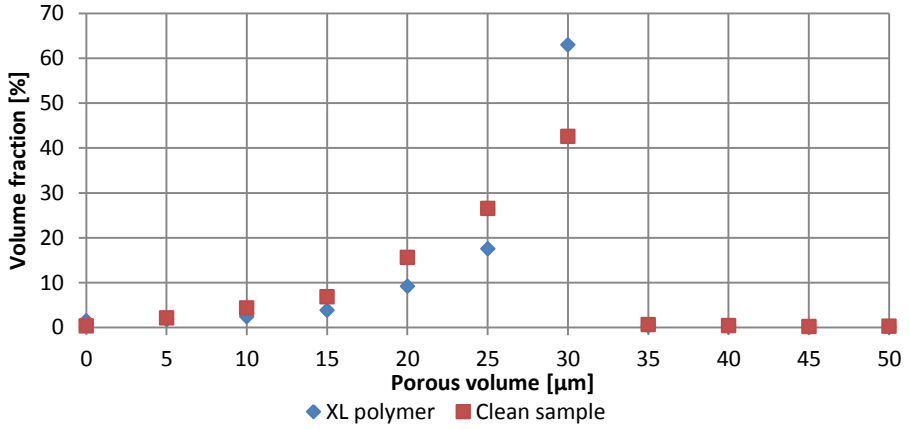


**Figure 2.19**- Pore size distribution of the Boise core before and after the injection of the XL polymer

## 2.4. Conclusions

In addition to studying the cross-linking process in bulk, we demonstrated its behavior at the core scale (1 m length) as well as on the pore scale. The gelation time in bulk suggested that the PEC could effectively delay the time of the crosslinking even at high brine mineralization. However the delay experienced in the core flood experiment was much shorter. The early increase of the differential pressure observed in the core flood experiment can be explained by the mechanical entrapment of formed gel particles. The filtration test showed that the growth of the particles is observed over time. This suggests that bulk gelation experiments may not be relevant for use in porous media. Filtration tests offer a much more useful alternative to the conventional bulk gelation tests. Tracer tests demonstrated that the XL polymer reduced the pore volume by roughly 6 % (in absolute terms). The micro-CT images showed that most of the XL polymer was retained in the smaller pores of the core. The large increase in the dispersion coefficient suggests that this must have resulted in the creation of a few dominant flow paths isolated from each other by the closure of the smaller pores.

# Chapter 3

## Nano-Spheres for Conformance Control. The Characterisation of the Size and Swelling Kinetics of Co-Polymer Nano-Spheres Extracted From an Emulsion

A nano-spheres suspension can be an alternative to cross-linking polymer for in-depth diversion in heterogeneous reservoirs. The small size of individual spheres makes the propagation of the suspension potentially viable. However, the propagation of the spheres is highly dependent on the swelling and agglomeration rates which can be experimentally estimated by the measurement of the size of spheres over time. Since the spheres are synthesized via an inverse emulsion polymerisation method and later are diluted in the brine for practical application, the study of the swelling and agglomeration rates is difficult due to the oil droplets in the oil in water (O/W) emulsion.

In this chapter we first describe the procedure for the separation of the spheres from the emulsion with acetone. Several washing steps are proposed with the subsequent drying of particles under vacuum. The obtained powder is later dispersed in the brine and treated with ultrasound to get a well dispersed suspension of nano-spheres. The high efficiency of the procedure is confirmed with transmission electron microscopy (TEM) and dynamic light scattering (DLS). This procedure can be adapted for a variety of acrylamide based polymers initially diluted in the emulsion.

The swelling rate of nano-spheres separated from the emulsion is studied with TEM and DLS. A procedure for the study of agglomeration and swelling rates with TEM is designed. Next, TEM results are compared against DLS results. It is demonstrated that the size distribution for agglomerates (clusters) of particles match well with the size distribution obtained from DLS. Hence, less time consuming DLS tests can be used for the sufficiently accurate estimation of the size of nano-spheres in the future.

The prediction of the size of spheres over time is done with a population balance model. The results of calculations show that agglomerates of spheres might lead to large scale blockages within months of starting the injection. This approach helps to understand how well the spheres can propagate in the reservoir over time.

## 3.1. Introduction

The practical application of nano-spheres is broad. They can be used in enhanced oil recovery technologies (Randy et al., 2015), drug-delivery systems (Farooqi, 2015) and templates for nanomaterials (Farooqi, 2015). In our work the nano-spheres are considered as a candidate for the improvement of oil recovery in heterogeneous reservoirs. When they are injected into a reservoir, due to their initially small size (~100 nm), they can initially propagate in higher permeable layers to a target zone. During flow in porous media, retention can occur due to the swelling and agglomeration of the spheres. Therefore, the study of the size and kinetics of the swelling of nano-spheres is important for its practical application.

Copolymer nano-spheres are synthesised using an inverse emulsion polymerisation method (Barari, 2011). The resulting particles are co-polymer networks which are able to swell over time when they are in contact with a good solvent (Saunders et al. 1999; Lietor-Santos et al. 2001; Rubinstein and Colby, 2003; Barari, 2011; Farooqi, 2015). The size of particles determines their propagation in porous media and has to be studied prior to the injection into a reservoir. However, since nano-spheres are initially dispersed in the emulsion, the study of their size is difficult due to the presence of oil droplets in the aqueous phase. Therefore, it is important to design a procedure to separate spheres from oil droplets.

One of the main components of the spheres is polyacrylamide (Barari, 2011). Polyacrylamide precipitates when it is in contact with a poor solvent (Stahl and Schulz, 1988), providing a mechanism for the separation of nano-spheres from the emulsion. In our work, we designed a detailed procedure for the nano-spheres separation from the oil including solvent type, washing steps, and mixing procedure. The effectiveness of the procedure was proven through size measurement tests.

After the spheres were extracted according to the designed procedure, the average size, swelling and agglomeration rates were determined. Finally, the

size distribution curves were matched against a population balance model that allows us to predict the size distribution evolution over time.

## 3.2. Literature overview

Generally, the kinetics of the swelling is slow and is governed by the level of crosslinking in the spheres, their internal structure, pH, ionic strength and the solvent composition (Figure 3.1, Fernandez-Nieves et al., 2011). The swelling process is largely reversible (Saunders, et al.,1999; Rubinstein and Colby, 2003). In the case of nano-spheres, the swelling time might be up to 2 weeks. After 2 weeks of aging, it is expected that particles keep their size and do not completely dissolve in the solvent as the polymer-polymer interaction is stronger than the polymer-solvent interaction.

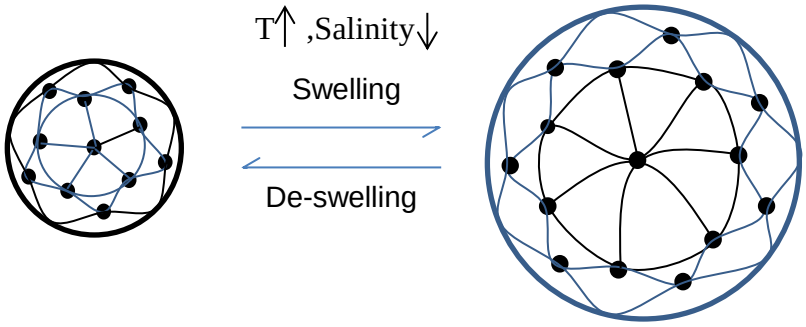


**Figure 3.1**- Swelling of a nano-sphere

According to Fernandez-Nieves et al. (2011), Shibayama and Tanaka (1993), there are three intermolecular forces which govern the swelling of crosslinked micro gels: van der Waals, hydrogen bonding and electrostatic interactions.

Van der Waals forces become active when the interaction between multiple interconnected monomers of the cross-linked particles takes place (Fernandez-Nieves et al., 2011). Depending on the solvent composition, there is always the influence of attractive and repulsive forces on a pair of interacting monomers. Swelling of the particles can happen due to this interaction.

As it was stated previously, the swelling of the polymeric particles may also be dependent on hydrogen bonding . It can be defined as an attractive interaction between fixed dipoles. If this interaction does take place in a

polymeric gel particle, then with an increase of the temperature, the particle may swell back due to weakening of hydrogen bonds (Giussi, J.M. et al., 2015).

The swelling of particles might also occur due to the imbalance between the ions distribution inside and outside of a particle. The difference in the distribution contributes to the osmotic pressure which has an effect on the swelling (Fernandez-Nieves et al., 2011).

Another important characteristic of nano- and micro- gels is their colloidal stability (Saunders, et al., 1999; Farooqi, et al., 2013). It is determined by the interaction of particles with each other and can be attractive or repulsive (Vincent and Saunders, 2011) (Figure 3.2). Long range interaction between particles comprises of van der Waals attraction and electrostatic repulsion if particles have a charge.

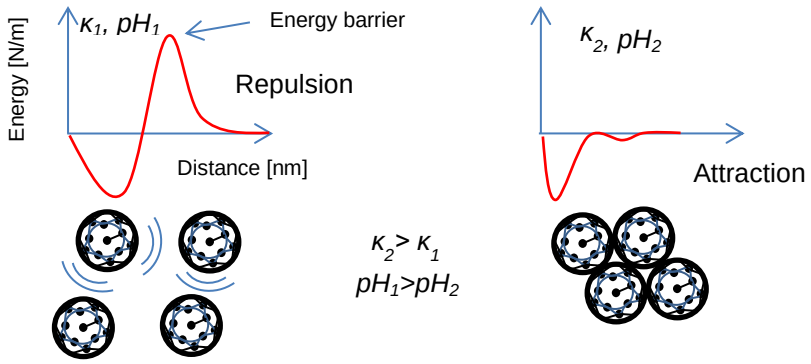


**Figure 3.2**- Interaction between particles according to repulsion-attraction forces (*inspired by* Zenamarkos and Bacchin, 2016 ): $\kappa$ electrolyte concentration; pH- potential of hydrogen.

Depending on how swollen the particles are the interaction can be different. If the particles are swollen, the van der Waals forces are negligible and the suspension is stable.

Electrostatic interaction between micro gel particles mostly occurs due to charged groups on the surface of the particles (Vincent and Saunders, 2011). Polyelectrolytes (e.g. polyacrylic acid), which are included as monomers into the structure of the micro gel particles, can induce fluctuation, by bridging, or provide electrostatic stabilization (Denton, 2003). The type of the interaction depends on the concentration of the polyelectrolyte and the method of attaching the PE to the surface of the particle (adsorption or grafting). Fluctuation

between charged micro gel particles can be enhanced if the electrostatic interaction is screened by counter ions (Denton, 2003).

Temperature influences the stability of micro gels as well (Farooqi, et al., 2013). Colloidal stability tests with poly-N-isopropylacrylamide-co-acrylic acid showed that the increase in temperature, salt concentration and decrease in pH results in aggregation of micro gels due to the increase of polymer–polymer interaction.

The monitoring of the size of nano-particles and micro gels in particular can be done by a variety of methods. The selection of methods for the size measurement is determined by the chemical composition of the particles and the objectives of the experiments. However, the measurement of the size of nano-particles is a difficult problem and there is no ubiquitous method for the size characterisation (Domingos, et al., 2009). The methods for particles characterisation can be divided into two main groups: indirect and direct.

One of the most common indirect tests for the acquisition of the hydrodynamic size of particles and size distribution is dynamic light scattering or photon correlation spectroscopy (Zetasizer Manual, 2004; Li, et al., 2014; Bantz, et al.,2014). The advantage of using DLS is that each single measurement is fast and it gives a hydrodynamic radius of particles and their size distribution in a solvent. Moreover, there is a possibility to obtain the size distribution at different temperatures. However, the mechanism behind the particle growth (swelling vs aggregation) remains unclear, since DLS does not visualise individual particles.

The main principle of the instrument is based on the relation between the size of particles, which move in a solvent due to the Brownian motion, and their speed according to the Stokes-Einstein equation. A sample is illuminated with a laser and the particles will scatter the light towards the detector. The motion of particles causes a fluctuation of the intensity of the scattered light. One of the disadvantages of DLS is a possible masking of the scattered light by dust particles or clusters of particles.

Direct methods, such as electron (TEM, cryo-TEM, and SEM) or optical microscopy methods can visualise the shape of particles on a substrate (Saunders, et al., 1999; Vincent and Saunders, 2011).

The main advantage of EM is its high resolution allowing direct imaging of individual particles (Pyrz et al., 2008). Additionally, agglomeration and swelling of the particles can be assessed by the comparison of multiple images

together which are taken over different time intervals using a statistical analysis. The disadvantages of EM are time consuming tests, high operational costs and the lack of reproducibility of specimen preparation. In the case of TEM applied in our study, samples for the analysis have to be dried in a vacuum (Pyrz, et al., 2008; Bantz, et al., 2014). When micro gels are dried, they can lose some solvent content and shrink.

Some of the experiments conducted with the SEM to visualize micro gels showed that the particles in the swollen state after evaporation of the solvent can be flattened (Saunders and Vincent, 1997). However, particles keep the original round shape when they are in the un-swollen state.

Another direct visualisation method that can be used for the estimation of the nano-particle sizes is dark-field microscopy (CytoViva Optical Microscope User Manual; Bayles, et al., 2016). However, the images of nano-particles are blurred which does not allow for the measurements of their diameter with an acceptable accuracy. Hence, instead of the calculation of the area of particles depicted in the microscope, trajectories of particles moving in a solvent due to Brownian motion are recorded. The recorded trajectories allow the estimation of the particle diffusion coefficients. Subsequently, the diameter can be calculated using the Stokes-Einstein equation (Savin, 2008; Giavazzi et al., 2016). The advantage of this technique compared to DLS is the robustness of the measurements of concentrated and heterogeneous samples (Bayles, et al., 2016). Contrary to TEM, dark field microscopy allows keeping the nano-particles in a solvent. This reduces the time to prepare the samples and avoids the de-hydration issues mentioned above.

Despite their drawbacks, the most commonly used methods remain TEM and DLS. All listed methods have their pros and cons and only the combination of methods can provide a robust characterisation of the nano-spheres (size distribution, agglomeration and swelling rates).

## 3.3. Experimental material and procedures

### The separation of the nano-spheres from the emulsion and the sample preparation

The polymeric nano-spheres studied in this work are synthesized using an inverse emulsion polymerization method. A mixture of monomers such as acrylamide and derivatives of acrylamide are reacted with an organic cross

linker to create copolymer spheres. The spheres are dispersed in an emulsion containing a mineral oil and a surfactant which are used for the synthesis of the spheres (Figure 3.3). Before the size distribution of the nano-spheres is determined, the spheres are separated from the emulsion by applying a specially designed procedure (Table 3.1). According to that procedure, the emulsion, containing spheres, is washed 4 times with acetone to separate polymeric spheres from the mineral oil (Figure 3.4). Acetone is a poor solvent for our polymers (Rubinstein, et al., 2003) causing them to precipitate. Subsequently we dry the precipitated polymer at 30 ˚C in a vacuum for 24 hrs after which we gently crumble it into small pieces (Figure 3.5). The mass of the extracted polymer accounts for 30 % of the total mass of the suspo-emulsion. The dried polymeric particles are later re-dispersed into a brine (Figure 3.6, Table 3.2). The diffusion speed of particles into the brine depends on the temperature, the size of clusters of particles, the interaction between particles and the brine salinity (Khorasani, et al. 2014). After mixing the polymeric particles for a few hours in the brine, ultrasound is applied to disperse the particles uniformly in the media (Figure 3.7).

**Table 3.1**- Procedure of the spheres extraction from the emulsion

| Action | Objective |
|---|---|
| 1. Extraction of the polymeric spheres from the suspension with acetone | To separate the mineral oil and surfactant from the sample |
| 2. Drying the particles at 30 ºC for 24 hrs in a vacuum oven. | To remove liquid droplets from the surface of the polymer particles. |
| 3. Dispersion of the particles (600 ppm) in brine with ultrasound at 80 W for 5 min. | To reintroduce the solvent (brine) |
| 4. The prepared nano-spheres suspension was stored in an oven at 30 ºC for aging. | Aging of the nano-spheres (for different time periods) to study the time evolution of the spheres size distribution |

**Table 3.2**- Brine composition

| Ions | Concentration, mg/l |
|---|---|
| NaCl | 4871.6 |
| $CaCl_2$ | 128.4 |

Prepared suspensions of nano-spheres (Figure 3.8) were tested by means of DLS, TEM and dark field microscopy to characterise the size distribution of the spheres and its change over time.

**Figure 3.3**- Emulsion containing the spheres

**Figure 3.4**- Separation of the spheres from mineral oil with acetone

**Figure 3.5**- Extracted powder of the spheres

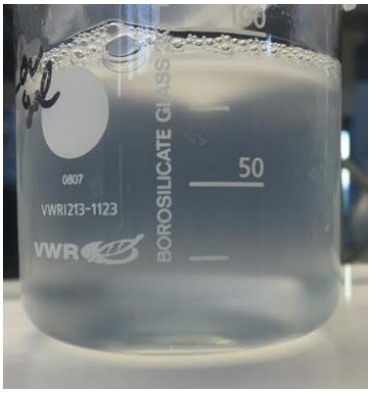


**Figure 3.6**- Suspension of the spheres

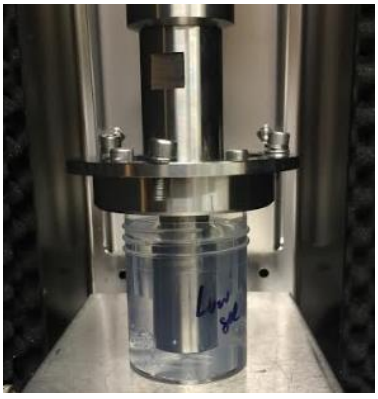

**Figure 3.7**- Treatment of the suspension with ultrasound

**Figure 3.8**- Purified suspension

### Characterisation of the nano-spheres using dynamic light scattering

A Zetasizer Nano instrument (Zetasizer Nano Series User Manual, 2004) was used to analyse the average size and the size distribution of the nano-spheres over time at the constant temperature of 25 ºC. The concentration of the spheres in samples was 600 ppm which is the recommended concentration for the application in practise. Aging of samples for the analysis was done in an oven at 25 ºC.

Tests were carried out using transparent disposable cuvettes which can store approximately 1 ml of the fluid each. Brine was selected as a dispersant (or solvent) with the refractive index (RI) of 1.33. Nano-spheres are defined for the instrument as polyacrylamide particles with the RI of 1.45.

### Characterisation of the nano-spheres using electronic microscopy

In addition to DLS, the size of the nano-spheres was studied using transmission electron microscopy (TEM). The advantage of this technique is that it directly visualises nano-particles (Pyrz, et al. 2008; Williams and Carter, 2009). As a result of the interaction between electrons and the specimen, high resolution images are obtained. They can be used to assess the relative impact of swelling and aggregation on the nano-spheres growth. The extracted nano-spheres were dispersed in the brine (table 3.2) at a concentration of 600 ppm. Subsequently they were divided in 3 samples that were aged for 48, 144 and 480 hrs respectively. The preparation procedure designed for the TEM experiments is listed in (table 3.3).

**Table 3.3-** Procedure of the sample preparation with the negative staining for TEM

| Name of steps | Action |
|---|---|
| 1. Preparation of a grid for the microscope. | Coating of a copper grid (100 mesh) with pioloform and carbon. Subsequently it was made hydrophilic by glow-discharging for 30 s with a current of 20 mA. |
| 2.Placing a sample on the grid. | A droplet of 3 µl of the nano-particle suspension was kept on the grid for 1 minute. Next, the excess suspension on the grid is absorbed by filter paper (Whatman #1). That is followed by staining for 1 minute on a droplet of distilled water containing 2.3% aranyl acetate. The excess of the staining solution was absorbed after which the grid was air-dried. |

The negatively stained specimens were examined with a Tecnai 12 Biotwin transmission electron microscope (FEI, The Netherlands), equipped with a lanthanum hexaboride (LaB6) source operated at an acceleration voltage of 120 keV. The specimens were imaged in focus and a series of images with binning 2 were recorded on a 4kx4k Eagle CCD camera. The acceleration voltage and magnification were chosen to get the best contrast between the nano-spheres and the grid. At higher acceleration voltages, a sample damage was observed. The resolution of the image is 3.4 nm/pixel. Note that, as explained above, the sample preparation procedure for TEM requires drying of the particles in a vacuum. This may cause the nano-spheres to shrink (dehydrate).

**Procedure for the analysis of the transmission electron microscopy (TEM) images (using ImageJ)**

Two dimensional images acquired with TEM have the size of 2048 by 2048 pixels. If no filter is applied, then the images are noisy and it is difficult to distinguish the particles from the background (Figure 3.9) (Pyrz at al., 2008). A Bandpass filter was applied to sharpen the edges of the objects shown on the images. The resulting image is shown in Figure 3.10.

Subsequently, the background of the image was subtracted using the rolling ball algorithm (Castle and Keller, 2007). The local background value is determined for each pixel through averaging over an area with a radius of 60 pixels (Figure 3.11). Next, the contrast of the resulting image was enhanced by 5 % and Yen's thresholding algorithm was applied (Figure 3.12). Objects with intensities lower than a cutoff value of 20 %, were defined as particles. Once thresholding has been done, the opening algorithm, which includes erosion with a subsequent dilation, is applied to binary images. This makes the objects smoother and deletes isolated pixels. Finally, watershed segmentation was applied to the images (Figures 3.13 and 3.14). Ultimately the algorithms yield the number of particles and clusters separately, as well as the corresponding cross section area of particles.

The chosen magnification limits the smallest particle size with the size no less than 5 nm because they might be recognised incorrectly using only an intensity histogram (Pyrz, et al., 2008).. Therefore, a 5 nm threshold was applied.

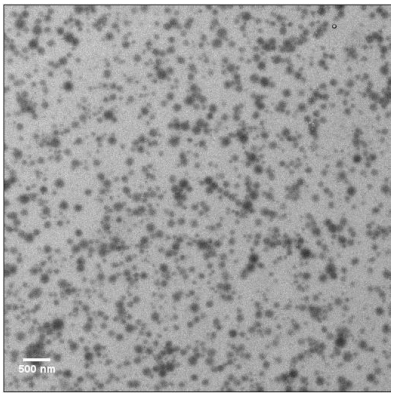


**Figure 3.9**-Initial image for the analysis

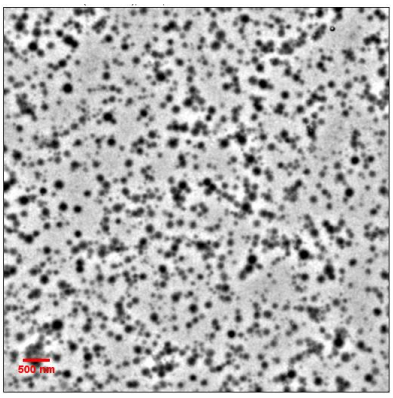


**Figure 3.10**-Image after the bandpass filter

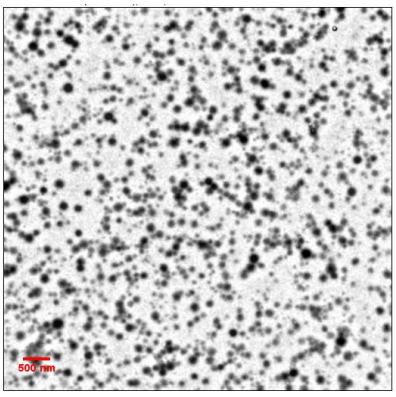


**Figure 3.11**-Image after the background was subtracted

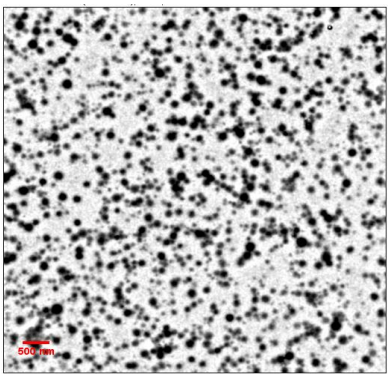


**Figure 3.12**- Image after the contrast was enhanced by 5 %

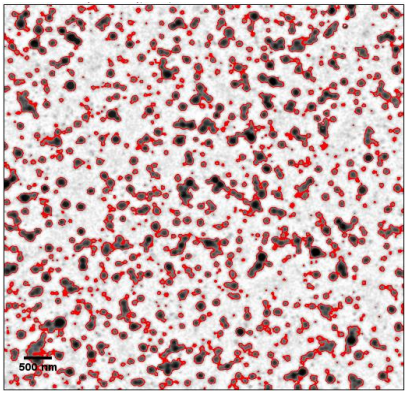


**Figure 3.13**- Thresholded image

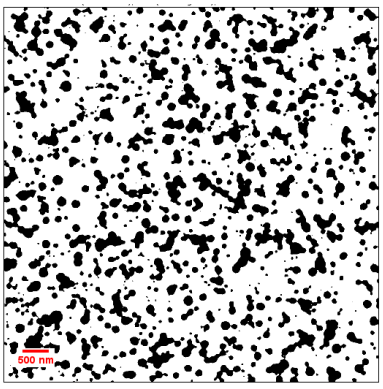


**Figure 3.14**- Binary image

In this work we used volume mean diameter D(4,3) and projected area mean diameter to describe the size distribution of nano-spheres. D(4,3) can be calculated as the sum of the product of volume fractions and particles dimeter divided by the sum of volume fractions. Projected area mean diameter is calculated as the sum of the product of projected area fractions and particles dimeter divided by the sum of area fractions. We use D(4,3) to describe the results of DLS, whereas a combination of D(4,3) and projected area mean diameter are used for the analysis of TEM results.

Initially, the algorithm for the analysis of TEM images provides projected area of nano-spheres. The obtained area of the spheres allows for reconstructing the size distribution curve according to the area. That gives the projected area mean diameter. Next, the area is converted into the volume of the spheres and the size distribution curve according to volume is plotted. From that histogram, the corresponding volume mean diameter D(4,3) is calculated.

## 3.4. Results and analysis

**The efficiency of nano-spheres separation from the emulsion according to dynamic light scattering (DLS)**

An example of a DLS test of the aged spheres in the original sample is shown in Figure 3.15. The first small peak (below 100 nm) is the expected size of the individual nano-particles. However, most of the volume is located in micrometre-plus agglomerations. This can be clearly seen in the corresponding TEM image (Figure 3.16).

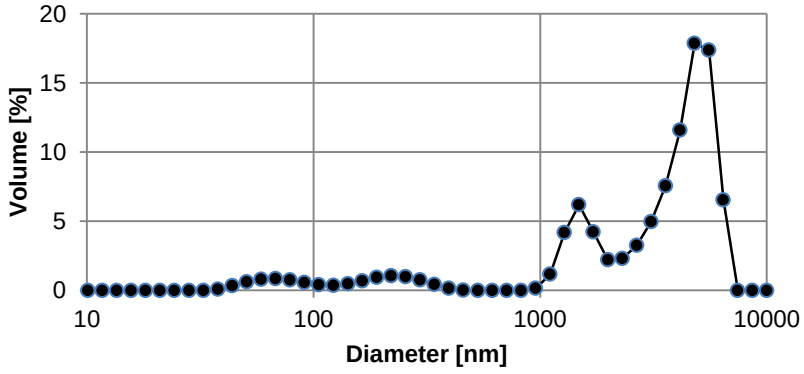


**Figure 3.15**- Size distribution of nano-spheres according to DLS

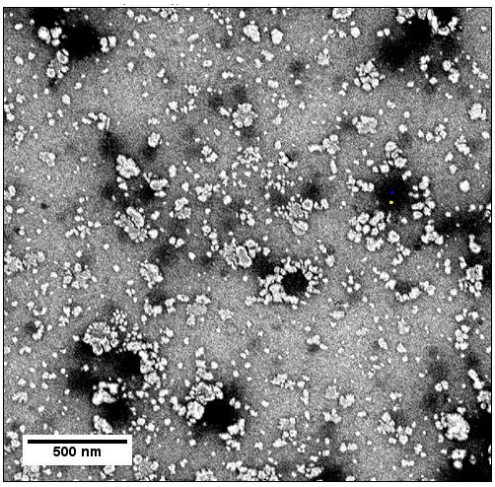


**Figure 3.16** – TEM image of the original sample: black particles are nano-spheres

The agglomerations are most likely caused by the presence of oil droplets and surfactant. In order to remove the oil, we wash the sample with acetone. Subsequently the sample is re-introduced in the DLS, which now gives the result depicted in Figure 3.17. The large aggregates have disappeared, as the dominant volume peak is now just below the 1 micrometre scale. Although the nano-particle peak (~ 38 nm) is more distinct after the acetone wash, it is clear that we still have a large volume of aggregates in the sample.

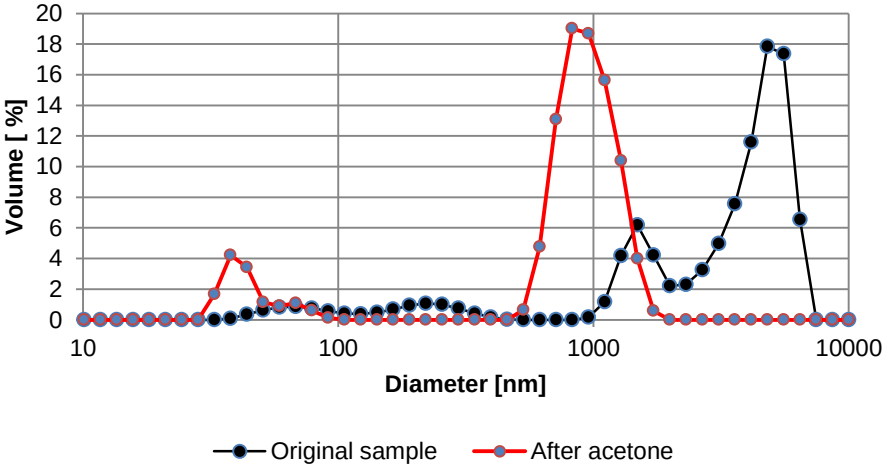


**Figure 3.17**- Size of particles after the oil was removed with acetone (brine TDS 5 g/l)

Next we expose the sample to ultrasound to break up the remaining aggregates. By the time the ultrasound was applied, nano-spheres had been mixed for 2 hrs and the DLS test resulted in the size distribution function shown in Figure 3.18. It appears that the ultrasound was successful in breaking up the large aggregates, leaving only small clusters containing a few nano-particles. The effectiveness of the sample preparation is reflected in the obtained polydispersity index which in all tests was less than 0.1 with a standard deviation of the average size of 2 nm.

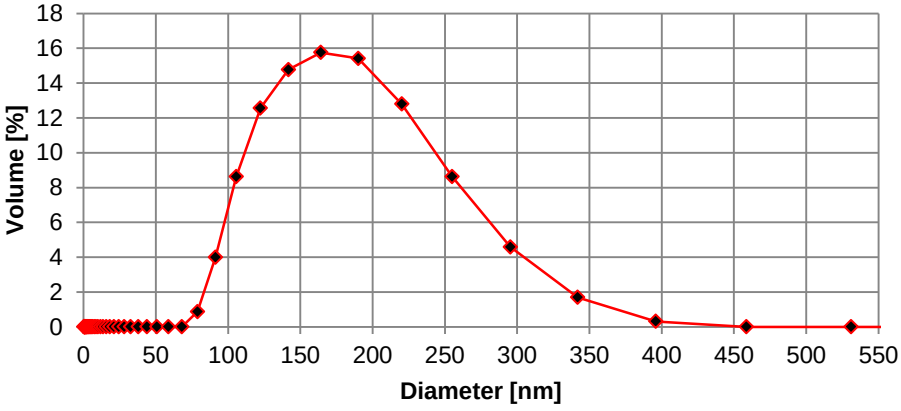


**Figure 3.18**- Size distribution of nano-spheres after ultrasound (brine 5 g/l)

Results of testes with DLS carried out for different concentrations of the spheres (100, 300 and 800 mg/l) showed that results are statistically insignificant, suggesting that our method is not sensitive to the concentration within the range explored.

**Swelling of nano-spheres according to DLS**

The size of the spheres will increase by swelling of the individual nano-spheres and by aggregation. The growth of nano-spheres prepared according to the designed procedure (table 3.1) in 5 g/l brine (table 3.2) was studied with DLS (Figure 3.19) over 1224 hrs (51 day) at 25 ˚C. According to the obtained results of the study the volume average diameter of the spheres increases. The growth of the spheres is non-linear and accounts for 18.3 % after 552 hrs (23 days) of aging from 175±2 nm to 207±2 nm. Later, the size increases slowly. Indeed, after 720 hrs of aging the change of the average size accounts for 1.9 % (1224 hrs). Most likely, on a later stage of the swelling, agglomeration is

responsible for the growth of the spheres. Additional study with TEM and optical microscope are required to reveal the mechanism behind the growth of the spheres.

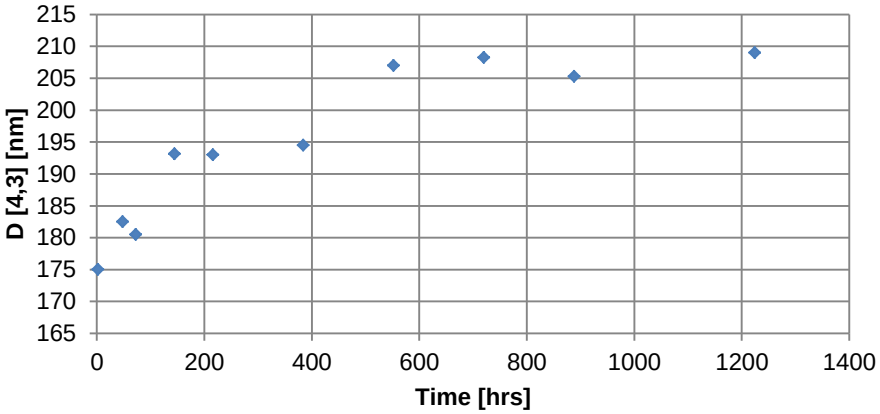


**Figure 3.19**- The growth of nano-spheres in 5 g/l brine over time according to DLS

Along with the volume average diameter of nano-spheres in the brine, the size distribution functions were plotted at different time steps over 888 hrs as well (Figure 3.20).

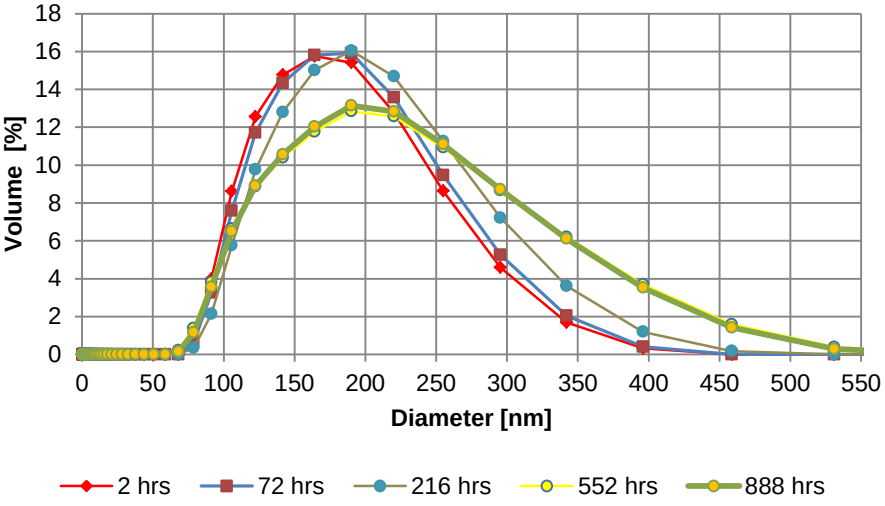


**Figure 3.20**- Size distribution of the nano-spheres obtained with DLS at different aging time steps: 2, 72, 216, 552, and 888 hrs

From the graph it can be seen that initially, after 2 hrs of aging, the size distribution is narrower than what was achieved after 552 hrs of aging. Indeed, after 552 hrs, the distribution function became wider with the increased mean diameter. Again, that indicates that the growth of the particles happens in the brine over time.

### The analysis of the TEM images

After the aging of the nano-spheres for 48, 144 and 480 hrs, their images are obtained with TEM. Eventually, we analysed 3 samples which represent every aging time. To analyse the statistics of the size distribution of the spheres, 100 images were processed with the designed image analysis algorithm. Binary images acquired in the end, show the distribution of the cluster (agglomerates) on the substrate. The distribution of individual spheres was obtained from the same binary images after their segmentation, when the clusters of the spheres were divided into individual particles.

The evolution of the size of clusters over time is shown on Figure 3.21.

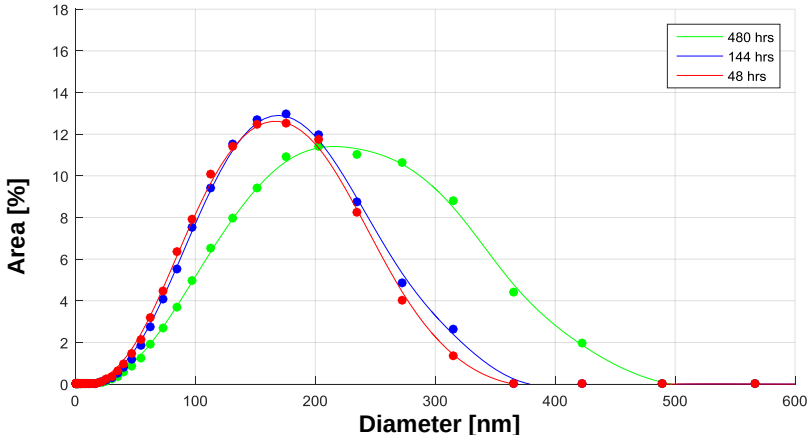


**Figure 3.21** –Size distribution of the clusters of particles over time according to their cross-sectional area obtained with TEM

From Figures 3.21 it can be seen that the projected (cross-sectional) area mean diameter for the initial distribution (48 hrs), which corresponds to 138 nm, increases to 186 nm over 432 hours later. A similar increase was observed in the DLS measurements. However, the averaged diameter for the size distribution function is higher for the DLS instrument (182.7 nm after 48 hrs) by a factor of 1.32. The difference might be explained by the disproportional influence of the size of aggregates on the scattered light in DLS system

explained by Domingos, et al., 2009. Another explanation may be the shrinkage of the spheres due to the evaporation of the solvent from the nano-spheres when samples prepared for the TEM.

Figure 3.21 also represents the volumetric distribution if the cluster observed under the TEM are disks with the thickness equal to unity (only a cross-sectional area is taken into account). Assuming they are spherical the distributions change to the those plotted in Figure 3.22. The true volumetric distribution will be somewhere in between these two representations. This is demonstrated through the comparison with the DLS data (Figure 3.23).

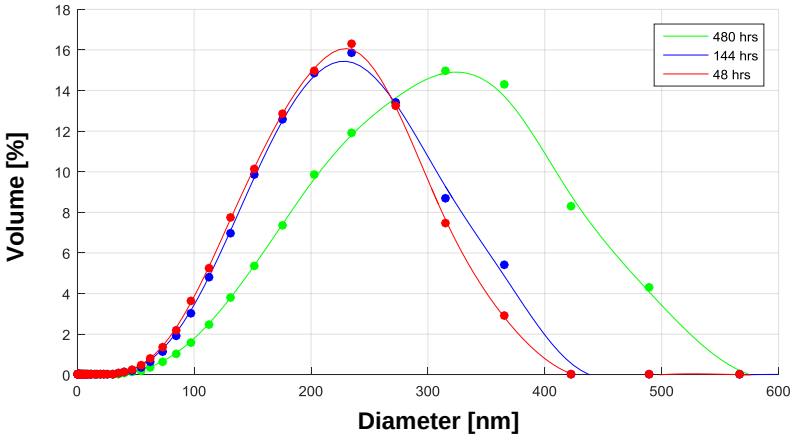


**Figure 3.22** - Size distribution of the clusters of particles over time according to their volume obtained with TEM

It appears (Figure 3.23) that the distribution obtained with the DLS (*DLS 552 hrs*) is closer to the area distribution (*TEM 480 hrs, Area*), suggesting that the clusters observed using the TEM are relatively flat.

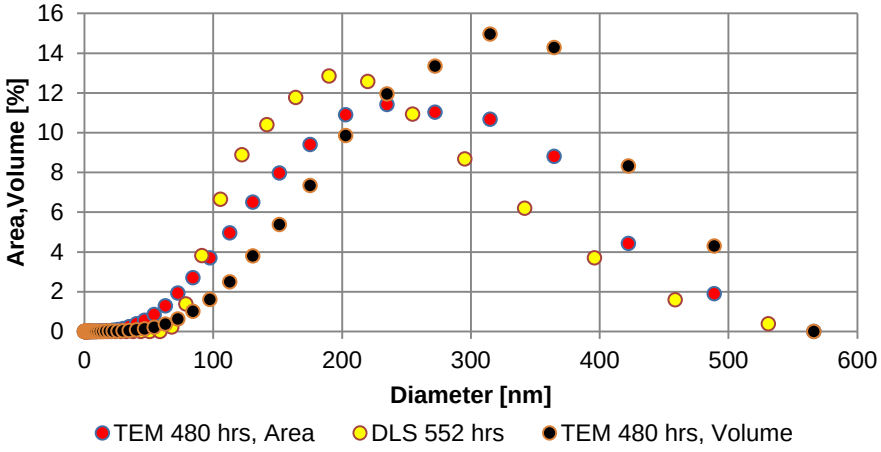


**Figure 3.23**- Size distribution of the clusters of the spheres at time steps: 480 and 552 hrs according to their cross-sectional area and volume obtained with TEM, as well as Size distribution after 552 hrs of aging obtained with DLS

The evolution of volume mean diameter D(4,3) of individual nano-spheres over time (48, 144,and 480 hrs of aging) is shown in Figure 3.24. From the figure it can been seen, that the volume mean dimeter increases from 151 until 175 nm over 432 hrs.

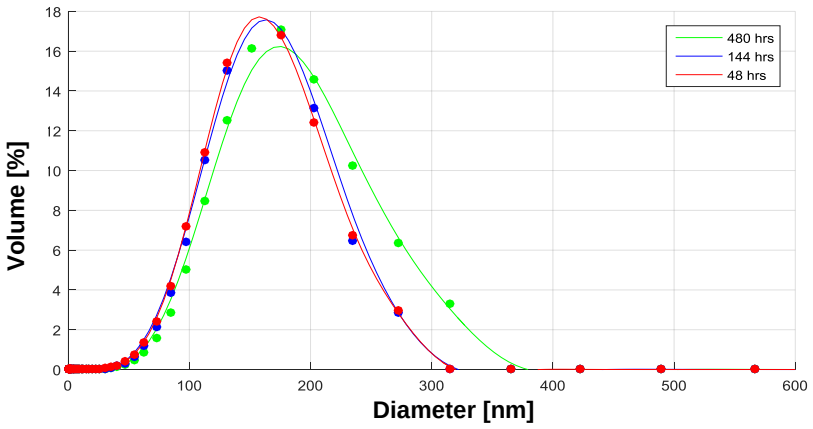


**Figure 3.24**- Size distribution of individual spheres over time according to their volume obtained with TEM

Figure 3.25 represents the size distribution curves plotted against the fraction of the cross-sectional area after 48 hrs of aging for clusters of nano-spheres obtained with TEM (*48 hrs clusters TEM*), as well as the cross-sectional

area of individual nano-spheres obtained with TEM (*48 hrs ind. TEM*). From that graph, it can be seen that the best approximation of the DLS results (*48 hrs DLS*) is the distribution curve obtained with TEM for clusters and plotted against area.

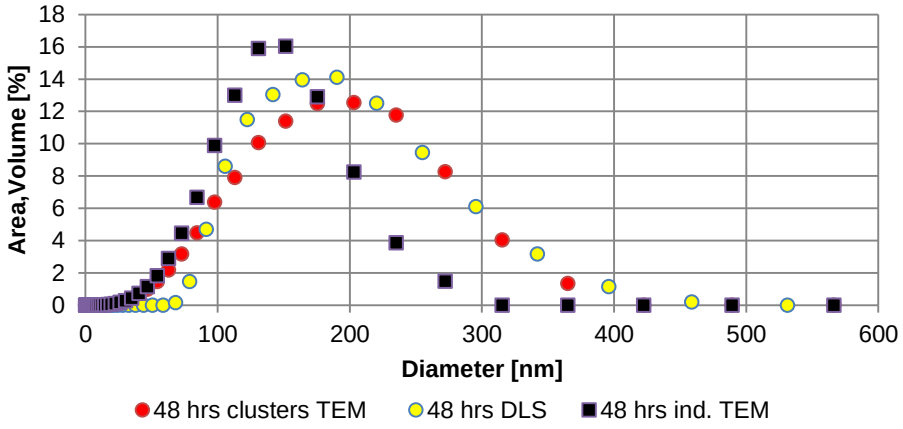


**Figure 3.25**- Size distribution of clusters and individual spheres after 48 hrs of aging according to their cross-sectional area obtained with TEM , as well as Size distribution after 48 hrs of aging obtained with DLS

In addition, we also explored dark field microscopy. The main results are presented in Appendix B. However, the images were too blurred to obtain reliable estimates of the size distribution.

## 3.5. Modelling of the agglomeration and swelling of nano-spheres with population balance model

Nano-spheres can be injected deep into a heterogeneous oil reservoir to improve sweep efficiency. The propagation of the spheres has to be enough to reach the target zone. However, due to the swelling and agglomeration of the spheres, their flow might be limited. Therefore, it is important to predict the growth of the spheres over time.

In our study, we assumed that the spheres with different sizes swell at the same rate. Hence, the size distribution curves can be corrected for the swelling effect and the prediction of the spheres' growth can be done using a population balance model accounting only for their agglomeration.

After 480 hrs of aging, the swelling appeared to reach a maximum constant factor of 1.2. Hence, the size distribution curve of the spheres aged for

480 hrs (*Aggl.+swell.*), obtained with TEM and plotted against the cross-sectional area, was divided by 1.2 to focus on the effect of agglomeration only (*Aggl.,* Figure 3.26). Next, the population balance model for the agglomeration case was applied to find the agglomeration rate and the size of the nano-spheres after 1000, 2086 and 3000 hrs of aging.

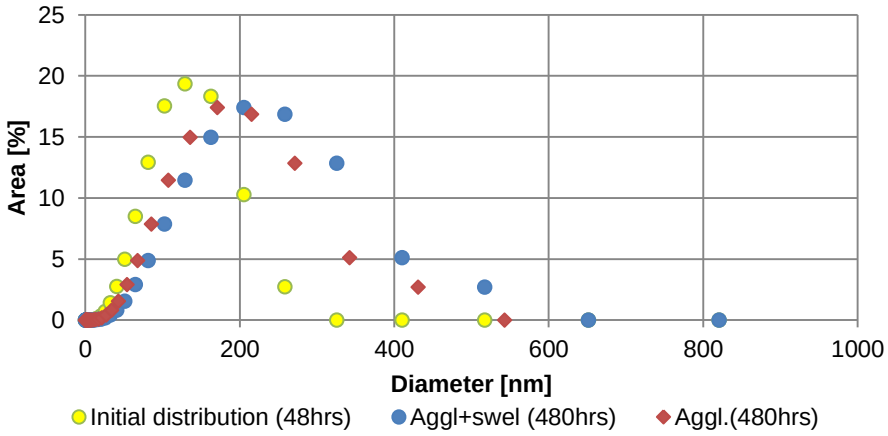


**Figure 3.26**- Size distribution functions which account for both (agglomeration and swelling) and only agglomeration after 480 hrs of aging according to the cross-sectional area of the spheres

The governing equation for the model which accounts for the agglomeration is shown below (3.1). It was first proposed by Hounslow et al. 1988 and only includes the aggregation kernel (see explanation in Appendix A). The latter is defined as a rate at which particles of different size aggregate with each other. According to Hounslow et al. 1988, equation 3.1 was obtained by the discretization of the computational domain according to the recommendations by Batterham et al. Indeed, the x-axis was divided according to progression $L_{i+1}/L_i=\sqrt[3]{2}$ where L is a length of a bin interval.

$$\frac{dN_i}{dt} = N_{i-1}\sum_{j=1}^{i-1} 2^{j-i+1}\beta_{i-1,j}N_j + \frac{1}{2}\beta_{i-1,i-1}N_{i-1}^2 - N_i\sum_{j=1}^{i-1} 2^{j-i}\beta_{i,j}N_j - N_i\sum_{j=i}^{\infty}\beta_{i,j}N_j \quad (3.1)$$

where $\beta_{ij}$ -aggregation kernel, $N_i$-number of particles; *t*-time; *i,j*- *i*th, and *j*th size intervals In the current study it is assumed that the aggregation kernel is size and time independent.

The aggregation kernel of equation 3.1 was selected as a matching parameter between TEM experimental results and the modelled data. In order to find the best match between experiments and the model, the aggregation kernel was adjusted according to the nonlinear optimization procedure using an L2-norm. The distribution curves obtained from the TEM experiments for 48 (initial distribution), 144 and 480 hrs of aging were used as the input for the optimization.

A good match between experimental and modelled data was obtained for a value of $4.07 \cdot 10^{-5}$ %/hr for the aggregation kernel $\beta$. The comparison between the modelled and experimental size distribution curves for 480 hrs of aging is shown in Figure 3.27.

By using the calculated agglomeration rate, the size distribution functions were plotted for 1000, 2086 and 3000 hrs of aging, showing substantial size increases over time. Depending on the pore throat distribution of the porous medium under consideration, large scale blocking can be expected within months of the start of the injection. It is also concluded for the first time that the pure swelling of nano-spheres is not responsible for the blockage of porous media

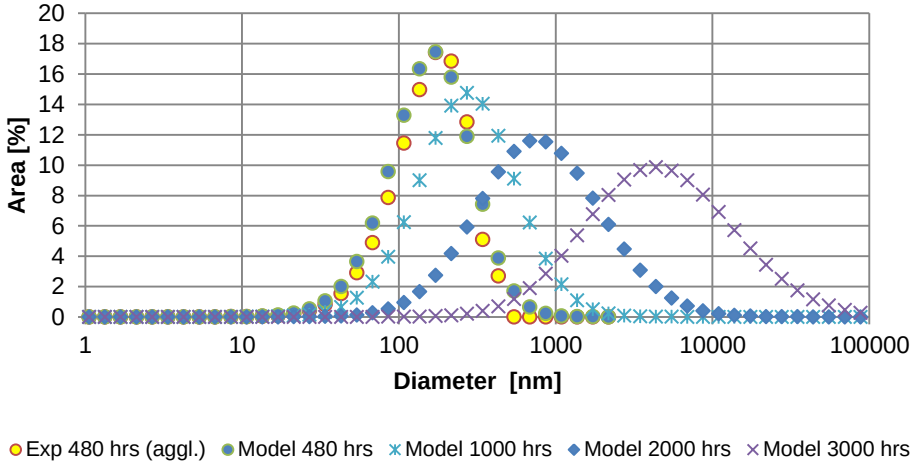


**Figure 3.27**- Modelled and experimental size distribution of nano-spheres

## 3.6. Conclusions

Care must be taken when preparing the nano-spheres for characterisation. The procedure defined in this paper allows study of the size distribution of the spheres and their time evolution. The combination of TEM and DLS, helped to mitigate the primary drawbacks of the individual techniques, lack of the solvent and direct information on the individual particle sizes, respectively. In addition, the comparison of the particles distribution obtained with TEM and DLS demonstrate a good match between two results. Thus, less time consuming tests can be used for the measurement of the size distribution of nano-spheres.

The images obtained with dark field microscopy (Appendix B) were too blurred to obtain reliable estimates of the size distribution and can be recommended for the similar studies.

The forecast of the nano-spheres growth was done using a population balance model. These results suggest that large scale blockages may occur within months of the start of injection.

# Chapter 4

## Propagation of Co-Polymer Nano-Spheres in Outcrop Cores

As explained in chapters 1 and 3, nano-spheres can be used for the conformance control in heterogeneous reservoirs. It is desired that the spheres can propagate deep in the reservoir with a resistance factor build-up over time. Finally, reservoir layers with the reduced permeability divert the flow of subsequently injected water into unswept areas with higher oil saturation.

Theoretically, a good propagation of the spheres can be achieved if their size is significantly smaller than the radius of pore throats. However, due to the interaction of nano-spheres with each other and their swelling behaviour, they can be retained with no further propagation. Depending on the characteristics of the reservoir, the required deep propagation might not be realistic. Hence, it is important to study the influence of essential reservoir characteristics, such as salinity of the brine, saturation of the core, and mineralogy of rocks on the retention of the spheres in porous media.

A series of core flood experiments in Berea, Bentheimer and Boise outcrop cores was carried out to experimentally study the flow of nano-spheres in porous media with different mineralogy and permeability. Complementary to that, the dynamic of the pressure drop over cores and carbon content in the effluent were analysed at different injection flow rates. Dynamic light scattering tests indicated the size of nano-spheres in different types of brine and helped to understand better its influence on the propagation in porous media.

The results of the work show that the propagation of nano-spheres in porous media is highly dependent on the brine salinity in cores with single and multiphase saturations. For the same experimental conditions, the resistance factor of nano-spheres in porous media depends on the flow rate.

## 4.1. Introduction

The nano-spheres suspension is considered as an attractive fluid for conformance control in heterogeneous reservoirs (Yuqin et al. 2012; Irvine et al. 2015). The active matter in this suspension consists of preformed co-polymer nano- spheres which can contain the following polymerized monomers: acrylamide, acrylic acid, and 2-Acrylamido-2-methylpropane sulfonic acid. The particles have a small initial size ~175 nm and expand over time due to the absorption of water (Wang et al. 2010; Barari et al. 2011). The spheres have been designed to improve sweep efficiency in heterogeneous oil reservoirs and enhance oil displacement by profile modification. The advantage of using prefabricated gel particles versus in-situ gelation is a better plugging of target intervals deep in the reservoir and the absence of chromatographic separation between components of the fluid during its propagation in porous media (Bai et al., 2007; Spildo, 2010).

The implementation of the nano-spheres in practice **requires a deep propagation in porous media** and **resistance factor build-up over time**. Although recovery technologies involving the nano-spheres are applied in different oil fields (Wang et al. 2010; Yuqin et al. 2012; Irvine et al. 2015), there are only a few studies which experimentally describe the propagation of the nano-gels in porous media (Wang et al. 2010; Spildo et al. 2010; Almohsin et al. 2014). Indeed, the understanding of the mechanism of propagation has not been well established yet and is still a subject of study. Therefore, it is of interest to investigate nano-spheres propagation in porous media in different types of rocks, permeability, level of heterogeneity, saturation of the core, brine salinity and injection rates.

The propagation of nano-spheres in Bentheimer, Boise and Berea outcrop cores at different salinities and saturations was studied in our work. The dynamic of swelling was monitored with DLS and size distribution curves were obtained for different salinities and aging times. In order to exclude the swelling effect from the core flood experiments, nano-spheres were mostly injected into cores in a swollen state. It means that the hardness of the spheres to deformation was the same for all experiments.

During the injection of particles into porous media they can accumulate and increase the residual resistance factor. The latter is important for the subsequent diversion of water into low permeable layers of a heterogeneous

reservoir. Hence, another series of core flood experiments was carried out to study RRF in Bentheimer, Boise and Berea outcrop cores at different salinities and saturations.

## 4.2. Literature review

Propagation of nano-spheres in porous media might depend on retention and hydrodynamic acceleration. For example, these parameters have a significant influence on the flow of conventional polymers (e.g. HPAM) in porous media (Willhite, G.P. and Dominguez, 1977; Sorbie, 1991; Farajzadeh et al., 2015). However, in the case of nano-spheres, which have a size several times smaller than the average size of pore throats, most of the pore space is accessible for their flow. Thus, hydrodynamic acceleration should be less important than the retention. We did a literature review to outline different types of retention for the systems similar to nano-spheres: polystyrene latex nano-particles, polymer nano-gels, hydrolyzed polyacrylamide and colloidal dispersion gels (CDG).

According to K. Sorbie (1991), once retention takes place, it significantly impacts the permeability reduction parameter- residual resistance factor (RRF). The dependence of the RRF on the flow rate (velocity) for polymers is reviewed as well.

**Propagation and resistance factor of nano-particles (nano-gels) in porous media**

Retention of nano-particles in porous media can be described by clogging mechanisms of micro channels with charge-stabilized polystyrene latex particles (Sendekie and Bacchin, 2016). In the work of Sendekie and Bacchin (2016) the influence of the ionic strength (*KCl was used as a salt in brine*), flow rate and micro channel's entrance geometry on the filtration dynamics and clog fragility were studied. It was shown that while particles enter the micro channel, they might be retained, even if the individual size of particles is smaller than the size of the channel. For example, they demonstrated that nano-particles can form arches around the entrance of pore throats due to a strong repulsion between particles at low brine salinities (Figure 4.1, a). That can restrict further propagation along the channel.

The strength of the repulsion depends on the ionic strength of brine. If a moderate brine salinity is used, then the repulsive double layer decreases and, according to Sendekie and Bacchin, the transport of the particles improves

leading to a delay in clogging. They also showed that at high brine salinity there is a high probability for the formation of **aggregates** but they are **very fragile** and can be swept out from channels under higher flow rates.

From the series of conducted experiments, they concluded that particle – particle and particle-wall interactions are very important for the retention events. Thus, the interplay between ionic strength of brine and hydrodynamic forces is crucial for the propagation.

Propagation of nano-gels, which are similar to nano-spheres, was studied by Almohsin et al. (2014). The results of core flood tests with nano-gels showed that the particles with a smaller size had a higher resistance factor in porous media than the particles with a bigger size. That observation is supported by the hypothesis that the particles in a swollen state are more elastic and deformable than the particles with a small size (Almohsin et al. 2014). However, it is generally assumed (Wang et al., 2010;Yuqin et al., 2012) that the particles have a tendency to block porous media in a swollen state. Hence, that contradicts with the general perception of how the swelling of particles influences their transport in porous media. Nevertheless, the difference might be explained with the difference in materials that the particles are made of.

Additional series of core flood tests conducted by Almohsin et al. (2014) with nano-gels revealed the power law dependence between resistance factor and velocity: at higher velocities a lower resistance factor was obtained. According to this study, the relationship holds in the range of permeability 41-1038 mD. These results experimentally indicate a shear thinning behavior of nano-gels and can be explained by the adsorption of elastic and deformable layers of nano-gels on the rock surface. The thickness of the layers was bigger than the size of individual particles. Hence, it can be assumed that multiple layers are adsorbed on the surface of the rocks.

Similar salinity and velocity dependent propagation at different saturations of rocks is expected from the nano-spheres. However, no research has been done in this area.

**Retention of hydrolyzed polyacrylamide in porous media**

Retention of nano-spheres in porous media can also be similar to conventional polymers like HPAM. Although HPAM is a linear polymer and nano-spheres have the shape of a sphere, they both are synthesized of acrylamide and acrylic acid. Many experiments have been carried out with

HPAM and are described in the literature. Temperature of the reservoir, brine hardness, and hydrolysis degree can cause the precipitation of the polymer. Hence, it might limit the propagation in porous media. Polymer retention happens due to the adsorption of polymers on the available sites of a rock surface, as well as, due to the mechanical entrapment and hydrodynamic retention (Figure 4.1, b) (Cohen, and Christ, 1986; Sorbie, 1991; Chiappa et al., 1999; Zitha et al., 1998; Farajzadeh et al., 2015).

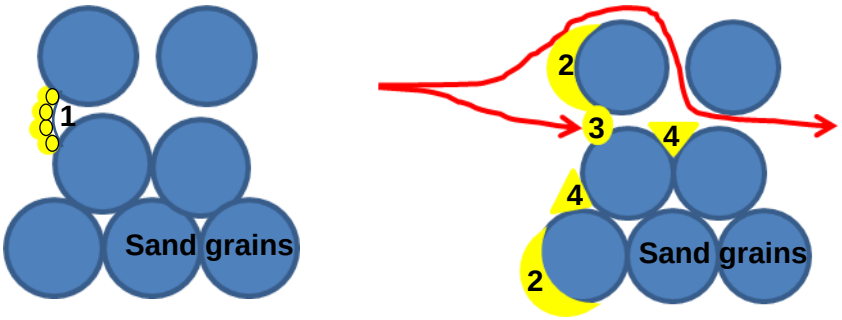


**Figure 4.1**- Different types of retention in porous media (Sendekie and Bacchin, 2016 (a); Sorbie, 1991 (b)):
a: 1-formation of arches from nano-particles; b: 2-polymer adsorption; 3- mechanical entrapment; 4- and hydrodynamic retention in stagnant zones.

Polymer adsorption on a rock surface can happen due to van der Waals forces and hydrogen bonding (Sorbie, 1991). Polymer molecules occupy available sites on the rock forming chemical bonds. Therefore, a thin layer of the polymer is formed on pore walls. That leads to reduction in the permeability of the porous media which is mostly controlled by the hydrodynamic thickness of the layer (Zitha et al., 1998). The layer build-up during the polymer flow cannot be fully avoided (Zitha et al., 1998).

Since the polymers are polyelectrolytes (e.g. anionic and cationic), they can also be adsorbed on the rock surface due to the electrostatic interaction (Chiappa et al., 1999). In the series of experiments conducted by Chiappa et al., 1999, the adsorption of (cationic, anionic and weakly anionic) polymers on quartzite (negatively charged at neutral pH) was studied. The results of their work demonstrated that the adsorption of cationic polymers is 2.3 times higher than anionic polymers on the surface of the pure quartz. The presence of clay

minerals enhances the adsorption of polymers due to their higher specific area and negative charge.

Mechanical entrapment and hydrodynamic retention are only observed when polymer flows through the porous media. The former happens when large polymer molecules flow through small pore throats (Willhite and Dominguez, 1977; Sorbie, 1991). As a result of the process, flow in porous media is restricted through small channels and permeability is reduced. The experimental evidence of mechanical retention suggests that the concentration of the polymer in the core is exponentially distributed along the length with the highest accumulation in the inlet (Sorbie, 1991).

Hydrodynamic retention is defined as a rate dependent retention. Experiments conducted with HPAM showed that the adsorption increases once the flow rate is increased (Sorbie, 1991). A physical explanation for the rate dependent retention is an accumulation of the polymer in stagnant zones and it also depends on the pore structure. This type of retention is reversible when the flow rate is reduced.

In the work of Cohen Y. and Christ F.R. 1986, resistance factor of HPAM (Mw= $5.5 \cdot 10^6$ and hydrolysis degree of 25 %) was studied experimentally using adsorbing and non-adsorbing porous media of equivalent properties (porosity, permeability, and pore size distribution). It was demonstrated that after the adsorption of the polymer on a rock surface has occurred, a polymer layer is formed. Experimental results suggest that at higher pressure drops over the core, the resistance to the flow is less. That can be explained by the deformation of the polymer layer. A similar pressure dependent resistance to the flow might be observed during the accumulation of nano-spheres in porous media.

**Retention of CDG in porous media**

Transport properties of nano-spheres are expected to be also similar to prefabricated nano-sized colloidal particles CDG. This assumption relates to the similarities in the size between CDG and nano-spheres, as well as, chemical composition. CDG particles are made by cross-linking the 600 ppm HPAM (Mw=20 mD) with 30-ppm $Al^{3+}$ in synthetic sea water (Spildo et al. 2009, 2010). Since the concentration of the polymer in the solution is low, it does not form a continuous interconnected network. Instead, separate cross-linked spherical particles are formed with a size in the range of 50-150 nm and the interaction between polymers is dominated by intramolecular cross-linking. The

main difference between CDG and nano-spheres is $Al^{3+}$ used as a cross-linker in CDG.

A series of core flood experiments studied the propagation of CDG in water-wet Berea cores (Spildo et al. 2010). Before the injection of CDG into porous media, it was aged for 3-8 days in high salinity brine at 40 ºC to ensure complete cross-linking. It was shown that the particles flow in porous media well without a chromatographic separation of $Al^{3+}$ and the polymer. Some small reduction in permeability of porous media was indicated after CDG passed the core. However, in previous laboratory tests, where CDG are injected into the core in lower salinity brine, a high retention of the particles was observed (Seright, 1995). Hence, brine salinity is an important parameter that influences the retention of acrylamide based particles in porous media.

During the flow in porous media, the retention of CDG might happen due to adsorption, mechanical entrapment and/or the jamming mechanism (Spildo et al., 2010). It was proposed that particles can extract additional oil from porous media by microscopic diversion, as well as the improvement in macroscopic sweep. Hence, particles block high permeable channels and influence redistribution of the pressure and flow in porous media. Oil mobilization increases with an increase in the permeability and heterogeneity.

## 4.3. Experimental material

### *Brine*

Four different types of brine were used in our study (Tables 4.1-4.4), as well as demineralized water. Before any of these types of brine were injected into the core, vacuum was applied and they were filtered with a cellulose filter with the size of 1.2 μm.

**Table 4.1**-Salts content in brine #1

| Ions | Concen., mg/l |
|---|---|
| $Na^+$ | **5295** |
| $Mg^{2+}$ | **137** |
| $Ca^{2+}$ | **199** |
| $Cl^-$ | **8917** |
| **TDS 15 g/l** | |

**Table 4.2**-Salts content in brine #2

| Ions | Concen., mg/l |
|---|---|
| $Na^+$ | **2008** |
| $K^+$ | **28** |
| $Mg^{2+}$ | **11** |
| $Ca^{2+}$ | **24** |
| $Cl^-$ | **3101** |
| $SO_4^{2-}$ | **159** |
| **TDS 5 g/l** | |

**Table 4.3**-Salts content in brine #3

| Ions | Concen., mg/l |
|---|---|
| $Na^+$ | **1916** |
| $Ca^{2+}$ | **35** |
| $Cl^-$ | **2986** |
| **TDS 5 g/l** | |

**Table 4.4**-Salts content in brine #4

| Ions | Concen., mg/l |
|---|---|
| $K^+$ | **7037** |
| $Ca^{2+}$ | **35** |
| $I^-$ | **248** |
| $Cl^-$ | **6480** |
| **TDS 30 g/l** | |

***Oil for reproducing multiphase saturation of the core***

Two different types of hydrocarbons were used in core flood experiments for the reproduction of multiphase saturation of the core. Experiments # 4 and 6 were carried out using decane, whereas a crude oil was used for the saturation of the core in a third flood experiment. The crude oil used for the study has a density of 941 kg/m$^3$ at 15 ˚C. Viscosity was measured at different temperatures with an AR-G2 viscometer (TA instruments). Results of the rheology test showed that the viscosity of the oil is 59 mPa·s at 50 ºC and 231 mPa·s at 25 ºC. Before the oil was injected into the core, impurities were removed by rotating oil in a centrifuge.

***Nano-spheres***

The nano-spheres were used as a conformance control agent in a series of core flood experiments. These acrylamide-based spheres are delivered in an emulsion form. In addition to the polymer, it contains mineral oil and surfactant. Since the main goal of this experiment is to study the propagation of particles in the core, the mineral oil and surfactant were removed from the composition. This was done by mixing the emulsion containing the spheres with acetone. While the emulsion was being mixed with acetone, the polymer precipitated. This enabled the collection of precipitant which was gently crumbled into a fine powder and washed again with acetone. This step was repeated 4 times to obtain a better extraction of the particles to make sure an effective separation between the polymer and oil is achieved. At the end, the particles were dried in the oven under a vacuum at 30 ˚C (Figure 4.2).

Later on, 600 ppm of the polymer was dispersed in the brine to obtain the suspension of nano-spheres (Figure 4.3). Before the suspension was injected into the core, it was aged in an oxygen free environment for 2 weeks at 22˚C. During the aging process, the nano-spheres swell over time by absorption of water. The visual observation of the aged suspension shows that the fluid demonstrates turbidity. The turbidity might be caused by the agglomerates of particles and the retention of oil droplets from the emulsion. Nevertheless, the content of oil in the purified suspension is low and does not influence significantly the results of the total organic carbon (TOC) analysis.

The flow of purified nano-spheres in a core allows for the physical modelling of the flow of the swollen spheres deep in a reservoir. In order to keep the particles suspended in the solvent and avoid segregation during the flood experiments.


**Figure 4.2**-Example of unpurified nano-spheres

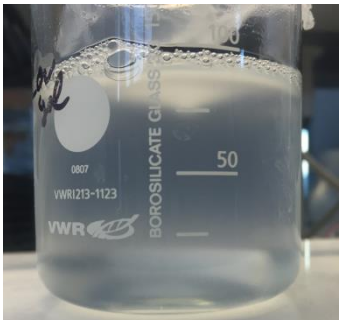


**Figure 4.3**-Example of purified nano-spheres

Next, the size of nano-spheres was studied with TEM and DLS. As an initial step, the particles were evenly distributed in the suspension by the treatment with an ultrasound in the low shear regime for 5 min. The obtained suspension is transparent and does not have any haziness.

A special procedure was applied to prepare nano-spheres for the tests with the TEM (Lenchenkov, et al. 2017). The obtained TEM micrographs show the distribution of the spheres on a substrate of the microscope (Figure 4.4**)**. It appears that the spheres can be individually distributed, as well as form agglomerates. Our earlier studies have shown that agglomeration and swelling are two processes which simultaneously influence the growth of the spheres in brine (Lenchenkov, et al. 2017).

From DLS tests, size distribution curves and the average size of the spheres were obtained at different aging times (Figures 4.5 and 4.6). It was found that a fresh suspension aged in 5 g/l brine (Table 4.3) mostly contains particles with an initial mean volume size D(4,3) of 175 nm. From Figure 4.5 it can be seen, that the size of the nano-spheres asymptotically increases over time reaching its maximum value after 552 hrs of aging. Hence, it might be an indication of the end of the swelling process.

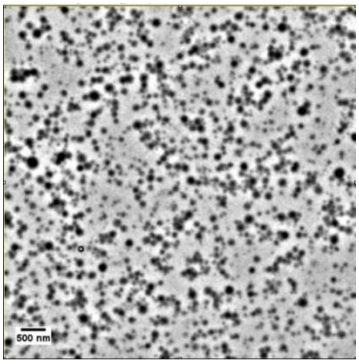


**Figure 4.4**-The TEM micrograph of the nano-spheres in 5 g/l brine

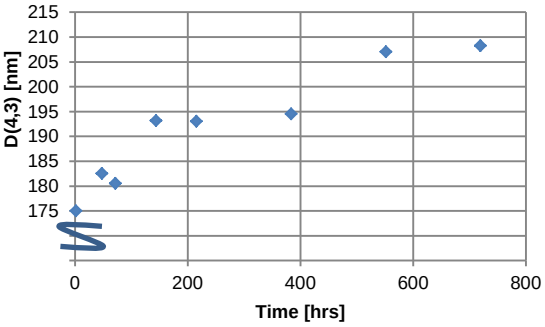


**Figure 4.5**- Change in the average diameter of nano-spheres over time in 5 g/l brine

Size distribution curves shown on Figure 4.6 indicate that there is a broad distribution of the size of nano-spheres. A shift of the mode of the distribution functions happens over time towards bigger size. Most likely, it happens due to the masking of the scattered light by the agglomerates.

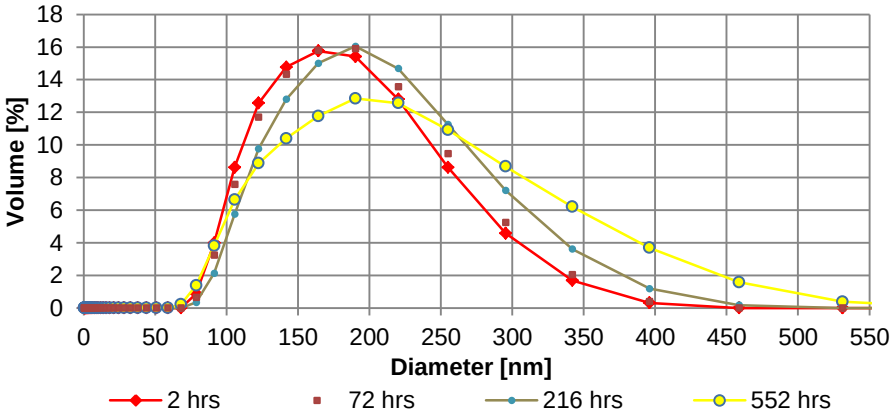


**Figure 4.6**-Distribution of the nano-spheres diameter in 5 g/l brine according to DLS

The influence of salinity on the average size of the spheres and their size distribution was studied in different types of brine: 1) 5 g/l brine (Table 4.3); 2) 30 g/l brine (Table 4.4); and 3) demineralised water. Results of DLS tests are shown on Figure 4.7. From the graph it can be seen, that the size distribution in demineralised water has a wider distribution than in 5 g/l brine or 30 g/l brine. Indeed, the volume mean diameter D (4,3) of the spheres in demineralised water is 391 nm, whereas the D (4,3) in 5 g/l brine and 30 g/l brine are 175 and

172 nm respectively. The conducted DLS tests also revealed that there is an insignificant difference between the size of particles aged in 5 g/l and 30 g/l brine. The difference in the size of the spheres dispersed in demineralised water and studied brines might be explained by the shrinkage of the spheres at high salinity brine. The similar decrease in the size of polyacrylamide with the increase of salt concentration happens due to the screening of negatively charged carboxylic groups of the polymer with cations. The relation between the size of the polyacrylamide and the salt concentration is found via a correlation between viscosity and the size of HPAM molecules (Sorbie, 1991). However, the reduction of the size of polyacrylamide due to the increase of salt concentrations is more significant than the size of nano-spheres. The difference occurs because HPAM is a linear polymer which shrinks at high salinities (Sorbie, 1991), whereas nano-spheres are cross-linked particles with a high polymer-polymer interaction.

The size of the spheres can influence their propagation in porous media. In turn, according to our study, the size of the spheres is affected by the salinity.

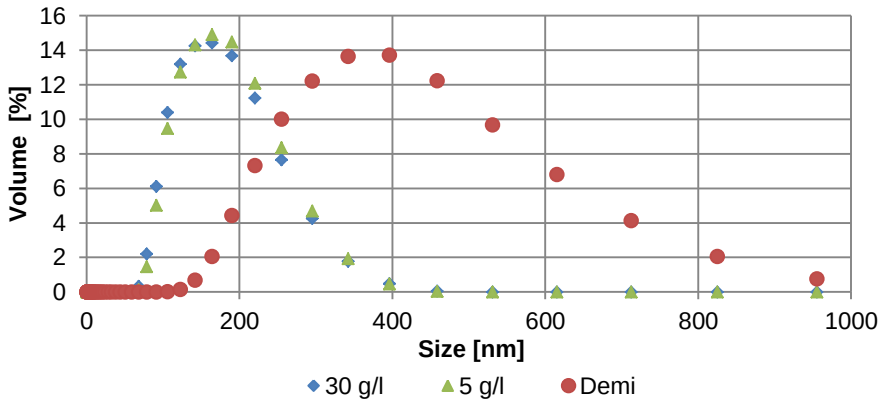


**Figure 4.7-** Size distribution of nano-spheres at different salinities: 30, 5 g/l and demi water at 25 ºC

### *Rheology of the nano-spheres*

The rheology of the nano-spheres was studied with rheometer MCR 302 (Anton Paar) using a cup and bob type measuring system. This series of tests was carried out at shear rates between 1 and 100 $s^{-1}$ at 25 ºC. The samples of the spheres were prepared separately in both demineralised water and brine with

15 g/l of NaCl. That helped to study the influence of the brine salinity on viscosity of the suspension.

The results of the test are shown on Figure 4.8. From the results it can be concluded that the viscosity of the suspension at the concentrations of nano-spheres below 2.4 g/l is low and equal to the viscosity of the brine. In addition to that, the viscosity does not depend on shear rate for the same interval of concentrations. However, at higher concentration of the spheres, above 2.4 g/l, the viscosity of the spheres in demineralised water is higher than in 15 g/l brine. Since acrylamide is the main component of the spheres, that difference in viscosity might be explained by a bigger size of the spheres in demineralised water rather than in brine. That results in the lower overlap concentration between particles for the lower brine salinities. Hence, if the salinity is decreased, then particles swell and the probability of particles to touch each other is increased.

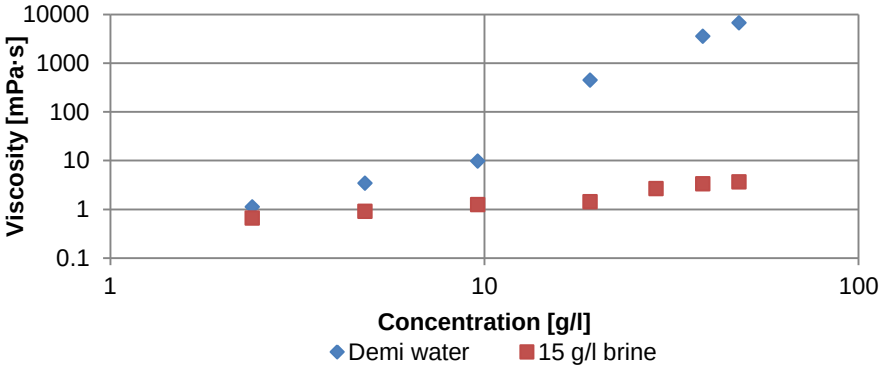


**Figure 4.8**- Viscosity of nano-spheres suspension in demineralised water and 15 g/l brine at the shear rate of 7 $s^{-1}$

***Core material***

Three different sandstone outcrops were used for the study: Boise, Bentheimer and Berea. The main characteristics of cores are presented in Table 4.5. These cores differ from each other by the level of heterogeneity and mineralogical composition.

In order to study the heterogeneity of the cores, micro CT scans were obtained. Samples of Boise, Bentheimer and Berea cores with a size of 10 mm to 40 mm were used for the micro CT study and a set of images was acquired at resolutions of 10 μm (Figures 4.9 and 4.10) and 17 μm (Figure 4.11). A stack of images was analysed with Avizo software (Avizo 9, 2015). From Figure 4.9 it

can be seen that the Boise core has two main zones with different size of grains. The difference in pore throat sizes of the Boise sample might cause an early breakthrough during the flood process. In contrast to that, the Bentheimer (Figure 4.10) and the Berea (Figure 4.11) samples have more homogeneous porous structure. Medical CT scan of the Boise core was obtained to visualise the porous structure of the core along the length. From the obtained image (Figure 4.12) it can be seen that the core has a layered structure with preferential flow paths.

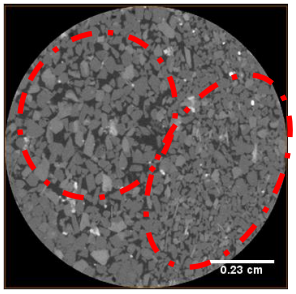


**Figure 4.9**-*A micro CT* image of the Boise core

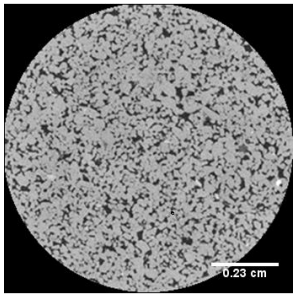


**Figure 4.10**-*A micro CT* image of the Bentheimer core

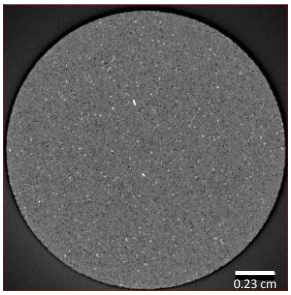


**Figure 4.11**-*A micro CT* image of the Berea core

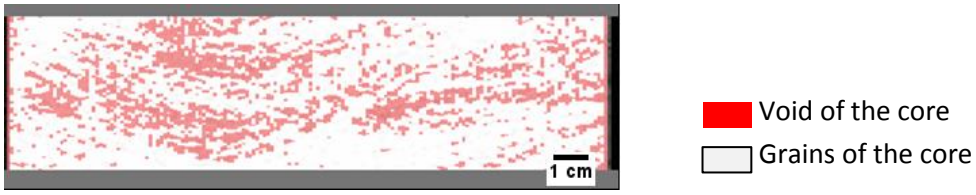


**Figure 4.12**-*A medical CT* image of the Boise core

**Table 4.5-** The main characteristics of the cores

| Parameter | Boise | Bentheimer | Berea |
|---|---|---|---|
| Length, cm | 17.0 | 17.0 | 17.0 |
| Diameter, cm | 3.5 | 3.5 | 3.5 |
| Porosity,% | 29.8 | 21.0 | 20.7 |
| Brine permeability, D | 2.6 | 2.6 | 0.050 |
| Mineralogical composition | 76 wt% quartz, 4 wt% illite, and mica, 9 wt% feldspar, 1 wt% illite-rich illite-smectite, 9 wt% of plagioclase and 1% of calcite and ankerite. | 85-92 wt% quartz, 2-5 wt% feldspar, and 3 wt% clay minerals: kaolinite, montmorillonite and illite/sericite (Peksa et al. 2015). | 94.4 % of quartz and 0.9 % of kaolinite. |

The pore throat size distribution of the Boise core was determined with the mercury intrusion method (Burdine, 1950). According to this method, the non-wetting phase- mercury is injected into the porous volume of the core. The resulting size distribution curve has a peak between 30- 40 µm (Figure 4.13).

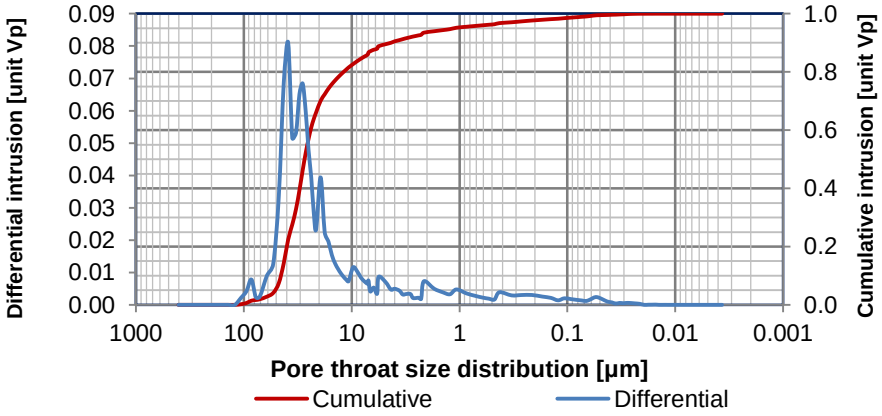


**Figure 4.13**- Pore throat size distribution of the Boise core

## The set-up of core flood experiments

Core flood experiments were carried out using different set-ups. The set-up was slightly adjusted to the specific goals of an experiment every time. A common description of the set-up is shown below.

The injection of fluid starts from the Quizix Q6000 pump (1) at the constant flow rate mode (Figure 4.14). During the injection of the fluid, the pressure on the pump is monitored, and if the safety pressure has been reached, the pump automatically stops. It makes the operation of the setup flexible and safe. After that, the pumped fluid flows to the core holder (2), where it enters the core. The pressure in the core is measured with differential pressure transducers ($dP_1$-$dP_{total}$). The inlet and the outlet sections have the length of 6.5 cm each. Therefore, the pressure transducers ($dP_1$, $dP_3$), which monitor pressure over these sections, have the range of 500 mbar. The middle section has the length of 4 cm and the pressure transducer ($dP_2$) over this section has the range of 100 mbar. The overall pressure transducer ($dP_{total}$) measures pressure over the whole core and has the range of 3 bar. This system of pressure transducers shows the contribution of pressures from each section to the overall pressure drop along the core.

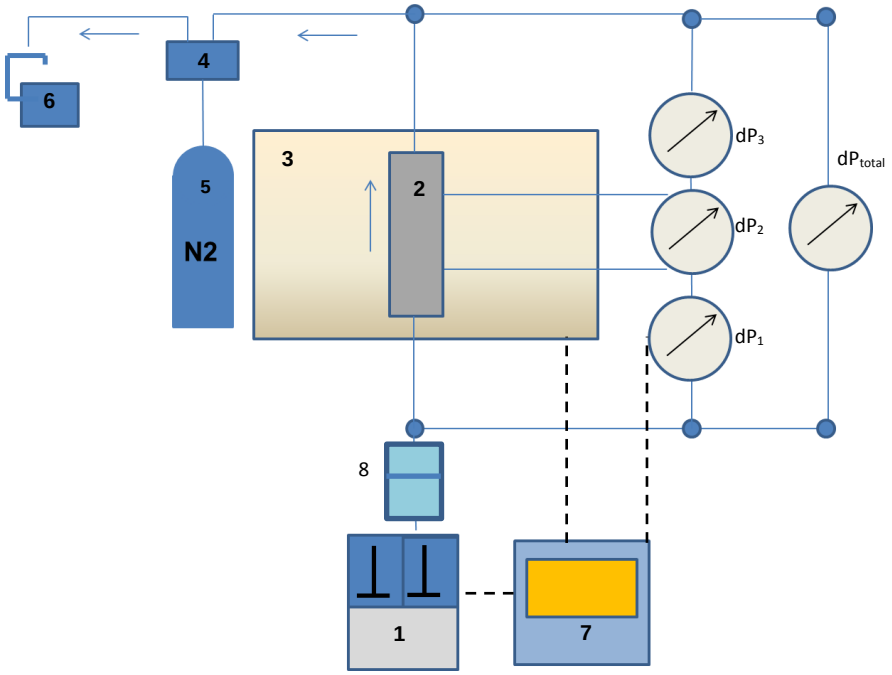


**Figure 4.14**-Core flood set-up: 1-Quizix Q6000 pump; 2- core holder; $dP_1$,$dP_3$-500 mbar PT; $dP_2$-100 mbar PT; $dP_{total}$-3 bar PT; 3-oven; 4- BPR; 5- high pressure transfer vessel with nitrogen; 6-fraction collector; 7-data acquisition system; 8- transfer vessel for the injection of the spheres into the core (optional).

The core holder (2) is made of the PEEK material and is designed for a core with the length of 17.0 cm and the diameter of 3.5 cm. It is placed vertically in the oven (3) to provide the flow from the bottom to the top side of the core.

High pressure in the core can be maintained with the back pressure regulator BPR (4), which is connected to the outlet of the core holder. The BPR contains a flexible membrane pressurised with $N_2$. When the fluid comes out from the core, it flows to the BPR. Overcoming the pressure of the membrane in the BPR, it flows to the fraction collector (6), where the effluent is collected over time. Effluent is analysed using the TOC analyser and DR 6000™ UV-VIS Spectrophotometer. An injection of the spheres into a core was done using a transfer vessel (8) where particles were placed in the bottom (Figure 4.15). That allowed for the injection of all prepared particles into the core. To prevent the segregation of the particles during the experiment, a rotating stirring bar was

placed into the vessel as well. The nano-spheres suspension was injected into a core by pushing the piston of the transfer vessel with water from the pump.

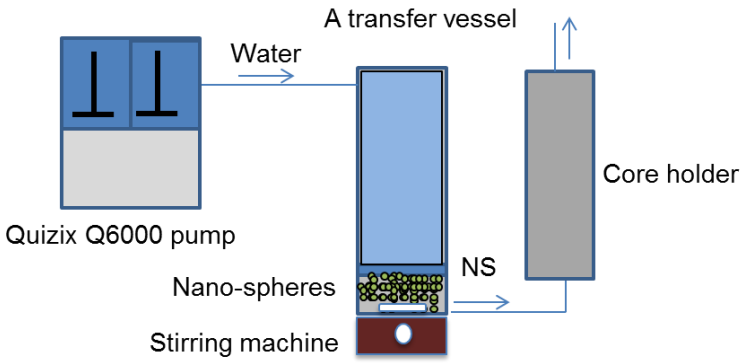


**Figure 4.15-** A transfer vessel for the injection of nano-spheres into the core

## 4.4. Procedure of experiments

Three core flood experiments were carried out in this study (#1, 4, and 5). Another two additional experiments (#2 and 3), conducted earlier, were used for the comparison of the results and discussion. Here we present the detailed procedures of the experiments conducted in this study. However, procedures of additional experiments (#2 and 3) were published in (van Dalen, 2014) and are briefly outlined in this chapter to give an overview of the major steps

Every experiment has specific goals which define the differences in procedures. Nevertheless, the initial steps of the experiments were the same (Table 4.6). As can be seen from Table 4.6, at the beginning a core is being saturated with brine. After the injection of multiple PV's of brine, the permeability test is carried out. The following steps depend on the goals of experiments (Tables 4.7-4.10**)**.

**Table 4.6** –General procedure for core flood experiments

| | Name of steps | Description | Objective |
|---|---|---|---|
| 1. | Vacuum the set-up. | The outlet of the set-up is connected to a vacuum pump. | Removal of air from the set-up. |
| 2. | Injection of $CO_2$. | Inject $CO_2$ into the core. | Removal of air from the core. |
| 3. | Saturate the core with brine against zero back pressure. | While the outlet of the set-up is connected to the vacuum pump, inject 1 PV of brine into the core at the flow rate of 1 ml/min. The pressure of the $N_2$ on the membrane | Fill the dead volume of the lines of the set up with brine, as well as, saturate the core with brine. |

| | | | |
|---|---|---|---|
| 4. | Increase the back pressure. | of the back pressure is increased to 5 bar. | Increases the average pressure in the core. |
| 5. | Brine injection. | 20 PV of brine is injected | Obtain the equilibrium between rock and fluid. To assure the injected brine composition is preserved. |
| 6. | Permeability test. | Brine injection at different flow rates: 0.1, 0.5, 1, 2 ml/min. | Estimation of the core's permeability. |

In the following experiments, pressure drop over a core was monitored during and after nano-spheres injection. The obtained pressure drop is used for the calculation of the resistance factor (RF) and residual resistance factor (RRF) at the constant flow rate.

$$RRF = \frac{\Delta P_{after}}{\Delta P_{before}} \tag{4.1}$$

where $\Delta P_{after}$ –pressure drop over a core during brine injection after a slug of nano-spheres was injected into the core, bar; $\Delta P_{before}$- pressure drop over a core during brine injection before a slug of nano-spheres was injected into the core, bar. In contrast to *RRF*, *RF* is determined as a ratio between pressure drops during nano-spheres injection and pressure drop during initial brine injection. Both parameters can change over time because of the nano-spheres propagation in porous media.

***Core flood experiment #1*** described in Table 4.7 studies the RRF of freshly made nano-spheres, as well as aged spheres in the Berea core. This experiment is divided into two stages: an injection of the fresh nano-spheres into the core which is followed by the shut off period for 2 weeks with the subsequent injection of the aged nano-spheres into the same core. That gives RRF at a sweep of flow rates: 0.05, 0.1, 0.2, 0.4, 0.8, 1, 1.6 ml/min. Thus, a relationship between the RRF of nano-spheres in porous media and the flow rate (velocity) is obtained.

**Table 4.7 –** Core flood experiment #1. Study of the RRF in the Berea core

| | Name of steps | Description | Objective |
|---|---|---|---|
| 7. | Injection of fresh nano-spheres. | Injection of the nano-spheres at 1 ml/min for 0.2 PV. | Saturation of the core with the nano-spheres. |
| 8. | Brine injection | Injection of brine at a flow rate of 1 ml/min (**Test 1**). | Study RRF after the injection of brine into the Berea core. |

| | | |
|---|---|---|
| 9. Injection of fresh nano-spheres. | Injection of the nano-spheres at 1 ml/min for 2 PV. | Saturation of the core with the nano-spheres. |
| | **Aging the core for 2 weeks** | |
| 10. Brine injection | Injection of brine at different flow rates: 0.05, 0.1, 0.2, 0.4, 0.8, 1, 1.6 ml/min (**Test 2**). | Study the RRF during the injection of brine into the Berea core. |
| 11. Injection of aged nano-spheres into the core. | Injection of the nano-spheres at 0.05 ml/min. | Saturation of the core with the nano-spheres. |
| 12. Brine injection. | Injection of brine at different flow rates: 0.05, 0.1, 0.2, 0.4, 0.8, 1, 1.6 ml/min (**Test 3**). | Study the RRF during the injection of brine into the Berea core. |

***Core flood experiment #2*** studies the RRF in a brine saturated Bentheimer core after the injection of 0.79 PV of the aged spheres. In contrast to that, ***Core flood experiment #3*** was carried out in a Bentheimer core at the residual oil saturation and studies the RRF of aged spheres in the core after 7.6 PV of the spheres was injected. Aging of the spheres was done in 15 g/l brine for 2 weeks. Characteristics of Bentheimer cores are similar to those shown in Table 4.5 (Bentheimer core).

***Core flood experiment #4a*** described in Table 4.8 explains the propagation of nano-spheres at 50 ºC in the Boise core which has a multiphase saturation. Crude oil was used for changing the saturation of the core with the subsequent injection of brine to reach the residual oil saturation. The injection of nano-spheres was started at a residual oil saturation when no more oil was produced. The experiment is complemented with a series of tracer tests before and after the injection of nano-spheres. In addition to that, the results of a TOC analysis of the effluent indicate the propagation of nano-spheres through the core.

**Table 4.8 –** Core flood experiment #4a. Propagation and the RRF of aged nano-spheres in the Boise core at multiphase saturation (injection of slugs of nano-spheres)

| Name of steps | Description | Objective |
|---|---|---|
| 7. Brine injection and heating up the core to 50 ºC. | During the brine injection the core's temperature is increased to 50 ºC. | Obtain the equilibrium between rock and fluid. To assure the injected brine composition is preserved. |
| 8. Saturation of the core with oil. | Core is saturated with oil and aged for 4 weeks | Saturation of the core with oil. |

| | | |
|---|---|---|
| 9. Brine injection. | Brine injection into the core at the sweep of flow rates: 1, 2 and 5 ml/min. | Reaching residual oil saturation. |
| 10. Tracer injection. | An injection of brine together with potassium iodide (20 ppm) into the core at 0.1 ml/min (2 ft/day) for 2 PV. The concentration of KI is detected by a spectrophotometer. | Estimation of the porous volume of the core and the dispersion coefficient. |
| 11.Brine injection. | Injection of brine for 2 PV. | Flush out the tracer from the core. |
| 12. Injection of slugs of nano-spheres. | Injection of slugs (0.5 PV) of nano-spheres into the core at 1 ml/min. | Study the RF of nano-spheres in the core. |
| 13. Effluent analysis. | TOC analysis was done to study the carbon concentration in the effluent. | Study the propagation of nano-spheres in porous media. |
| 14. Tracer injection. | Injection of KI into the core. | Determine the porous volume and dispersion coefficient. |

It is expected that the propagation of slugs of nano-spheres is different to the propagation of the spheres during its continuous injection. Therefore, the spheres were injected continuously into the same core (***experiment # 4b***). Effluent was collected and analyzed with the TOC analyzer. That allowed studying the propagation of the spheres in the core.

**Table 4.9 –** Core flood experiment #4b. Propagation and the RRF of aged nano-spheres in the Boise core at multiphase saturation (continuous injection of the nano-spheres)

| Name of steps | Description | Objective |
|---|---|---|
| 15. Continuous injection of nano-spheres | Continuous injection of nano-spheres into the core at | Study the RF of nano-spheres during its continuous injection. |
| 16. Effluent analysis. | TOC analysis was done to study the carbon concentration in the effluent. | Studies the propagation of nano-spheres in porous media. |

***Core flood experiments #5 and #6*** represent the flow of nano-spheres in a Bentheimer and a Boise core respectively both at high salinity brine (Table 4.10). The Boise core in experiment #6 was saturated with mineral oil (Table 4.10 and step 7a) and later the oil was displaced by water at the sweep of flow rates (Table 4.10 and step 7b) to reach the residual oil saturation. The

propagation of the nano-spheres in porous media was analyzed via the dynamic pressure drop over the core and effluent analysis.

**Table 4.10** – Core flood experiments #5 and #6. Injection of nano-spheres at high salinity brine

| Name of steps | Description | Objective |
|---|---|---|
| 7a. Saturation core with oil | Injection mineral oil for into the core (Exp. #6) | Saturation of the core with oil. |
| 7b. Displacement of oil | Injection of brine at the sweep of flow rates (Exp. #6) | Reaching residual oil saturation |
| 8. Continuous injection of the nano-spheres into the core. | Continuous injection of the nano-spheres into the core at 1 ft/day. | Studies the pressure build-up during the injection of nano-spheres in porous media. |
| 9. Effluent analysis. | TOC test was done to study the carbon concentration of the polymer. | Studies the propagation of nano-spheres at high salinity brine. |

## 4.5. Results and Analysis

### Results of the nano-spheres injection

***Experiment #1***

During the first experiment, nano-spheres aged in 15 g/l brine were injected into the Berea core. The subsequent injection of brine was done at different flow rates: 0.05-1.6 ml/min. That allowed for the study of the relationship between RRF and superficial velocity (Table 4.7).

At the beginning of the experiment, 0.2 PV of fresh nano-spheres was injected into the core. Subsequently injected brine showed an increase of the RRF to 1.42 (**Test 1**, Figure 4.16) which indicates an accumulation of the spheres in porous media. The injection of brine was carried out for 3 PV and it was followed by an injection of 2PV of fresh nano-spheres. Next, the core was shut off for 2 weeks and an injection of brine was started at the sweep of flow rates: 0.05; 0.1; 0.2; 0.4, 0.8 and 1.6 ml/min (**Test 2**). The results of Test 2 also showed that the RRF declines asymptotically to the minimum value with the flow rate. Indeed, the increase in a flow rate resulting in the decrease of the RRF. A maximum value for RRF is equal to 24 at 0.05 ml/min and the minimum 3.5 at 1 ml/min. During Test 2, 11 PV of brine was injected into the

core. That was followed by the injection of 0.2 PV of aged nano-spheres which increased the RRF again.

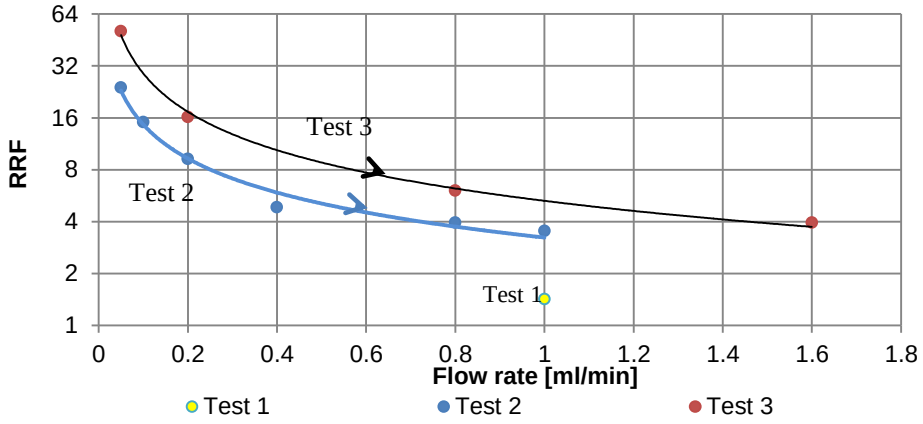


**Figure 4.16**- The relationship between RRF and flow rate (ml/min).
Total volume of the spheres inj: Test1: 0.2 PV; Test2: 2.2 PV; Test3: 2.4 PV

The increase in the RRF was estimated by a brine injection at the sweep of flow rates: 0.05; 0.2; 0.8 and 1.6 ml/min (**Test #3**). A similar velocity dependent relationship between the RRF and flow rate was obtained in Test #3. In addition to that, the RRF was increased by 1.5 times after the last slug of injected spheres.

Similar flow rate (velocity) dependent RRF was obtained during the injection of nano-gels in a series of core flood experiments by Almohsin, et al. (2014). In that study they experimentally showed that the increase in the velocity leads to the decrease in the resistance factor for high and low permeability cores. That confirms the shear-thinning behaviour of nano-spheres in porous media.

***Experiments # 2 and #3***

Core flood experiments #2 and #3, carried out by the injection of nano-spheres into the brine saturated Bentheimer core, as well as the Bentheimer core at residual oil saturation respectively, demonstrated again the asymptotic decline of RRF with the flow rate (Figure 4.17, van Dalen, 2014). This suggests that despite the difference in the saturation of rocks (*single phase vs multiphase saturation*), the RRF after nano-spheres injection asymptotically declines with the flow rate. However, RRF is smaller in the multiphase saturated core

(Figure 4.17, Exp. #3) than in a single phase saturated core (Figure 4.17, Exp. #2). Hence, the RRF might be less in a core with a residual oil saturation due to less adsorption on the rock surface. The obtained results of the experiments also suggest that the resistance factor build-up in porous media is similar for purified (with acetone) and unpurified nano-spheres. However, it is still essential to purify the spheres to study their propagation in the core with TOC (Total Organic Analyser).

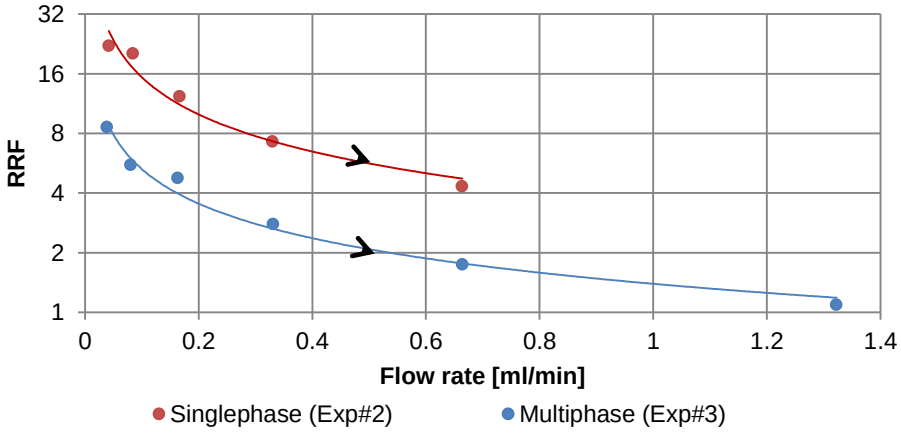


**Figure 4.17-** The relationship between RRF and flow rate (ml/min) in single and multiphase saturations

### *Experiment #4a*

Experiment #4 aims to study the propagation of nano-spheres aged in 5 g/l in Boise core. After the injection of multiple PV's of brine into the core, it was saturated with oil and aged for 4 weeks. Next, the water flood was carried out to reach the residual oil saturation in the core. After the residual oil saturation was achieved, the effective porous volume was reduced from 48 ml to 25.5 ml. Finally, nano-spheres were injected into the core and their propagation was studied via effluent analysis, as well as the pressure drop (Table 4.8).

Four slugs of nano-spheres were injected into the Boise core at a rate of 1 ml/min with slugs of brine in between at a flow rate of 0.05 ml/min (Figures 4.18 and 4.19). The high injection rate of nano-spheres was chosen to get closer to near wellbore velocities and the volume of each slug of spheres is equal to 13.5 ml (0.53 PV). During the flow of the spheres in porous media, the pressure drop was monitored over different sections of the core.

From experimental results, it can be concluded that during the injection of particles, the overall resistance factor increases. The largest contribution to the overall resistance factor comes from the inlet section of the core. It indicates that the spheres may have accumulated in the inlet section of the core. Furthermore, during the injection of the 2$^{nd}$ slug, it was still evident that the biggest pressure drop happens in the inlet section (the section is defined in Figure 4.14) of the core (Figure 4.18).

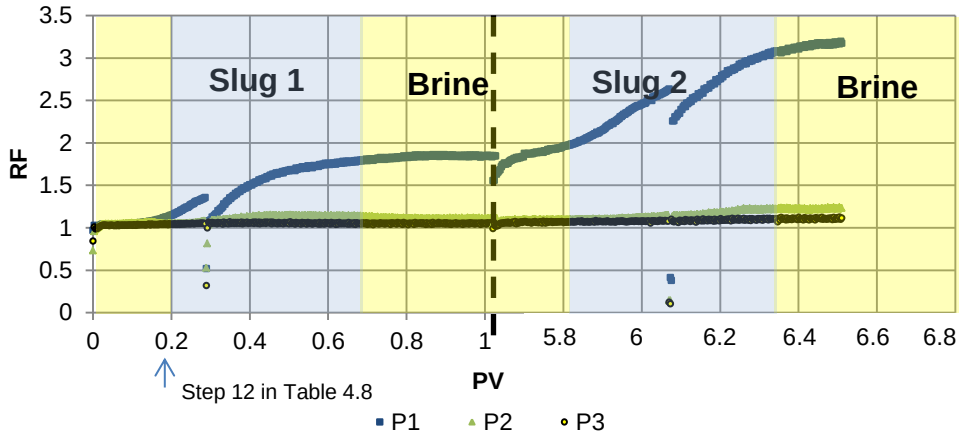


**Figure 4.18-** Resistance factor over PV injected: 1 and 2 slugs of nano-spheres (1 PV= 28 ml): P1-inlet pressure transducer, P2-pressure transducer in the middle section of the core, P3-pressure transducer in the outlet section.

The following slugs of nano-spheres (3 and 4) confirm a poor propagation of the spheres in porous media (Figure 4.19).

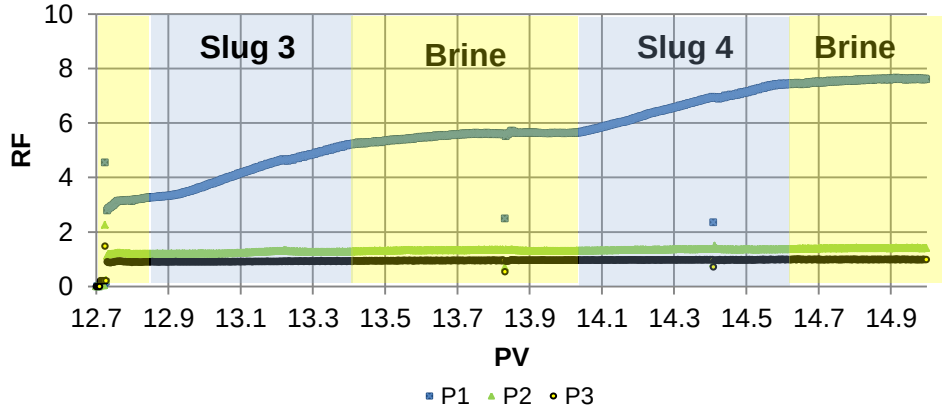


**Figure 4.19-** Resistance factor over PV injected: 3 and 4 slugs of nano-spheres (1 PV= 28 ml)

After all the slugs were injected into the core, a tracer injection was conducted with the KI at 20 ppm. The obtained tracer breakthrough curve is shown on Figure 4.20. For comparison, the tracer breakthrough curve for the time when the spheres had not yet been injected in the core (before the NPS) is shown as well. From the shape of the curves it can be concluded that there is no significant reduction in the pore volume of the core and there is a slight reduction in the dispersion after 4 slugs of the spheres were injected. The reduction of the dispersion coefficient can be explained by some diversion in the core entrance due to a poor propagation of the spheres. That slightly improves the sweep of the core. The resulting porous volume of the core is equal to 25.5 ml.

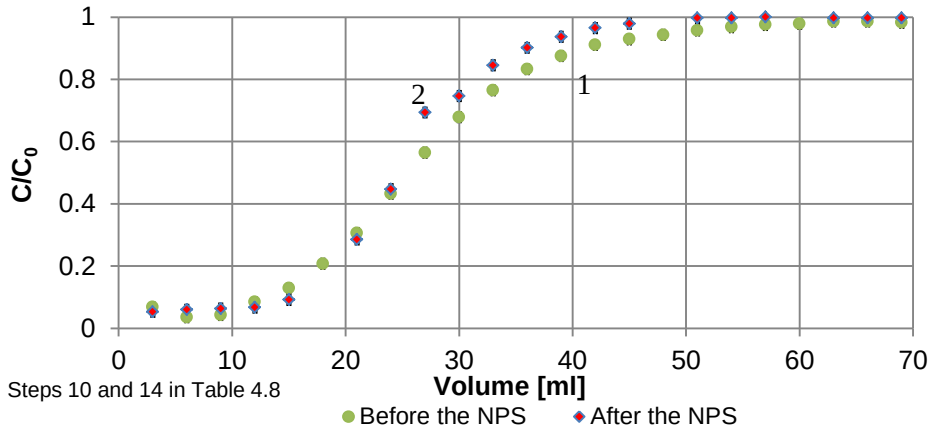


**Figure 4.20**-Tracer breakthrough curves: 1- before the spheres were inj.; 2- after the spheres were inj.

***Experiment #4b***

The dynamic of the pressure drop changes when the spheres are continuously pushed into the core. Hence, that was studied via a continuous injection of spheres for an additional 5 PV into the same Boise core with multiphase saturation (Table 4.9, Figure 4.21). It was observed that after 1 PV of the spheres was injected again (21 PV on the graph), the RF started to rise in the middle section of the core ($dP_2$). However, the pressure in the outlet section of the core did not change. After 3.4 PV of the spheres were additionally injected (23.4 PV on the graph), the RF started to rise in the outlet section.

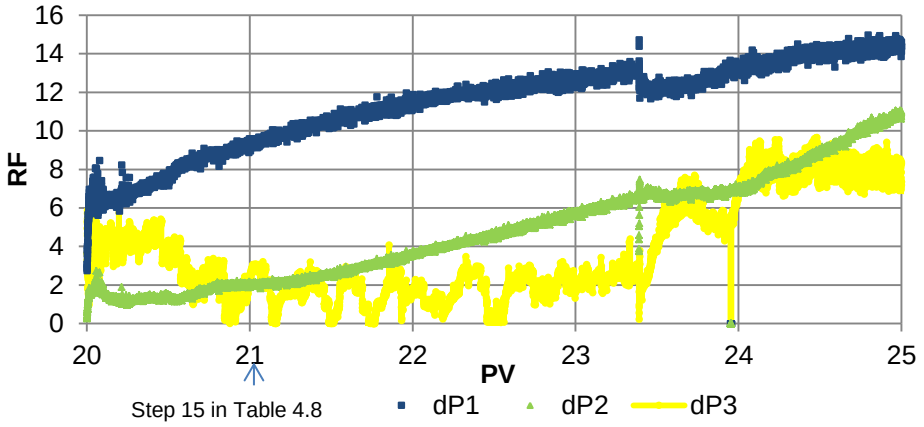


**Figure 4.21**-Continuous injection of the spheres

***Total organic carbon (TOC) analysis of the effluent in Experiments 4a and 4b***

The spheres propagation through the core was studied with the TOC analysis of the effluent (TOC analysis, User Manual), which was collected during the experiments (Tables 4.8 -4.10). At the beginning of the analysis, a calibration curve was obtained. That curve represents a relationship between the dimensionless concentration ($C/C_0$) of nano-spheres suspension and its carbon content corresponding to pure nano-spheres (Figure 4.22**)**. The calibration test was done with different concentrations of nano-spheres suspension in the brine: 600 ppm ($C/C_0$=100%), 300 ppm ($C/C_0$=50%), 150 ppm ($C/C_0$=25%), and 0 ppm. The highest concentration (600 ppm) is determined by the concentration of nano-spheres used in the core flood expeirments. Results of the tests showed that the carbon content corresponding to $C/C_0$=100% is equal to 138 ppm, where the same parameter for polyacrylamide is equal to 220 ppm. It also appears from Figure 4.22 that the relation between $C/C_0$ and the carbon concentration is linear. The later observation is well expected for this type of test.

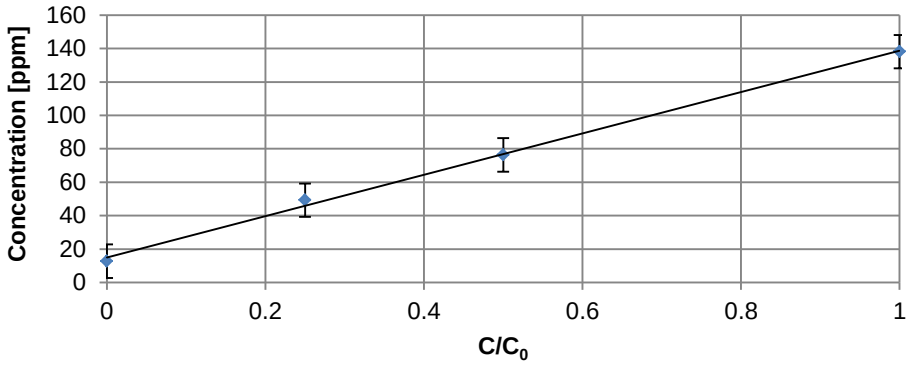


**Figure 4.22**- Calibration curve for the organic content of nano-spheres

Propagation of nano-spheres through the Boise core with multiphase saturation during slugs (***Exp. 4a***) and continuous injection (***Exp. 4b***) was studied using TOC analyser (Figure 4.23). Results of the TOC analysis in Figure 2.23 showed that the carbon content of the produced fluid remains small, even after 2 PV of particles had been injected into the core $C/C_0$=~9 % (until **NS4**). The pressure drop dynamics and the effluent analysis have shown that the injection of the spheres' slugs results in poor propagation through the core.

The propagation of the spheres slightly improves during its continuous injection. The effluent analysis showed a slight increase in carbon content in the effluent $C/C_0$ up to 14 % (Figure 4.23, NS5).

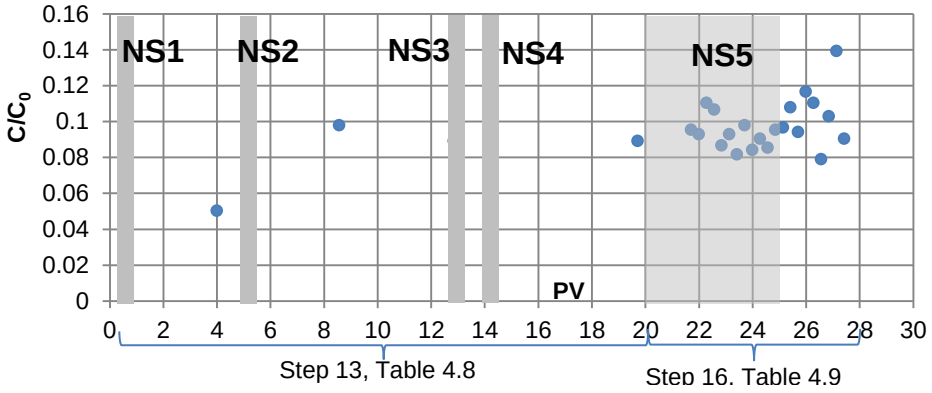


**Figure 4.23**-Results of the effluent analysis (initial concentration $C_0$-138 ppm)

Retention (µg/g) of the spheres in the core during its continuous injection for 5 PV was calculated according to eq. 2 (Manichand and Seright, 2014):

$$R=\frac{C_{in}\cdot\Sigma\left(\Delta V\cdot(1-Cp/C_{in})\right)}{M_{rock}} \quad (4.2)$$

where $M_{rock}=V_{swept}\cdot(1-\varphi)/\varphi\cdot\rho_{rock}$ – mass of the rock, mg; $C_{in}$=600 mg/l- initial concentration of the injected spheres; $\Delta V$-incremental produced volume, l; $C_p$-produced concentration, mg/l; $\rho_{rock}$=2.65 g/cm$^3$- density of the rock; φ-porosity; $V_{swept}$- effective volume, l.

The obtained value of the retention is high and accounts for 592±12 µg/g. This retention number represents a minimum limit, as after the injection of 7PV of the spheres, the producing concentration is still only 10 % of the injected concentration. Therefore, we concluded that there is a high retention of the spheres in the porous media with very few passing the inlet section of the core (~ 6 cm).

***Experiment #5***

Another experiment (Table 4.10) carried out in the study shows the propagation of nano-spheres at high brine salinities 30 g/l in the Bentheimer core. During the injection, the resistance factor over the core was obtained. The resulting increase in RF is marginal and is equal to 0.2 units over 60 PV of injected nano-spheres (Figure 4.24**)**. The reason for the slow resistance factor build-up might be a better propagation of the nano-spheres at high brine salinities. That is supported by the results of the TOC analysis (Figure 4.24). The analysis showed that the average concentration of the carbon in the effluent accounts for 85±2% of the initial concentration (137 ppm). Apparently, the rest of the particles are retained in the core and this volume is responsible for the slight resistance factor build-up.

The possible explanation of better propagation of nano-spheres in the core at higher salinities is lower repulsion between the spheres.

Variation in the TOC data throughout the experiment implies that the propagation of nano-spheres is a complex dynamic process which consists of plugging and releasing the spheres in the core. Indeed, we assume that after the pugging of the core, the carbon concentration in the effluent decreases and the pressure increases. The opposite takes place when particles get released from the core, pressure decreases and the carbon content increases.

In order to compare the level of retention in 5 g/l brine with the 30 g/l brine, the retention was calculated for the Experiment #5 as well. The calculated

value for the retention in 30 g/l brine is equal to 81.2±9 µg/g. That is 7.3 times smaller than the retention of the spheres aged in 5 g/l brine.

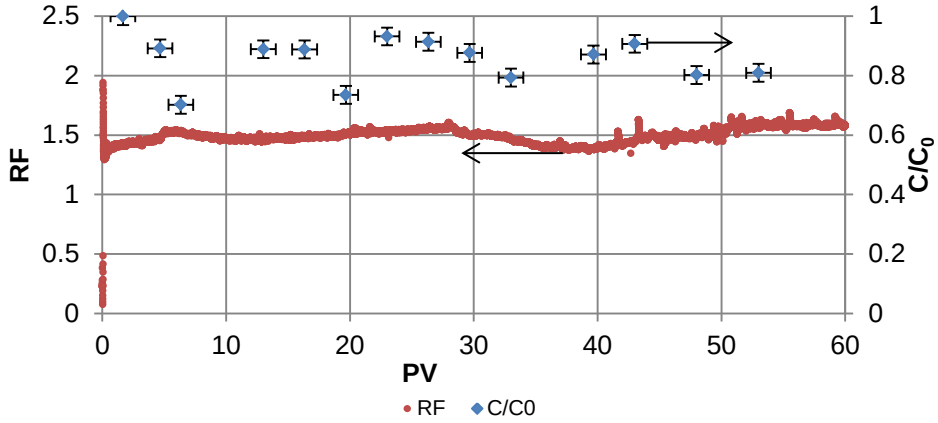


**Figure 4.24**- Relationship between $C/C_0$ , RF and PV injected

***Experiment #6***

An additional core flood experiment # 6 was conducted by the injection of nano-spheres aged in 30 g/l brine into a Boise core at multiphase saturation (Table 4.10). After a residual oil saturation was achieved, the spheres were continuously pushed into the core at 1 ft/day. The resistance factor build-up during the injection was marginal and equal to 1.5 over 2PV (Figure 4.25). Although the TOC analysis was not done in this experiment, the pressure drop dynamic indicates a good propagation in the core. The following slug injection did not show any rapid increase in the resistance factor.

Summarizing the results of Experiments #5 and 6 it can be concluded that regardless of core mineralogy and saturation, a good propagation can be achieved by increasing the brine salinity.

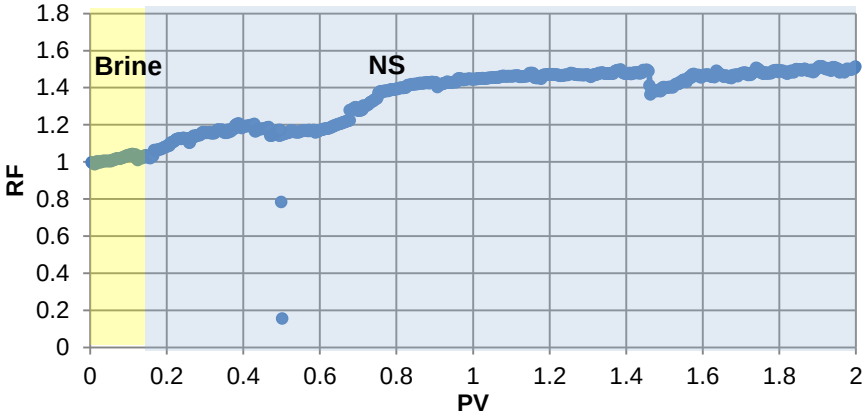


**Figure 4.25**- Relationship between RF and PV injected (multiphase saturation)

## 4.6. Discussion

The flow of nano-spheres in porous media is mostly affected by the retention and is considered to be an important phenomenon which influences the economic aspects of their implementation in practice (Sorbie 1991; Farajzadeh et al., 2015). There are different possible mechanisms responsible for the retention in porous media: mechanical entrapment, hydrodynamic retention, jamming and adsorption on a rock surface. These mechanisms for conventional polymers were studied by Sorbie (1991), Denys (2003), Spildo (2009), Farajzadeh (2015). However, there are limited studies that have been conducted for the flow of nano-spheres in porous media.

The experiments in single phase and multiphase saturations in Berea, Boise and Bentheimer cores were carried out in our study. An overview of six core flood experiments is shown in table 4.11.

**Table 4.11**- Summary of core flood experiments

| Name of the experiment | Description | Objective | Results |
|---|---|---|---|
| Core flood experiment #1 | Injection of nano-spheres into the the brine saturated Berea core at a variety of flow rates. | Study the RRF in outcrop cores with single and multiphase saturations. | The asymptotic decline of RRF with the flow rate was obtained. |
| Core flood experiment #2 | Injection of nano-spheres into the brine saturated Bentheimer core. | | The asymptotic decline of RRF with the flow rate was obtained. |

| | | | |
|---|---|---|---|
| Core flood experiment #3 | Injection of nano-spheres into a Bentheimer core at residual oil saturation. | Study the propagation and RF in outcrop cores with single and multiphase saturations. | The asymptotic decline of RRF with the flow rate was obtained. |
| Core flood experiment #4 | Injection of nano-spheres into the Boise core at residual oil saturation and at low brine salinity. Propagation of the particles was studied via the pressure drop dynamic and the effluent analysis. | | Poor propagation of spheres through the core was observed at low brine salinities. The pressure drop analysis showed that particles accumulate mostly in the inlet section of the core. The effluent analysis showed that the maximum recovery of the particles accounts for 12% of the total mass. |
| Core flood experiment #5 | Injection of nano-spheres into the Bentheimer core at high brine salinities. | | A good propagation of the nano-spheres through the core was achieved. Effluent analysis showed the recovery of 85% of the total mass. Pressure drop did not increase much over time as well. |
| Core flood experiment #6 | Injection of nano-spheres into the Boise core at residual oil saturation and at high brine salinities. | | Pressure drop analysis and effluent analysis showed a good propagation of nano-spheres through the core with marginal resistance factor build-up. |

One of the possible mechanism of the spheres retention in porous media is a jamming effect. It happens when particles simultaneously migrate through a pore throat. They form a clog of arrested particles which will reduce the permeability (Sendekie, and Bacchin, 2016). Porous media contain multiple pore throats which makes the jamming effect more evident. This effect can be an explanation of the clogging which occurs when the size of the particles is smaller than size of pore throats. Indeed, the comparison of pore throat size distribution of the Boise core and nano-spheres size distribution has shown that there is a significant difference between modes of the distributions (Figure 4.26). It means that spheres might easily propagate through the core without entrapment. However, the results of the core flood experiment #4, conducted at low brine salinities 5 g/l, suggest that the spheres are trapped in the first section of the core during the slug injection.

The results of experiment #6 demonstrated that at high brine salinities (30 g/l) the propagation of nano-spheres is the best. However, the resistance factor

build-up is low and might not be enough for the effective diversion of water. That might be explained by the attraction between particles at high brine salinities and the formation of agglomerates. However, these agglomerates are soft and do not cause a significant permeability reduction resulting in better propagation through a core.

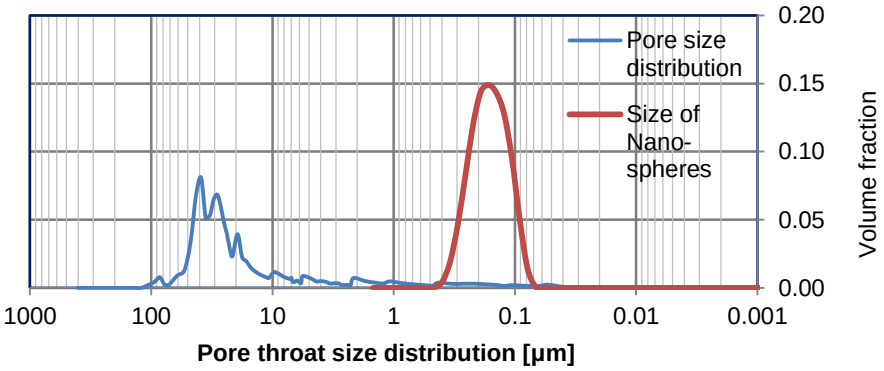


**Figure 4.26-** Comparison of the pore throat size distribution of the Boise core with size distribution of nano-spheres aged at 5 g/l

To demonstrate the difference in the propagation of the spheres in outcrop cores with different salinities, the RF build-up curves obtained during the nano-spheres injection in core flood experiments # 4b, #5 and #6 were plotted on the same graph to compare their dynamic (Figure 4.27). From the data it can be seen that in low brine salinity 5 g/l the increase in the RF is much faster than in high brine salinity 30 g/l regardless of the saturation and minerology of the cores. It confirms the influence of brine salinity on the propagation in porous media.

Although there is no significant difference between the size distributions of the spheres aged in 5 g/l brine and 30 g/l, the difference in propagation of the spheres aged in these types of brine is substantial (core flood experiments #4 and #6). That might be also explained by the differences in the resistivity to deformation of the particles. A similar difference in the resistivity to deformation at different salinities was observed with Preformed particles gels (PPGs) (Imqam et al., 2015), which have similar chemical composition to the nano-spheres. In the case of PPGs, the resistivity has a higher influence on propagation rather than the ratio between the pore throat size and the particles size.

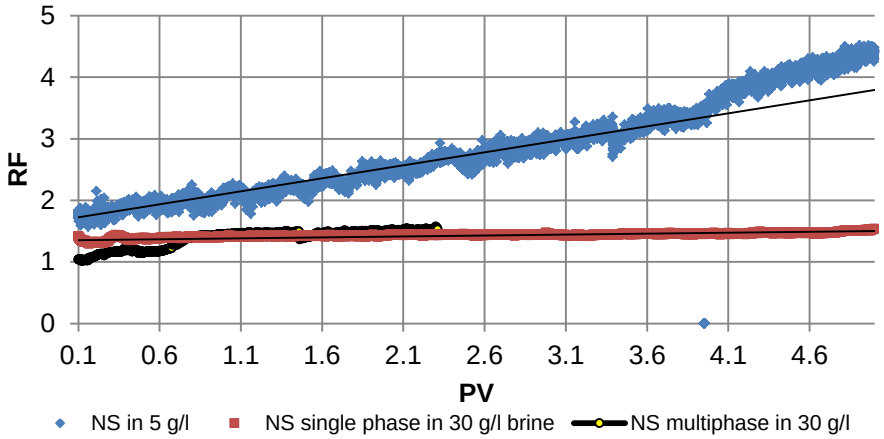


**Figure 4.27-** Combined RF curves from core flood experiments # 4b (represents overall RF from the core), #5 and #6

Electrostatic interaction between the spheres and rock surface can also be responsible for the propagation of the spheres in porous media. Indeed, in high brine salinities, particles attract each other forming soft agglomerates. At the same time, since the nano-spheres are negatively charged, and the rock minerals are negatively charged as well, significant repulsion might take place. However, in high brine salinity, ions screen a charge on the rock surface allowing for the propagation of the aggregates.

In our experiments, it was also observed that a non-linear correlation between the flow rate and a permeability reduction factor does exist in outcrops (Boise, Bentheimer and Berea) regardless of saturation. Probably, nano-spheres are able to form deformable layers on the surface of rocks. The thickness of the adsorbed layer might contain multiple particles together which can be explained by agglomeration of particles. Agglomeration of particles was confirmed with TEM and DLS tests (Chapter 3). A hypothesis about the clustering of particles on a surface of rocks was also proposed by Almohsin et al. (2014) for experiments conducted with nano-gels.

Summarising the discussed mechanisms of the spheres' retention, it is probable that the spheres adsorption and jamming might take place in porous media. Moreover, salinity is a major factor which affects the retention of the spheres. Therefore, in order to decrease the retention of the spheres, its

chemistry has to be designed specifically for the conditions of the oil field (brine salinity, temperature, type of oil and mineralogy of porous media).

The results of our study showed that due to the small size of nano-spheres, they can propagate into both higher and less permeable layers. Therefore, the injection of the spheres into the reservoir might regulate the mobility ratio in the whole reservoir by affecting the permeability for water and not oil.

## 4.7. Conclusions

1. The workflow for the study of nano-spheres propagation in porous media was designed.

2. The pressure drop dynamics and the effluent analysis at the conditions of the experiment (brine salinity 5 g/l, porous media: Boise and Bentheimer outcrops) showed that nano-spheres have poor propagation during its injection into cores at low brine salinities in single and multiphase saturated cores. The continuous injection of the spheres results in its propagation, however, according to the pressure drop behaviour and effluent analysis, this process is slow. Nevertheless, it was experimentally demonstrated that the propagation is improved in high salinity brine - 30 g/l for both single and multiphase saturated cores but resistance factor build-up is small.

3. Marginal residual oil recovery was obtained from the Boise outcrop core during the injection of nano-spheres aged in 5 g/l brine. The spheres did not propagate well in the core and it was restricted by the inlet section of the core.

4. A non-linear correlation between the flow rate and a permeability reduction factor exists in outcrop cores (Boise, Bentheimer and Berea) regardless of saturation. An increase of the flow rate (velocity) resulting in the decrease of the RRF. That relation is reversible and at lower flow rates higher values of RRF were observed.

5. Core flood experiments carried out in single phase and multiphase saturated outcrop cores revealed that the RRF is smaller in the multiphase saturated core than in the single phase saturated core .

6. Further work is required to evaluate the conditions under which the performance of the nano-spheres can be improved. The influence of the concentration of nano-spheres on the resistance factor in porous media should be studied. An optimal brine salinity has to be found where both the resistance

factor build-up and propagation are sufficient for in-depth profile modification. Additional micro fluidic experiments can be carried out to better understand the mechanism of the particles propagation in porous media.

# Chapter 5

## Summary and Conclusions

The main results of the thesis are discussed in this chapter. It is mostly linked to the studies with crosslinking polymer and nano-spheres for the conformance control in heterogeneous reservoirs. Some results of the study can be applied to a wide pool of fluids (e.g. cleaning acryl-based polymers from an emulsion, propagation of gelants in porous media, and microscopy of suspensions). The advantages and disadvantages of the studied technologies are outlined which can be used as a guideline for the application in a field.

Finally, recommendations for future research are given. They are mostly connected to studies which are presented in the thesis.

The improvement of sweep efficiency in heterogeneous reservoirs is a complex problem which can be addressed by the injection of polymer fluids deep into the formation. The injected fluids increase the residual resistance factor in high permeable layers and divert the flow of subsequently injected water into low permeable layers (*the case with a cross-flow*). The efficiency of this process depends on the chemical composition of the fluids, as well as reservoir characteristics. In our work, a crosslinked polymer and a nano-spheres suspension were studied. These fluids have the potential for application in practise because of possible deep propagation into a reservoir and later residual resistance factor build up. However, their propagation and residual resistance factor might be limited in certain reservoir characteristics (Imqam et al. 2105; Glasbergen et al., 2014). Hence, it is important to study the main factors which influence the propagation and resistance in porous media. It also helps to select criteria important for the development of the new gel systems.

***Firstly***, ***crosslinking HPAM was selected*** as a candidate for in-depth diversion (Chapter 2). It increases the resistance factor in porous media by the viscosity build-up over time. In order to delay the cross-linking reaction, a polyanion was used. Together with PEI (polycation crosslinker), it forms Poly Electrolyte Complex (PEC) which hides PEI from the interaction with the polymer. A series of rheology tests showed that the initial viscosity of the polymer system is low and equal to the viscosity of the polymer. However, due to the gelation process, the viscosity increases over time until the gel point is reached. The kinetics of the gelation process depends on the temperature, brine salinity and the concentration of the cross-linker (PEI). The selected composition successfully delays the gelation of the HPAM in bulk for 8 days. *Nevertheless, it is important to understand what the difference between the kinetics of the gelation process in bulk and in porous media is?*

The injection of the gelant into the 1 m core and a series of filtration ratio tests revealed that despite the initial viscosities of the gelant and HPAM being equal in bulk, the initial resistance factor of the gelant (HPAM+PEI+retardant) in the core is higher than the resistance factor of HPAM. That difference might be explained by the creation of micro gel particles after the mixing of the components of the recipe. Subsequently the flow of gel particles may block pore throats resulting in an additional pressure drop over the core. However, the concentration of the particles is low and it does not affect the viscosity of the gelant much. Hence, the sensitivity of the rheometer is not enough to measure

the influence of the particles on the viscosity. The hypothesis about the formation of micro gel particles in a crosslinking polymer was supported with a series of filtration ratio tests conducted in our study. The results of these tests suggest that the interaction between the cross-linker and the polymer happens after mixing components together which is unfavourable. It can also be recommended that filtration ratio tests are a better approach to study the gelation of cross-linking systems.

The continuous injection of the crosslinking polymer into the core revealed the increase of the pressure drop in the core over time. Most likely, it indicates the in-situ gelation of the polymer. The results of the tracer analysis after the crosslinked polymer was injected into the core showed the reduction of the effective porosity by 6.2 % and a 20 times larger dispersion coefficient. That confirms the formation of a gel in porous media.

Micro CT experiments conducted with the samples drilled from the core after the flood experiment was finished showed that the polymer is distributed mostly in smaller pores of the core. It is assumed that the gel is formed mostly in smaller pores because it is easier to form cross-linking networks in smaller openings than in bigger pores. The large increase in the dispersion coefficient suggests that this must have resulted in the creation of a few dominant flow paths isolated from each other by closure of the smaller pores. Thus it explains that the gel easier blocks smaller pores than the bigger ones which is undesired.

While the cross-linking polymer flows in porous media, chromatographic separation might take place between the components of the gelant (Li et al., 2009). Hence, the final gel might lose its resistance. To avoid the separation, gel or gel particles must be formed on the surface and later injected into a reservoir. That can be achieved with ***nano-spheres which is a suspension of prefabricated elastic polymer particles***. Another advantage of nano-spheres over the cross-linking polymer is the simplicity of preparation in a field. Indeed, a mother solution is being mixed with water in a tank to obtain a selected concentration of the spheres. Afterwards, the suspension is ready for injection.

It is widely accepted that the spheres preferably flow along the most permeable layers of a heterogeneous reservoir. Initially, the average size of spheres is small (~175 nm at 5 g/l brine) and the pressure gradient is enough to push the spheres deep into the reservoir. However, when the spheres are swollen and they reach the region of the reservoir where the gradient of pressure is not high enough, they can accumulate without further propagation. Accumulated

spheres divert the flow of subsequently injected water into low permeable layers with higher oil saturation (*a case with a cross-flow*).

The polymer spheres can contain the following monomers: acrylamide, acrylic acid, and 2-Acrylamido-2-methylpropane sulfonic acid. The composition of spheres makes them negatively charged and determines their physical properties, such as swelling over time by the absorption of brine, interaction with ions of brine and elasticity. The synthesis of the spheres is done according to the inverse-emulsion polymerisation method. Hence the spheres are dispersed in an emulsion when they are ready for the injection. However, to study the size distribution of nano-spheres it is required to separate the spheres from the emulsion in order to exclude the negative influence of oil on the characterisation.

It is also important to separate the polymeric spheres (polymers) from mineral oil where the spheres are initially dispersed for the study of their propagation in core flood experiments. Normally, according to a standard procedure, an effluent is analysed to estimate the propagation via an organic content of the produced fluid. A polymer concentration in the produced fluid is related to the organic content. However, there has not been any reliable procedure for the study of the nano-spheres separation from an emulsion.

A procedure for the separation of spheres from emulsion with acetone was designed (chapter 3.1). The extracted polymeric particles were dried under vacuum. Later they were dispersed in brine and subsequently treated with ultrasound to obtain a homogeneous suspension. The efficiency of the separation of the nano-spheres were confirmed with DLS and TEM.

Size distribution of the spheres and their swelling over time were done with TEM according to the specially designed procedure which includes the image analysis algorithm. That algorithm can be used for the estimation of agglomeration and swelling rates of the spheres with TEM. It was demonstrated that after several months of injection, the nano-spheres will likely block the reservoir, which is unfavourable (chapter 3.5). The procedure of the estimation of the particles growth can be applied to similar polymeric nano-particles and polymers distributed in an emulsion form.

It is reported in literature (Yuqin et al., 2012; Almohsin et al., 2014) that application of the spheres in practise is not limited by brine salinities and temperatures. However, the results of our experiments revealed that the brine

salinity plays a crucial role in the propagation in porous media due to the chemical content of the spheres (chapter 4).

The mechanism of nano-spheres propagation in porous media at different salinities was studied in this work. According to our study it was demonstrated, that in low brine salinities (5 g/l) the spheres have a poor propagation in porous media but in high brine salinities (30 g/l) the propagation improves. Apparently, the size of individual spheres is not responsible for the difference in the propagation because the average size of the swollen spheres is more than 100 times smaller than the average size of pore throats (the size is compared with the size distribution of pore throats of the Boise core). Thus, the difference in propagation might be explained by the repulsion between particles in low brine salinities which prevents particles from going into pore throats. At moderate brine salinities, particles are attracted to each other which improves the transport through porous media. If the salinity of the brine is high, then the repulsion is mostly screened and agglomerates are formed. These agglomerates are soft and might cause a pressure fluctuation without preventing the particle propagation. The influence of salinity on the propagation of the spheres in porous media was observed for different outcrop cores (Boise, Bentheimer and Berea ) regardless of their saturation with oil. It is also possible that at different brine salinities the resistance to the deformation of the spheres changes as well. For example, at high brine salinities the particles are softer and the propagation is better.

It is assumed in the literature (Goudarzi et al., 2014) that preformed particles gels (e.g. micro spheres) can reduce residual oil in porous media. To study this, a core flood experiment was conducted with nano-spheres aged in 5 g/l brine using a heterogeneous Boise core at the residual oil saturation (Chapter 4.5, experiments 4a and 4b). Results of our experiment suggest that the propagation of the spheres is poor and is mostly limited to the inlet section of the core. The injection of slugs of nano-spheres, as well as continuous injection in a tertiary mode showed a marginal oil recovery. Most likely, some oil recovery was observed due to the small-scale heterogeneity of the core.

Another important phenomenon which was experimentally demonstrated for the flow of nano-spheres in porous media is an asymptotic decline of the residual resistance factor to its minimum value with the flow rate (Chapter 4, experiments 1-3). A series of core flood experiments at single and multiphase saturations showed that the increase of the pressure drop over the core leads to

the decrease in the residual resistance factor. Probably, nano-spheres are able to form deformable layers on the surface of rocks. The thickness of the adsorbed layer might contain multiple particles together, since particles form agglomerates over time. Another experimental observation was that at high flow rates there was a lower resistance factor. That can be used in practise when the spheres are being injected into a reservoir at higher flow rates having a lower resistance to the flow, whereas deep in the reservoir, the flow rates are lower and the resistance factor is higher.

Core flood experiments carried out in single and multiphase saturated outcrop cores also showed that the RRF might be smaller in a multiphase saturated core due to possibly less adsorption on the rock surface.

Finally, it can be stated that every fluid has its own area of application. There is no system which can be equally efficient in a variety of reservoir characteristics. Therefore, for every practical case, an appropriate solution has to be selected. The advantages and disadvantages of the studied systems and main conclusions which are relevant for the practical applications of the fluids are outlined in table 5.1.

**Table 5.1**- General recommendations for application in a field

| **Polymer systems for the in-depth diversion** | **Disadvantages** | **Advantages** |
|---|---|---|
| 1. Cross-linking polymer | a. Micro gel particles are created after mixing the polymer with the crosslinker. That increases the resistance factor of the gelant in comparison to the fluid injected before.<br>b. Gelation time is temperature and salinity dependent. Unfavourable reservoir characteristics can limit the application of the gel. | a. A good propagation can be achieved in low brine salinities with a prolonged gelation time.<br>b. Gelation time can be adjusted to temperature and salinity of a reservoir. |
| 2. Nano-spheres suspension | a. Poor propagation in the matrix of a reservoir in low brine salinity.<br>b. Although propagation in high brine salinity is good, the resistance factor build up is slow and the spheres have low resistance factor in porous media. | a. Easy to prepare a nano-spheres suspension in a field.<br>b. Can be successfully used for near well bore diversion (e.g. the isolation of fractures). |

## 5.1. Recommendations for future research

The flow of fluids such as cross-linking polymer and nano-sphere suspensions in porous media is a complex process which depends on the rock-fluid interaction and the interaction between the components of the fluids. It is influenced by the flow rate which are governed by hydrodynamic forces, concentration, brine salinities and temperatures. Additional experimental and simulation work is required to better understand the mechanisms which underline in-situ gelation and propagation in porous media. That will help to define criteria for the successful application and develop new systems which will combine the advantages of both fluids. A proposal for additional studies is outlined below.

The improvement of the polyelectrolyte comple to hide the organic cross-linker PEI from the interaction with the polymer has to be done for different salinities, pH and temperatures using, for example, differential scanning calorimetry (Vebrel et al., 1993; Spruijt, 2012). The latter is more sensitive method to estimate the cross-linking of a polymer than the measurement of the viscosity. Eventually, that might help effectively delay the cross-linking reaction in different reservoir characteristics.

A series of experiments on the chromatographic separation has to be carried out to show how robust the system is in different reservoir characteristics (e.g. temperature, brine salinity, and type of the rock).

Oil recovery by nano-spheres from outcrop cores can be studied at high brine salinities. According to our study, the propagation of the spheres in high brine salinity improves. Therefore, the residual oil recovery might be improved as well. Additional core flood experiments are required.

The mechanisms of clogging at pore scale by nano-spheres can be studied with a microfluidic device. The device might have transparent micro channels with a sinusoidal shape which includes consecutive pore throats and pore bodies. During the flow of nano-spheres through the channel they interact with each other and the walls of the channel. The visualisation of the process can be done with a camera. In addition to that, the experiment can be carried out at different temperatures and the flow process can be monitored with pressure transducers. That experiment might explain the difference in the propagation of nano-spheres at different salinities, temperatures, as well as possible influence of the flow rate and concentration on the clogging in the microchannel.

A theoretical explanation of the particles propagation can be made on the basis of pore scale modelling of the particles flow. The better propagation of the particles in high salinities rather than in low salinities can be simulated with a DLVO type of interaction.

Agglomeration and swelling of the spheres can be studied with a Cryo-SEM where the particles are submerged in a brine. This procedure of particles preparation for the experiment excludes an artefact when the evaporation of brine takes place influencing the interaction with each other. The image analysis algorithm which was applied for the study of the size of spheres with TEM can be used for the study with Cryo-SEM as well.

A new system for the conformance control might be designed as prefabricated soft gel particles. Hence, no chromatographic separation takes place in the reservoir. Another advantage is the facilities for the preparation of the particles in a field are minimised. The size distribution of the particles should be narrow with a standard deviation corresponding to the permeability contrast of the layers of the heterogeneous reservoir. It is desired that particles can propagate without high retention in porous media which later swell by many folds in a target zone. The trigger for the swelling should be a time effect. The time will be associated with the distance of propagation.

It is also recommended to design nano-particles which can reduce the permeability of water and leave unaffected the permeability to oil. These particles can be continuously injected into a reservoir with the propagation into less and higher permeable layers.

# Bibliography


1. Alberts, B., Johnson, A., Lewis J. 2002. Molecular Biology of the Cell. 4th edition. New York: Garland Science.

2. Al-Maamari, R.S., Al-Hashami, A.R., Al-Sharji, H.H., Dupuis, G., Bouillot, J., Templier, A., Zaitoun A. 2015. Development of Thermo-Gels for in Depth Conformance Control. SPE Asia Pacific Enhanced Oil Recovery Conference, 11-13 August, Kuala Lumpur, Malaysia. http://dx.doi.org/10.2118/174640-MS.

3. Almohsin, A., Bai, B., Imqam, A. et al. 2014. Transport of Nanogel through Porous Media and its Resistance to Water Flow. Presented at the SPE Improved Oil Recovery Symposium, Tulsa, Oklahoma, 12-16 April. SPE-169078-MS. http://dx.doi.org/10.2118/169078-MS.

4. Al-Muntasheri, G. A., Hisham A. Nasr-El-Din, H.A., Zitha, P.L.J. 2008. Gelation Kinetics and performance evaluation of organically cross-linked gel at high temperature and pressure. SPE Journal, 13(3), SPE-104071-PA. http://dx.doi.org/10.2118/104071-PA.

5. Al-Muntasheri, G. A., Zitha, P.L.J.2009. Gel under Dynamic Stress in Porous Media. New Insights using Computed Tomography, Paper SPE-126068-MS, presented at the SPE Saudi Arabia Section Technical Symposium, Al-Khobar, Saudi Arabia, 9-11 May. http://dx.doi.org/10.2118/126068-MS.

6. An, Y., Solis, F.J., Jiang, H. A Thermodynamic Model of Physical Gels. 41. http://imechanica.org/files/Physical%20Gel.pdf.

7. Avizo User's Guide. 2015. Avizo9, http://www.vsg3d.com.

8. Bai, B. and Zhang, H. 2011. Preformed-Particle-Gel Transport Through Open Fractures and Its Effect on Water Flow. SPE Journal. 16 (02) http://dx.doi.org/10.2118/129908-PA Document IDSPE-129908-PA.

9. Bai, B., Wei, M., and Liu, Y. 2013. Field and Lab Experience With a Successful Preformed Particle Gel Conformance Control Technology. Presented at the SPE Production and Operations Symposium, Tulsa,

Oklahoma, 23-26 March. SPE-164511-MS. http://dx.doi.org/10.2118/164511-MS.

10. Bailey, B., Crabtree, M., Tyrie, J., Elphick, J., Kuchuk, F., Romano, C., Roodhart, L. 2000. Water control, Oilfiled review, 30-51.

11. Bantz, C., Koshkina, O., Lang, T., Galla, H.-J., Kirkpatrick, C.J., Stauber, R.H., and Maskos, M. 2014. The surface properties of nanoparticles determine the agglomeration state and the size of the particles under physiological conditions. Beilstein J. Nanotechnology, 5:1174-1786.

12. Barari M., Abdollahi, M., and Hemmati, M. 2011. Synthesis and Characterisation of High Molecular Weight Polyacrylamide Nanoparticles by Inverse-emulsion Polymerization. Iranian Polymer Journal 20 (1): 65–76. http://journal.ippi.ac.ir.

13. Barth, H.G. 1984. Modern methods of particle size analysis.

14. Batchelor, G.K. 2000. An Introduction to Fluid Dynamics. Cambridge University Press.

15. Batterham, R.J., Hall, J.S. and Barton, T. 1981. Pelletizing kinetics and simulation on full scale balling circuits, 3rd International Symposium on Agglomeration: A136-A151.

16. Bayles, A.V., Squires, T.M., and Helgeson, M.E. 2016. Dark-field differential dynamic microscopy, Soft Matter, (12): 2440-2452.

17. Broesta, D., Medjahed, F., Lecourtierm, J. et al. 1995. Polymer Adsorption/Retention in Porous Media: Effects of Core Wettability on Residual Oil. SPE Advanced Technology Series 3 (1), 103-112. SPE-24149-PA.http://dx.doi.org/10.2118/24149-PA.

18. Burdine, N.T., Gournay, L.S., and Reichertz, P.P. 1950. Pore size distribution of petroleum reservoir rocks. Journal of Petroleum Technology. 2(7). SPE-950195-G. http://dx.doi.org/10.2118/950195-G.

19. Castle, M. and Keller, J. 2007. Rolling Ball Background Subtraction (ImageJ). http://imagej.net/Rolling_Ball_Background_Subtraction

20. Chiappa, L., Mennella, A., Lockhart, T.P. et al. 1999. Polymer Adsorption at the Brine-Rock Interface: The Role of Electrostatic Interactions and Wettability. J. Pet. Sci. Eng. 24(2-4): 113-122. doi: 10.1016/S0920-4105(99)00035-2.

21. Cohen, Y. and Christ, F.R. 1986. Polymer retention and adsorption in the flow of polymer solutions through porous media. SPE Reservoir Engineering. SPE-12942-PA. 1(02). http://dx.doi.org/10.2118/12942-PA.

22. Cordova, M., Cheng, M., Trejo, J., Johnson, S. J., Willhite, G. P., Liang, Jenn-Tai, and Berkland, C. 2008. Delayed HPAM Gelation via Transient Sequestration of Chromium in Polyelectrolyte Complex Nanoparticles, Macromolecules, 41 (12): 4398-4404.

23. Crespo, F., Reddy, B. R., Lewis, C.A., Eoff, L.S. 2013. Recent Advances in Organically Crosslinked Conformance Polymer Systems, Paper SPE-164115-MS presented at the SPE International Symposium on Oilfield Chemistry, The Woodlands, Texas, USA, 8-10 April. http://dx.doi.org/10.2118/164115-MS.

24. Crespo, F., Reddy, B.R., Larry Eoff, L., Christopher Lewis, C., Pascarella, N. 2014. Development of a Polymer Gel System for Improved Sweep Efficiency and Injection Profile Modification of IOR/EOR Treatments, Paper IPTC-17226-MS, presented at the International Petroleum Technology Conference, Doha, Qatar, 19-22 January. http://dx.doi.org/10.2523/IPTC-17226-MS.

25. CytoViva Optical Microscope User Manual.

26. Denton, A. R. 2013. Counter ion Penetration and Effective Electrostatic Interactions in Solutions of Polyelectrolyte Stars and Microgels. Phys. Rev. E 67, 011804.

27. Denys, K. 2003. Flow of Polymer Solutions Through Porous Media. PhD thesis, TU Delft: Delft University of Technology, Delft (November 2003).

28. Dickie, R. A., Labana, S. S., Bauer, R. S. 1988. Cross-Linked Polymers. Chemistry, Properties, and Applications, American Chemical Society. DOI: 10.1021/bk-1988-0367.

29. Domingos, R.F., Baalousha, M.A., Ju-Nam, Yon, Reid,M.M., Tufenkji, N., Lead, J.R., Leppard, G.G., and Wilkinson, K.J. 2009. Characterizing Manufactured Nanoparticles in the Environment: Multimethod Determination of Particle Sizes. Environmental Science and Technology, 43: 7277–7284.

30. Edited by Fernandez-Nieves, A., Wyss, H.M., Mattsson, J., and Weitz, D.A. 2011. Microgel Suspensions: Fundamentals and Applications. WILEY-VCH Verlag & Co. KGaA.

31. Ehrenfried D.H. 2013.Impact of Viscoelastic Polymer Flooding on Residual Oil Saturation in Sandstones. MS thesis, The University of Texas at Austin, Austin, Texas.

32. Elsharafi, M., Bai, B. 2015. Minimizing Formation Damage for Preformed Particle Gels in Mature Reservoirs. Paper presented at SPE Asia Pacific Enhanced Oil Recovery Conference, 11-13 August, Kuala Lumpur, Malaysia 174645-MS. http://dx.doi.org/10.2118/174645-MS.

33. Fang, Q., Chen, J., Lu, C., Yin, D., and Li, Y. 2015. Study on Relation between Hydrodynamic Feature Size of HPAM and Pore Size of Reservoir Rock in Daqing Oilfield. Advances in Materials Science and Engineering. (2015). http://dx.doi.org/10.1155/2015/139284.

34. Farajzadeh, R., Andrianov, A., Krastev, R., Hirasaki, G.J., Rossen, W.R. 2012. Foam-oil interaction in porous media: implications for foam assisted enhanced oil recovery. Advances in Colloid and Interface Science 183-184.1-13. http://dx.doi.org/10.2118/154197-MS.

35. Farajzadeh, R., Lotfollahi, M., and Bedrikovetsky, P. 2015. Simultaneous Sorption and Mechanical Entrapment During Polymer Flow Through Porous Media. Presented at SPE Kuwait Oil and Gas Show and Conference, Mishref, 11-14 October, SPE-175380-MS. http://dx.doi.org/10.2118/175380-MS.

36. Farooqi, Z.H., Khan, H.U., Shah, S.M., Siddiq, M. 2013. Stability of poly(N-isopropylacrylamide-co-acrylic acid) polymer microgels under various conditions of temperature, pH and salt concentration. Arabian Journal of Chemistry: 1878-5352. http://dx.doi.org/10.1016/j.arabjc.2013.07.031.

37. Frampton, H., Morgan, J.C., Cheung, S.K., Munson, L., Chang, K.T., Williams, D. 2004. Development Of A Novel Waterflood Conformance Control System. Presented at SPE/DOE Symposium on Improved Oil Recovery, 17-21 April, Tulsa, Oklahoma, USA. SPE-89391-MS. http://dx.doi.org/10.2118/89391-MS.

38. Gelhar, L.W. and Axness, C.L. 1983. Three- Dimensional Stochastic Analysis of Macrodispersion in Aquifers. Water Resources research, 19 (1): 161-180. DOI: 10.1029/WR019i001p00161.

39. Genuchten, van M. Th. and Parker, J.C. 1984. Boundary Conditions for Displacement Experiments through Short Laboratory Soil Columns. Soil Sci. Soc. Am. J. 48: 703- 708.

40. Giavazzi, F., Haro-Pérez, C. and Cerbino, R. 2016. Simultaneous characterization of rotational and translational diffusion of optically anisotropic particles by optical microscopy. Journal of Physics: Condensed Matter, Volume 28, Number 19.

41. Giussi, J.M., Velasco, M.I., Longo, G.S., Acostab, R.H., and Azzaroni, O. 2015. Unusual temperature-induced swelling of ionizable poly(N-isopropylacrylamide)-based microgels: experimental and theoretical insights into its molecular origin. Soft Matter, 11: 8879-8886. DOI: 10.1039/c5sm01853f.

42. Glasbergen, G., Abu-Shiekah, I., Balushi, S., van Wunnik, J. 2014. Conformance Control Treatments for Water and Chemical Flooding: Material Screening and Design, Paper SPE-169664-MS, presented at the SPE EOR Conference at Oil and Gas West Asia, Muscat, Oman, 31 March-2 April. http://dx.doi.org/10.2118/169664-MS.

43. Goudarzi, A., Almohsin, A., Varavei, A., Delshad, M., Bai, B., Sepehrnoori, K. 2014. New Experiments and Models for Conformance Control Microgels. SPE Improved Oil Recovery Symposium, 12-16 April, Tulsa, Oklahoma, USA. SPE-169159-MS. http://dx.doi.org/10.2118/169159-MS.

44. Green, D.W. and Willhite, G.P. 1998. Enhanced Oil Recovery. SPE Textbook Series, Vol. 6. Society of Petroleum Engineers.

45. Han, M., Alshehri, A.J., Krinis, D., Lyngra, S. 2014. State-of-the-Art of In-Depth Fluid Diversion Technology: Enhancing Reservoir Oil Recovery by Gel Treatments. SPE-172186-MS.

46. Heath, A.R, and Koh, P.T.L. 2003. Combined population balance and CFD modelling of particle aggregation by polymeric flocculant. Third international conference on CFD in the materials and process industries CSIRO, Melbourne, Australia. 10-12 December.

47. Hernando, L., Bertin, H. J., Omari, A., Dupuis, G., Zaitoun, A. 2016. Polymer-Enhanced Foams for Water Profile Control. Paper presented at SPE Improved Oil Recovery Conference, 11-13 April, Tulsa, Oklahoma, USA. SPE-179581-MS. http://dx.doi.org/10.2118/179581-MS.

48. Hounslow, M.J., Ryall, R.L., Marshall, V.R. 1988. A discretized population balance for nucleation, growth, and aggregation. AIChE Journal, 34(11).

49. Hourdet, D., L'Alloret, F., Audebert, R. 1997. Polymer, 38, 2535.

50. Hove, A.O., Nilse, V., and Leknes, J. 1990. Visualization of Xanthan Flood behavior in Core samples by means of X-Ray Tomography. SPE Reservoir Engineering.SPE-17342-PA. http://dx.doi.org/10.2118/17342.

51. http://imagejdocu.tudor.lu/doku.php?id=gui:process:binary

52. Huh, C. and Pope, G.A. 2008. Residual Oil Saturation from Polymer Floods: Laboratory Measurements and Theoretical Interpretation. Presented at SPE Symposium on Improved Oil Recovery, Tulsa, Oklahoma, 19-23 April. SPE-113417-MS. http://dx.doi.org/10.2118/113417-MS.

53. Hutchins, R. D., Dovan, H.T., Sandiford, B.B. 1996. Field Applications of High Temperature Organic Gels for Water Control, Paper SPE-35444-MS, presented at the SPE/DOE Improved Oil Recovery Symposium, Tulsa, Oklahoma, USA. 21-24 April. http://dx.doi.org/10.2118/35444-MS.

54. Iler, R.K. 1979. The Chemistry of Silica: Solubility, Polymerization, Colloid and Surface Properties and Biochemistry of Silica. John Wiley & Sons.

55. Imqam, A., Bai, B., al Ramadan, M., Wei., M., Delshad, M., Sepehrnoori, K. 2014. Performed Particle Gel Extrusion through open Conduits during Conformance Control Treatments. SPE-169107-MS. Paper presented at the SPE Improved Oil recovery Symposium, Tulsa, Oklahoma, USA, 12-16 April. http://dx.doi.org/10.2118/169107-MS.

56. Imqam, A., Bai, B., Delshad, M. 2015. Preformed Particle Gel Propagation Through Super-K Permeability Sand and Its Resistance to Water Flow During Conformance Control. SPE/IATMI Asia Pacific Oil & Gas Conference and Exhibition, 20-22 October, Nusa Dua, Bali, Indonesia. http://dx.doi.org/10.2118/176429-MS.

57. Imqam, A., Bai, B., Wei., M. 2015. Combining conformance treatment with mobility control improves oil sweep efficiency in non-cross flow heterogeneous reservoirs. SPE-176728-MS. Paper presented at the SPE Russian Petroleum Technology Conference in Moscow, Russia, 26-28 October 2015. http://dx.doi.org/10.2118/176728-MS.

58. Irvine, R., Davidson, J., Baker, M., Devlin, R., Park, H. 2015. Nano Spherical Polymer Pilot in a Mature 18° API Sandstone Reservoir Water Flood in Alberta, Canada. SPE Asia Pacific Enhanced Oil Recovery Conference, 11-13 August, Kuala Lumpur, Malaysia. SPE-174656-MS. http://dx.doi.org/10.2118/174656-MS.

59. Jayakumar, S., Lane, R.H. 2012. Delayed crosslink polymer flowing gel system for water shutoff in conventional and unconventional oil and gas reservoirs, Paper SPE-151699-MS, presented at the SPE International Symposium and Exhibition on Formation Damage Control, Lafayette, Louisiana, USA, 15-17 February. http://dx.doi.org/10.2118/151699-MS.

60. Jia, H., Pu, W.-F., Zhao, Jin-Z., and Fa-Yang Jin, F.-Y. 2010. Research on the Gelation Performance of Low Toxic PEI Cross-Linking PHPAM Gel Systems as Water Shutoff Agents in Low Temperature Reservoirs, Ind. Eng. Chem. Res., 49: 9618–9624. DOI: 10.1021/ie100888q.

61. Karsani, K. S. M. E., Al-Muntasheri, G.A., Sultan, A. S., Hussein, I.A. 2014. Impact of Salts on Polyacrylamide Hydrolysis and Gelation: New Insights. Journal of Applied Polymer Science 131(23).

62. Khorasani, F.B., Poling-Skutvik,R., Krishnamoorti, R., Conrad, J.C. 2014. Mobility of Nanoparticles in Semidilute Polyelectrolyte Solutions. Macromolecules, 47: 5328−5333. dx.doi.org/10.1021/ma501248u.

63. Kokufuta, E. 2001. Transitions in polyelectrolyte gels, in Physical Chemistry of Polyelectrolytes (ed. T. Radeva), Taylor & Francis Ltd.

64. Koroteev, D., Dinariev, O., Evseev, N., Klemin, D., Nadeev, A., Safonov, S., Gurpinar, O., Berg, S., van Kruijsdijk,C., Armstrong, R., Myers, M.T., Hathon, L., de Jong, H. 2014. Direct Hydrodynamic Simulation of Multiphase Flow in Porous Rock. Petrophysics, Vol. 55, 3: 294–303.

65. Lake, L.W. 2010. Enhanced Oil Recovery. Society of Petroleum Engineers.

66. Lapidus, L. and Amundson, N.R. 1952. Mathematics of Adsorption in Beds. VI. The Effect of Longitudinal Diffusion in Ion Exchange and Chromatographic Columns. J. Phys. Chem. 56 (8): 984–988. DOI: 10.1021/j150500a014.

67. Lenchenkov, N.S., Glasbergen, G., Kruijsdijk, C. 2017. Flow of a cross-linking polymer in porous media. Submitted to the Transport in Porous Media journal.

68. Lenchenkov, N.S., Glasbergen, G., van Kruijsduijk, C., Cassiola, F., Koning, R., Bos, E., Vulovic, M. 2017 The characterization of the size and swelling kinetics of copolymer nano-spheres extracted from an o/w emulsion. to be published.

69. Lenchenkov, N.S., Slob, M., van Dalen, E., Glasbergen, G., van Kruijsduijk, C. 2016. Oil Recovery from Outcrop Cores with Polymeric Nano-Spheres. SPE Improved Oil Recovery Conference, 11-13 April, Tulsa, Oklahoma, USA. SPE-179641-MS. http://dx.doi.org/10.2118/179641-MS.

70. Li, D., Shi, M., Wang, D., Li, Z., Fei, H. 2009. Chromatographic Separation of Chemicals in Alkaline Surfactant Polymer Flooding in Reservoir Rocks in the Daqing Oil Field. SPE International Symposium on Oilfield Chemistry, 20-22 April. The Woodlands. Texas. USA. SPE-121598-MS. http://dx.doi.org/10.2118/121598-MS.

71. Li, D., Shi, M., Wang, D., Li, Z., Fei, H. 2009. Chromatographic Separation of Chemicals in Alkaline Surfactant Polymer Flooding in Reservoir Rocks in the Daqing Oil Field. SPE International Symposium on Oilfield Chemistry, 20-22 April. The Woodlands. Texas. USA. SPE-121598-MS. http://dx.doi.org/10.2118/121598-MS.

72. Li, Z., Wang ,Y., Shen, J., Liu,W., Sun, X. 2014. The measurement system of nanoparticle size distribution from dynamic light scattering data. Optics and Lasers in Engineering, 56: 94-98.

73. Liang, J.-T., Sun, H., Seright, R.S. 1995. Why Do Gels Reduce Water Permeability More Than Oil Permeability? Published in SPE Reservoir Engineering journal, 10 (04). SPE-27829-PA. http://dx.doi.org/10.2118/27829-PA.

74. Lietor-Santos, J.J., Sierra-Martın,B., and Fernandez-Nieves, A. 2011. Bulk and shear moduli of compressed microgel suspensions. Physical Review E. 84: 060402(R). DOI: 10.1103/PhysRevE.84.060402.

75. Lindner, A., Coussot, P., and Bonn, D. 2000. Viscous Fingering in a Yield Stress Fluid. Phys. Rev. Lett. 85, 314. http://dx.doi.org/10.1103/PhysRevLett.85.314.

76. Liu, X., Wang, Y., Lu, Z., Chen,Q., Feng, Y. 2012. Effect of Inorganic Salts on Viscosifying Behavior of a Thermoassociative Water-Soluble Terpolymer Based on 2-Acrylamido-methylpropane Sulfonic Acid. Wiley Online Library. DOI 10.1002/app.36745.

77. Mack, J.C. and Smith, J.E. 1994. In-Depth Colloidal Dispersion Gels Improve Oil Recovery Efficiency. SPE-27780-MS. Presented at SPE/DOE Improved Oil Recovery Symposium, 17-20 April, Tulsa, Oklahoma. http://dx.doi.org/10.2118/27780-MS.

78. Manichand, R.N., Seright, R.S. 2014. Field vs Laboratory Polymer Retention Values for a Polymer Flood in the Tambaredjo Field. Presented at the SPE Improved Oil Recovery Symposium, , Tulsa, OK. 12-16 April. SPE-169027-MS. http://dx.doi.org/10.2118/169027-MS.

79. Marle, C. 1981. Multiphase Flow in Porous Media, Houston: Gulf Publishing.

80. McCool, C.S., Green, D.W., and Willhite, G.P. 1991. Permeability Reduction Mechanisms Involved in In-Situ Gelation of a Polyacrylamide/ Chromium (VI)/Thiourea System. SPE Reservoir Engineering Journal, 6 (01):77-83. SPE-17333-PA. http://dx.doi.org/10.2118/17333-PA.

81. Mondal, S. 2013. Flow of Particulate Suspensions through Constrictions: Multi-Particle Effects. The University of Texas at Austin.

82. Moradi-Araghi, A., Stahl, G.A. 1991b. Gelation of acrylamide-containing polymers with hydroxyphenyl alkanols. EP Patent 446 865, assigned to Phillips Petroleum Co., September 18.

83. Müller, M., Kebler, B., Fröhlich, J., Poeschla, S., and Torger, B. 2011. Polyelectrolyte Complex Nanoparticles of Poly(ethyleneimine) and Poly(acrylic acid): Preparation and Applications. Polymers, 3, 762-778.

84. Pancharoen, M., Thiele, M.R., and Kovscek, A.R. 2010. Inaccessible pore volume of associative polymer floods. Paper SPE-129910-MS, presented at the SPE Improved Oil Recovery Symposium, Tulsa, Oklahoma, USA, 24-28 April. http://dx.doi.org/10.2118/129910-MS.

85. Pancharoen, M., Thiele, M.R., and Kovscek, A.R. 2010. Inaccessible pore volume of associative polymer floods. Presented at SPE Improved Oil Recovery Symposium, Tulsa, Oklahoma, 24-28 April, SPE-129910-MS. http://dx.doi.org/10.2118/129910-MS.

86. Peksa, A.E., Wolf, K.-H.A.A, and Zitha, P.L.J. 2015.Bentheimer sandstone revisited for experimental purposes. Marine and Petroleum Geology. **67:** 701–719. doi:10.1016/j.marpetgeo.2015.06.001.

87. Pich, A.Z., Richtering, W., Albrecht, K. 2010. Chemical Design of Responsive Microgels. Springer.

88. Pyrz, W.D., and Buttrey, D.J. 2008. Particle Size Determination Using TEM: A Discussion of Image Acquisition and Analysis for the Novice Microscopist. Langmuir, 24:11350-11360.

89. Randy I., John, D., Mark, B.et al. 2015. Nano Spherical Polymer Pilot in a Mature 18° API Sandstone Reservoir Water Flood in Alberta, Canada, Presented at SPE Asia Pacific Enhanced Oil Recovery Conference, Kuala

Lumpur, 11-13 August. SPE-174656-MS. http://dx.doi.org/10.2118/174656-MS.

90. Reddy, B.R., Eoff, L.S., Crespo, F., Lewis, C.A. 2013. Recent Advances in Organically Crosslinked Conformance Polymer Systems. SPE International Symposium on Oilfield Chemistry, 8-10 April, The Woodlands, Texas, USA. SPE-164115-MS. http://dx.doi.org/10.2118/164115-MS.

91. Rossen, W.R. and Bruining, J. 2004. Foam Displacements With Multiple Steady States. Presented at SPE/DOE Symposium on Improved Oil Recovery, 17-21 April, Tulsa, Oklahoma, USA. SPE-89397-MS. http://dx.doi.org/10.2118/89397-MS.

92. Roy, D., Brooksb, W.L.A. and Sumerlin, B.S. 2013. New directions in thermoresponsive polymers. Chem. Soc. Rev., 42, 7214-7243.

93. Rubinstein, M., and Colby, R.H., 2003. Polymer Physics. Oxford University press.

94. Russ, J. C. 2011. The Image Processing Handbook, Sixth Edition. CRC Press.

95. Saadatfar, M., Arns, C. H., Knackstedt, M. A., Senden, T. J. 2005. Mechanical and transport properties of polymeric foams derived from 3D images. Colloids and Surfaces A: Physicochemical and Engineering Aspects 263.1-3: 284–289. DOI: 10.1016/j.colsurfa.2004.12.040.

96. Saunders, B.R. and Vincent, B. 1997. Colloid Polym. Sci., 275, 9.

97. Saunders, B.R., Vincent, B., 1999. Microgel particles as model colloids: theory, properties and applications, Advances in Colloid and Interface Science.80:1-25.

98. Seetha, N., Mohan Kumar,M.S., Hassanizadeh, S. M., Raoof, A. 2014. Virus-sized colloid transport in a single pore: Model development and sensitivity analysis. Journal of contaminant hydrology, 164: 163-180.

99. Sendekie, Z.B., and Bacchin, P. 2016. Colloidal Jamming Dynamics in Microchannel Bottlenecks. Langmuir, 32: 1478-1488. doi:10.1021/acs.langmuir.5b04218.

100. Seright, R. S., Zhang, G., Akanni, O.O., Wang, D. 2011. A comparison of polymer flooding with in-depth profile –modification, Paper SPE-146087-MS, presented at the Canadian Unconventional Resources Conference, Calgary, Canada, 15-17 November. http://dx.doi.org/10.2118/146087-MS.

101. Seright, R.S. 1995. Propagation of an Aluminium Citrate- HPAM Colloidal Dispersion Gel through Berea Sandstone. In Seright, R. Improved Techniques for Fluid Diversion in Oil Recovery Process. Annual Report. Report No. DOE/BC/14880-10. U.S. DOE, Office of Fossil Energy, Washington, D.C. (September 199 and March 1995). 51-64.

102. Seright, R.S., Peihui, H., Dongmei, W. 2006. Current colloidal dispersion gels are not superior to polymer flooding. 1000-3754 (2006) 05-0071-10.

103. Seright, R.S.; Mac Seheult, J.; Talashek, T. 2008. Injectivity Characteristics of EOR Polymers. SPE Annual Technical Conference and Exhibition, 21-24 September, Denver, Colorado, USA. SPE-115142-PA. http://dx.doi.org/10.2118/115142-MS.

104. Shibayama, M. and Tanaka, T. 1993. Volume phase transition and related phenomena in polymer gels, in Responsive Gels, Volume Transitions I, Advances in Polymer Science, vol. 109 (ed. K. Dusek), Springer Verlag.

105. Shiran, B. S. and Skauge A. 2015. Wettability and Oil Recovery by Polymer and Polymer Particles. Presented at SPE Asia Pacific Enhanced Oil Recovery Conference, 11-13 August, Kuala Lumpur, Malaysia. SPE-174568-MS. http://dx.doi.org/10.2118/174568-MS.

106. Sorbie K.S. 1991. Polymer Improved Oil Recovery. Glasgow, UK: Blackie and Son.

107. Sorbie, K.S., Seright, R.S. 1992. Gel Placement in Heterogeneous Systems With Crossflow. SPE/DOE Enhanced Oil Recovery Symposium, 22-24 April, Tulsa, Oklahoma, USA. SPE-24192-MS. http://dx.doi.org/10.2118/24192-MS.

108. Spildo, K., Skauge, A., Aarra, M.G., Tweheyo, M.T. 2009. A New Polymer Application for North Sea Reservoirs. SPE Res Eval & Eng 12(3):427-432. SPE-113460-PA. http://dx.doi.org/10.2118/113460-PA.

109. Spildo, K., Skauge, A., and Skauge, T. 2010. Propagation of colloidal dispersion gels (CDG) in laboratory cores. Paper SPE 129927. Presented at the SPE Improved Oil recovery Symposium. Tulsa, Oklahoma. 24-28 April. http://dx.doi.org/10.2118/129927-MS.

110. Spruijt, E. 2012. Strength, structure and stability of polyelectrolyte complex coacervates. PhD thesis, Wageningen University, Wageningen, The Netherlands.

111. Stahl, G.A., and Schulz, D.N. 1988. Water-Soluble Polymers for Petroleum Recovery. Plenum Publishing Corp., New York.

112. Stavland, A., Jonsbraten, H.C., Vikane, O., Skrettingland, K., Fischer, H. 2011. In-Depth Water Diversion Using Sodium Silicate on Snorre - Factors Controlling In-Depth Placement. Presented at SPE European Formation Damage Conference, 7-10 June, Noordwijk, The Netherlands. SPE-143836-MS. http://dx.doi.org/10.2118/143836-MS.

113. Sydansk, R.D. 1988. A New Conformance-Improvement-Treatment Chromium (III) Gel Technology, Paper SPE-17329-MS, presented at the SPE Enhanced Oil Recovery Symposium, Tulsa, Oklahoma, USA, 16-21 April. http://dx.doi.org/10.2118/17329-MS.

114. Sydansk, R.D., Southwell, G.P. 2000. More Than 12 Years of Experience with a Successful Conformance-Control Polymer Gel Technology, Paper SPE-62561-MS, presented at the SPE/AAPG Western Regional Meeting, Long Beach, California. USA, 19-22 June. http://dx.doi.org/10.2118/62561-MS.

115. Thierry Savin. 2008. Micro rheology of heterogeneous systems, online tutorial http://web.mit.edu/savin/Public/.Tutorial v1.2.

116. Todd, B.J., Willhite, G.P., and Green, D.W.1993. A Mathematical Model of In·Situ Gelation of Polyacrylamide by a Redox Process. SPE Reservoir Engineering Journal, 8 (01):51-58. SPE-20215-PA. http://dx.doi.org/10.2118/20215-PA.

117. Total Organic Carbon Analyzer. User manual. http://www.ecs.umass.edu/eve/facilities/equipment/TOC/TOCV/TOC-V_CP_Users_Manual_E.pdf.

118. Turner, M. L., Knüfing, L., Arns, C. H., Sakellariou, A., Senden, T. J., Sheppard, A. P., Sok, R. M., Limaye, A., Pinczewski, W. V., Knackstedt, M. A. 2004. Three-dimensional imaging of multiphase flow in porous media, Physica A: Statistical Mechanics and its Applications, Volume 339, Issue 1: 166-172. DOI: 10.1016/j.physa.2004.03.059.

119. van Dalen, E. 2014 Conformance control for heterogeneous reservoirs with nano-particles suspension. MS thesis, TU Delft: Delft University of Technology (December 2014).

120. van der Hoek, J.E., Botermans, W., Zitha, P.L.J.2001. Full Blocking Mechanism of Polymer Gels for Water Control. Paper SPE-68982-MS presented at the SPE European Formation Damage Conference, The Hague, The Netherlands, 21-22 May. http://dx.doi.org/10.2118/68982-MS.

121. van Krevelen, D.W., and te Nijenhuis, K.2008. Properties of polymers, Fourth edition, Elsevier.

122. Vasquez, J., Civan, F., Shaw, T.M., Dalrymple, E.D., Eoff, L., Reddy, B.R., Brown, D. 2003. Laboratory evaluation of high temperature conformance polymer systems, Paper SPE-80904-MS, presented at the SPE Production and Operations Symposium, Oklahoma City, USA, 23-26 March. http://dx.doi.org/10.2118/80904-MS.

123. Vebrel, J., Grohens, Y., Kadmiri, A. and Gowling, E.W. 1993. Differential scanning calorimetry study of the cross-linking of styrene and an unsaturated polyester: The chemistry of canoe manufacture. J. Chem. Educ., 70 (6), p 501. DOI: 10.1021/ed070p501.

124. Wang, D., Cheng, J., Yang, Q. et al. 2000. Viscous-Elastic Polymer Can Increase Microscale Displacement Efficiency in Cores. Presented at SPE Annual Technical Conference and Exhibition, Dallas, Texas, 1-4 October. SPE-63227-MS. http://dx.doi.org/10.2118/63227-MS.

125. Wang, L., Zhang, G., GE, J. Li, G., Zhang, J., Ding, B. et al. 2010. Preparation of Microgel Nanospheres and Their Application in EOR. Presented at International Oil and Gas Conference and Exhibition in China, Beijing, 8-10 June. SPE-130357-MS. http://dx.doi.org/10.2118/130357-MS.

126. Willhite, G.P. and Dominguez, J.G. 1977. Improved Oil Recovery by Surfactant and Polymer Flooding, eds Shah, D. O. and Shecter, R. S., Academic Press Inc., New York.

127. Williams, D.B., Carter, C.B., 2009. Transmission Electron Microscopy: A Textbook for Materials Science. Springer.

128. Winter, H.H. 1987. Can the gel point of a cross-linking polymer be detected by the G′-G″ Crossover? Polymer Engineering & Science, Volume 27, Issue 22, pp 1698–1702. DOI: 10.1002/pen.760272209.

129. Yao, C., Xu, X., Wang. D., Lei, G., Xue, S., Hou, J., Cathles, L.M., Steenhuis, T.S. 2016. Research and Application of Micron-Size Polyacrylamide Elastic Microspheres as a Smart Sweep Improvement and Profile Modification Agent. SPE Improved Oil Recovery Conference, 11-13 April, Tulsa, Oklahoma, USA. http://dx.doi.org/10.2118/179531-MS.

130. Yeramilli, S.S. 2012. Analysis of Polymer Injectivity in Porous Media: Experiments and Modelling. Master thesis, TU Delft: Delft University of Technology, Delft.

131. Yerramilli, R. 2012 Water Injectivity Prediction: Experiments and Modeling. Master thesis, TU Delft: Delft University of Technology, Delft.

132. Yuqin, T., Lushan, W., Yanyan, T., Chengjie, L., Chao, Ma, Tao, W. 2012. Research and Application of Nano-Polymer Microspheres Diversion Technique of Deep Fluid, SPE-156999-MS. Presented at International Oilfield Nanotechnology Conference and Exhibition, 12-14 June. Noordwijk, The Netherlands. http://dx.doi.org/10.2118/156999-MS.

133. Zetasizer Nano Series User Manual. 2004.

134. Zhang, Q., Zhou, Ji-Sheng. 2008. Effect of salt solutions on chain structure of partially hydrolysed polyacrylamide. Journal of Central South University of Technology. Volume 15, Supplement 1.

135. Zhu, Y., Xu, Y., Huang, G. 2013. Synthesis and Aqueous Solution Properties of Novel Thermosensitive Polyacrylamide Derivatives. J. APPL. POLYM. SCI. DOI: 10.1002/app.39192.

136. Zitha, P.L.J. and Botermans, C.W. 1998. Bridging-Adsorption of Flexible Polymers in Low Permeability Porous Media. SPE Prod & Fac. 13(1). SPE-36665-PA. http://dx.doi.org/10.2118/36665-PA.

137. Zitha, P.L.J., Botermans, C. W., Hoek, v. d. J. and Vermolen, F.J. 2002. Control of flow through porous media using polymer gels. Journal of Applied Physics, 92, 1143. http://dx.doi.org/10.1063/1.1487454.

138. Zitha, P.L.J., Nguyen, Q.P., Currie, P.K. 2003. Effect of Flow Velocity and Rock Layering on Foam Flow: an X-ray Computed Tomography Study. Presented at SPE Asia Pacific Oil and Gas Conference and Exhibition, 9-11 September, Jakarta, Indonesia. SPE-80530-MS. http://dx.doi.org/10.2118/80530-MS.

139. Zitha, P.L.J., van Os, K.G.S., Denys, K.F.J. 1998. Adsorption of Linear Flexible Polymer during Laminar Flow through Porous Media: Effect of Concentration. Presented at the SPE/DOE Improved Oil Recovery Symposium, Tulsa, OK. 19-22 April. SPE-39675-MS. http://dx.doi.org/10.2118/39675-MS.

# Appendix A

## Population balance model

The simulation of the aggregation of nano-spheres over time was done according to the one-dimensional binary aggregation population balance equation (A.1). This equation assumes that the particles collide with any other particle in the system.

$$\frac{\partial n(\upsilon)}{\partial t} = \frac{1}{2}\int_0^{\upsilon} \beta(u, \upsilon - u) n(u) n(\upsilon - u) du - n(\upsilon)\int_0^{\infty} \beta(u, \upsilon) n(u) du \quad \text{(A.1)}$$

where n is the number density function of the spheres of size υ; β is the aggregation rate kernel which represents a frequency of collision between particles $\upsilon$ and $u$. In the current work a size independent kernel is used.

The discretization of eq. 1 was done according to the method proposed by Hounslow using volume (length) as an internal coordinate. The geometric grid used for the discretization is divided into intervals according to the progression $\upsilon_{i+1}=2\cdot\upsilon_i$ where υ is a particle volume or $L_{i+1}/L_i=\sqrt[3]{2}$ where L is a length. In the work of Hounslow it is explained that this discretization technique enables covering a wide range of particles sizes and corresponds well to the output of a dynamic light scattering instrument.

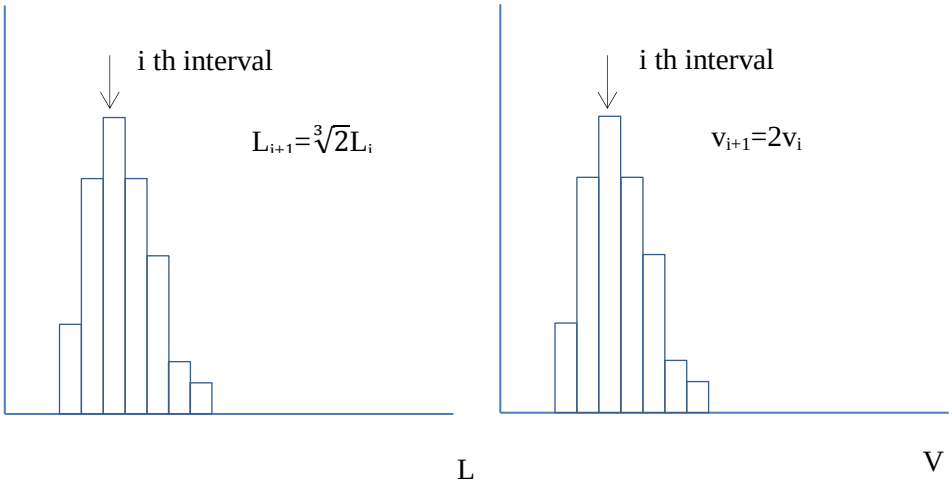


a. Length as an internal coordinate

b. Volume as an internal coordinate

**Figure A.1**- Discrete size distributions with length or volume as internal coordinates (Hounslow et al.)

Hounslow et al. outlined four binary interaction mechanisms between particles which are considered for the numerical solution of the equation: 1) birth in i th interval due to the aggregation between the particles in (i-1) th and the first to (i-1)th intervals; 2) aggregates are formed via collisions between particles in an (i-1) interval; 3) death of a particle in the i th interval by aggregation; 4) death of a particle in the i th interval due to the aggregation of particles from the same to higher intervals.

Combining the outlined mechanisms together and applying it to eq. A.1, we obtain eq. A.2.

$$\frac{dN_i}{dt} = N_{i-1}\sum_{j=1}^{i-1} 2^{j-i+1}\beta_{i-1,j}N_j + \frac{1}{2}\beta_{i-1,i-1}N_{i-1}^2 - \\ -N_i\sum_{j=1}^{i-1} 2^{j-i}\beta_{i,j}N_j \; -N_i\sum_{j=i}^{\infty}\beta_{i,j}N_j \qquad \text{(A.2)}$$

The main drawback of this approach is the division of the computation domain only according to the progression $L_{i+1}/L_i=\sqrt[3]{2}$. Therefore, we cannot select other numbers for the analysis.

# Appendix B

## Characterisation of the nano-spheres using dark field optical microscopy

The study of the size of nano-spheres in the brine was also done with the CytoViva enhanced dark field optical microscope (CytoViva Optical Microscope User Manual). The advantage of the method is that the Brownian motion of the spheres can be directly visualised in a solvent. The objective of the microscope captures only light which is scattered by particles and no light from the source is detected. This produces high resolution images with a dark background. The advantage of the dark field microscope over conventional optical microscopes used in similar studies is the high signal to noise ratio. The preparation of samples for the microscope does not require fluorescent labelling. Every test can be carried out faster than any of the tests with electron microscopy.

A sample of nano-spheres at the concentration of 600 ppm dissolved in the brine (Chapter 3, table 3.2) was prepared for a series of experiments with the microscope. In order to study the increase in the size of nano-spheres in the solvent, 5 sets of video micrographs were taken over time: 1, 6, 13, 20 and 30 days of aging. Instead of acquiring single images, the more representative picture of particles behaviour can be obtained by recording video micrographs for 50 s each time. The video consists of a sequence of individual micrographs and depicts the Brownian motion of the particles. The requirements for the micrographs is a high concentration of the bright movable particles in a field of view of the microscope.

During the image analysis it was noticed that all images contain bright spots which do not move while the video is being recorded. Most likely, these are impurities on a substrate for the sample or particles which stick to the substrate. That artifact has to be excluded from images. It was done by subtracting the background from all images (Figures B.1, a-d).

Finally, the resulting images contain only movable spheres. By applying a Bandpass filter and thresholding each image, size distribution according to cross-sectional area is obtained at Day 1 (Figure B.2).

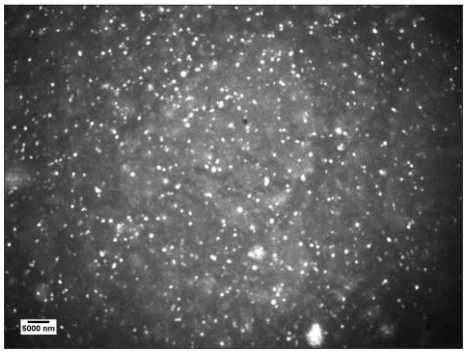


a. Initial image of the suspension

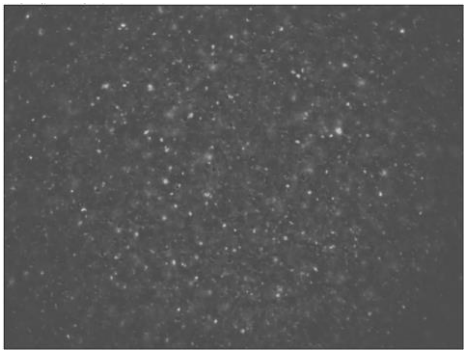

b. An image after the subtraction of the background

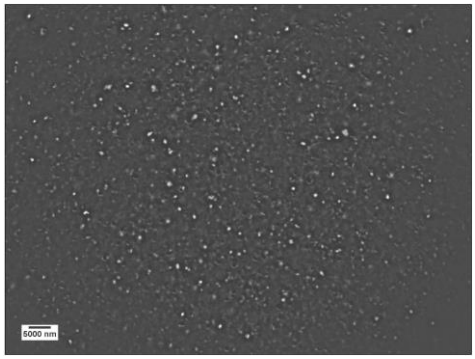


c. The image after the application of the Bandpass filter

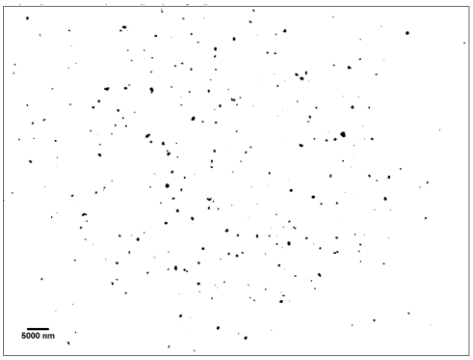


d. Binary image

**Figure B.1** –Resuls of the image analysis of the micrographs at a maginifcation of 40x

As can be seen from Figure B.2 the particles distribution is wider than what was obtained with DLS (Chapter 3, Figure 3.20). Indeed, according to the optical microscopy, the cross-sectional area average dimeter of the distribution at day 1 is 386 nm, whereas the mean from DLS is 175 nm. The difference between results can be explained by the interference of the light with edges of particles at high magnification in the optical microscopy (Alberts B et al., 2002). That gives slightly blurred particles with an increased size. Moreover, if particles are located in a close vicinity to each other, then due to the edge effect it will appear as a single particle.

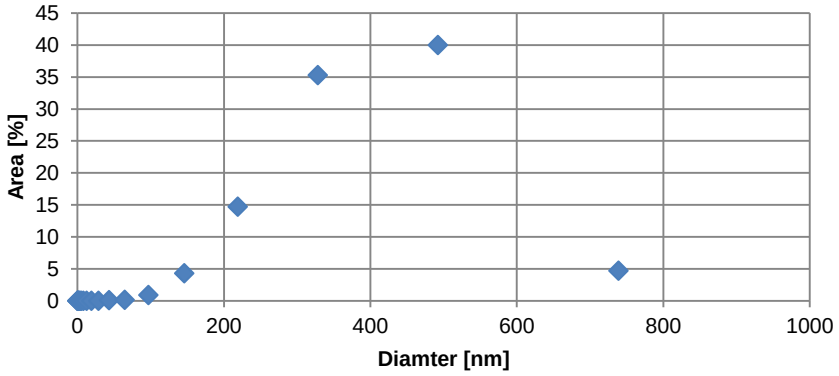


**Figure B.2-** Distribution of the size of particles at day 1

In order to overcome the optical limitations of the dark field microscopy and to obtain another estimation of the size of particles, a tracking of the nano-spheres' trajectories can be done over time.

That gives an indication of the displacement of the particles which randomly move in a solvent in a two dimensional space. The displacement of the particles can be used for the calculation of their diffusion coefficient according to equation B.3.

$$D=\frac{\langle r^2\rangle}{4dt} \tag{B.3}$$

where $\langle r^2\rangle$ ($m^2$)- a mean squared displacement of a particle in the solvent; *dt* (s)- time lack; *D* ($m^2/s$)- diffusion coefficient.

An example of obtaining the average squared displacement $\langle r^2\rangle$ of a particle in the solvent is shown on Figure B.3. The particle moves in the solvent and its trajectories can be monitored with a series of micrographs with an increment in time of 0.1 s. The distance between two subsequent positions can be measured using peaks of grey value distribution. By combining all coordinates of the particle's positions, it is possible to reconstruct the change in the mean square displacement over time. The shape of the curve, which is shown on Figure B.4, suggests that it is a superposition of the isotropic and confined random walk motion.

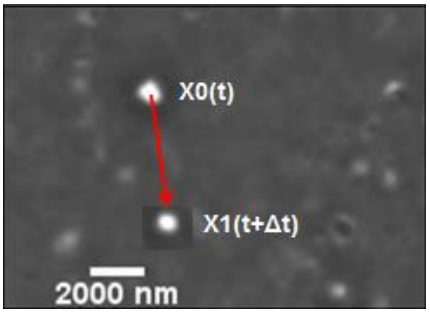


**Figure B.3**- An example of the displacement of a particle in the solvent over *dt*=3 s

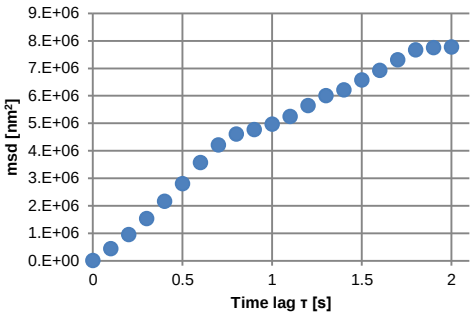


**Figure B.4**- Mean square displacement *msd* ($nm^2$) vs time lag $\tau$ (s) Day 1

The resulting displacement $\langle r \rangle$ of the particle depicted on Figure B.3 accounts for 659 nm over 0.1 s and the corresponding value of the diffusion coefficient is equal to $10.8 \cdot 10^{-13}$ $m^2/s$.

The obtained diffusion coefficient is used for the calculation of the diameter of particles using the Stokes-Einstein equation for a sphere (equation B.4).

$$D = \frac{k_B T}{3 \cdot \pi \cdot \mu \cdot d} \qquad \text{(B.4)}$$

where $r$ (m)-discplacement; $\mu$ (Pa·s)-viscosity; $d$ (m)-diameter; $k_B$ - the Boltzmann constant; $T$ (K)-temperature.

Although the motion of the particles happens in the 3 dimensional space, the projection of the particles trajectory on two dimensional space is observed in the microscope. That influences the results of the calculations and the obtained diameter of particles might be larger than it is in reality. To decrease this effect, at least 40 frames of the video were taken to estimate the average displacement with a time lack of 0.1 s. For the case of Figure B.3, the calculated diameter of a particle is 394 nm.

By maintaining a constant temperature over experiments-20-24 ˚C, and viscosity of the solvent $1\text{-}0.91 \cdot 10^{-3}$ Pa·s, it is possible to compare the size of the particles at different time steps (Figure B.5).

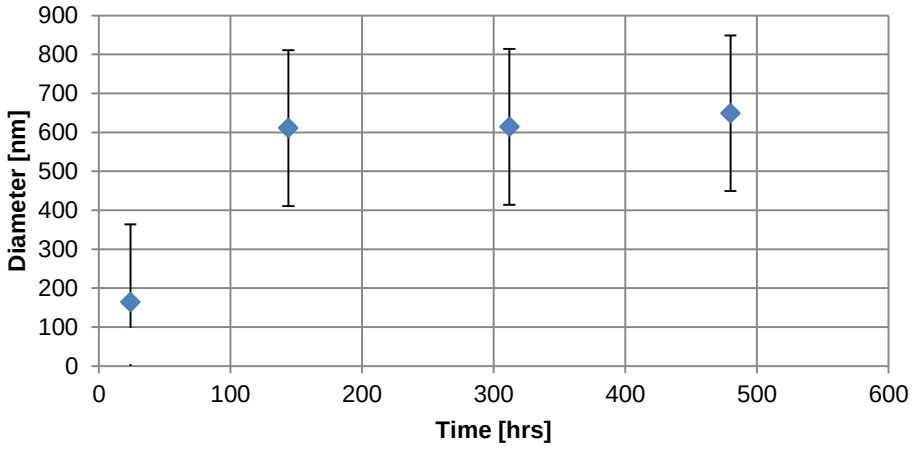


**Figure B.5-** The change of the average particles size over time at 5 g/l brine

The dynamic of the spheres growth depicted in Figure B.5 shows that the initial size of the nano-spheres is about 184 ±60 nm. After 120 hrs of aging, it reaches the size of 611±60 nm. Later, that size does not change much, remaining at the same level.

Although the difference in the size between the optical microscopy and DLS is evident, the former method supports the idea about nano-spheres growth, as well as showing the maximum size that can be reached by the particles.

In addition to that, the visual inspection has shown that fewer particles appear in the view of the microscope over time. This implies that the agglomeration between particles takes place in the suspension. That hypothesis can be supported by the increase of the size of the nano-spheres in the solvent.

# Nomenclature

## Greek

| Symbol | Units | Description |
|---|---|---|
| $\mu$ | [Pa·s] | Viscosity |
| β | [$s^{-1}$] | Aggregation kernel |
| υ | [m] | Size of the spheres |
| ϕ | - | Porosity |
| ρ | [$kg \cdot m^{-3}$] | Density |
| π | - | Constant (≈3.14) |
| κ | - | Ionic strength |

## Latin

| Symbol | Units | Description |
|---|---|---|
| $D$ | [$m^2 \cdot s^{-1}$] | Diffusion coefficient |
| $T$ | [K] | Temperature |
| $r$ | [m] | Displacement of a particle |
| $\langle r^2 \rangle$ | [$m^2$] | A mean squared displacement of a particle in the solvent |
| $d$ | [m] | Diameter of a particle |
| $t$ | [s] | Time |
| $N$ | - | Number of particles |
| $l$ | [m] | Length of a tube |
| $g$ | [$m/s^2$] | gravitational acceleration |
| $L$ | [m] | Core length |
| $Npe$ | - | Peclet number |
| $Vp$ | $m^3$ | Accessible pore volume |
| $x_D$ | - | Dimensionless distance |
| $C_D$ | - | dimensionless concentration |
| $C_I$ | - | Initial concentration |
| $C_J$ | | Injection concentration |
| $q$ | [$m^3 \cdot s^{-1}$] | Flow rate |
| $u$ | [$m \cdot s^{-1}$] | Velocity |
| $M_{rock}$ | [kg] | Mass of a rock |
| $\Delta V$ | [L] | Incremental produced volume |
| $V_{swept}$ | [L] | Effective volume |
| $C_p$ | - | Produced concentration |
| $C_{in}$ | - | Initial concentration |

# Acronyms

| | |
|---|---|
| AFM | Atomic Force microscopy |
| An RGB image | The image which has three channels: red, green, and blue |
| BPR | Back pressure regulator |
| CDG | Colloidal Dispersion Gels |
| Cryo-TEM | Cryo-electron microscopy |
| CT | Computer tomography |
| DLS | Dynamic light scattering |
| HCl | Hydrochloric acid |
| HPAM | Partially hydrolyzed polyacrylamide |
| ICP | Inductively Coupled Plasma Spectrometry |
| Ind. | Individual particles |
| KI | Potassium iodide |
| Micro CT | Micro computational tomography |
| Mw | Molecular weight |
| NaClO | Sodium hypochlorite |
| NPS or NS | Nano-spheres |
| PBM | Population balance model |
| PE | Polyelectrolyte |
| PEC | Polyelectrolyte complex |
| PEI | Polyethyleneimine |
| ppm | Parts per million |
| PV | Porous volume |
| RF | Resistance factor |
| RRF | Residual resistance factor |
| SEM | Scanning electron microscopy |
| TDS | Total dissolve solids |
| TEM | Transmission electron microscopy |
| UV | Ultraviolet |
| XL agent | Cross linker |
| XL polymer | Crosslinking polymer: a mixture of PEC and HPAM |
| O/W emulsion | Oil in water emulsion |

# Acknowledgements

This thesis is a result of intensive work which has been possible only due to the help and support of the group of people who have surrounded me.

I am deeply indebted to my supervisors, Drs. Gerard Glasbergen and Prof. Cor van Kruijsdijk, for their scientific guidance during the entire period of my PhD project. Without their help, this journey would be much harder to overcome and less productive with respect to the results! Our regular meetings helped me to learn many of the physical aspects of complex fluid flow in porous media and improved my critical thinking. After the time which we spent together, they became a part of my family.

I am profoundly thankful to Shell Global Solutions International for their financial support of the project and the opportunity to publish the results in journal papers. During my PhD project I also was seconded to Shell in the EOR group with a focus on conformance control in heterogeneous reservoirs with polymer technologies. That unique opportunity gave me an overview of the impact which my research can cause. Discussions of my research results with my colleagues, Dr. Marco Welling, Dr. Steffen Berg, Dr. Koenraad Elewaut, Dr. Ramez Nasralla, Mr. Andrew Parker, Dr. Johan Romate, Mr. Efraim Keijzer, Dr. Mariya Krymskaya, Dr. Anke ten Berge-Leferink op Reinink, Ms. Leandra David, Dr. Diederik Boersma, Ms. Roelien Broos, Dr. Marten Buijse, Dr. Nair Nitish, Dr. Flavia Cassiola, Dr. Hans Groot, Dr. Diego Wever, Ms. Henneke de Vries, Dr. Ali Fadili, Mr. Adi Anand, Mr. Ko Wisse, Dr. Li Li, Mr. Menno van Haasterecht, Dr. Katie Humphry, Mr. Sander de Kruijf, Mr. Fons Marcelis, Mr. Carl van Rijn, Mr. Axel Makurat, Dr. Esther Vermolen, Ms. Merit van der Lee, Dr. Ryan Armstrong, Ms. Linda Wiegman, allowed me to learn new techniques for the analysis of experimental data and broaden my approach for tackling challenging problems within reservoir engineering.

I would like to thank Delft University of Technology for the opportunity to successfully accomplish my Doctoral program. My regular presentations at different meetings at the University made my presenting skills stronger and gave me the opportunity to have fruitful discussions with professors of the Petroleum engineering section, Prof. Pacelli Zitha, Prof. Bill Rossen, Prof. Hans Bruining, Dr. Karl Heinz Wolf, Dr. Rouhi Farajzadeh, Dr. Dennis Voskov, Prof. Jan-Dirk Jansen, Dr. Hadi Hajibeygi, and Dr. Paul van den Hoek who shaped my research into a well –rounded message.

I am grateful to the members of my doctoral defence committee, Prof. Michael Golombok, Prof. Timo Heimovaara, Prof. Pacelli Zitha, Dr. Johan Padding, and Prof. Ken Sorbie, who found time to examine my thesis and gave me valuable recommendations on how to improve it. It is especially my honour to have Prof. Ken Sorbie as a member of my committee. The book Polymer-Improved Oil Recovery by Prof. Ken Sorbie has become my favorite technical book.

Some of my research would have not been possible without the collaboration with my colleagues from various departments at Delft University. I successfully collaborated with Dr. Milos Vulovic on the Transmission Electron Microscope, which became a part of a bigger project with Leiden University on the characterisation of nano-spheres. Thus, I would like to thank Mr. Erik Boss and Dr. Roman Koning for their technical support. I also would like acknowledge Mr. Michiel Slob who helped me to build up and technically supported my laboratory set up during the entire project. Finally, our joint work resulted in the chapter of the thesis on the flow of nano-spheres in porous media.

I very much appreciate the help of Prof. Jens Harting and Dr. Dennis Hessling from Eindhoven University on the modelling of nano-particles flow in in micro channels. Our collaboration and critical discussions allowed me to set up a new problem which theoretically might explain a propagation of nano-spheres in porous media.

The experimental study on the nano-spheres flow in a pore scale using the PIV technique was also started in collaboration with Prof. Cristian Poelma and Mr. E.F.J. Overmars. I am very thankful to these scientists for their time and contribution.

I kindly remember my joint work with Mr. Ernst van Dalen who did his MSc project under my supervision. Results which we obtained together were very useful for the theory of nano-spheres flow in porous media and became one of the bases for Chapter 4.

This work was very enjoyable for me mainly because I was surrounded by my colleagues from TU Delft who gave me constant support and attention. I would like to specifically thank Dr. Phil Vardon, Mr. Matei Tene, Mr. Eduardo De Barros, Mr. Swej Shah, Mr. Bander Alquaimi, Dr. Asya Kudarova, Ms. Anna Peksa, Dr. Siavash Kahrobaei, Mr. Matteo Cusini, Mr. Rafael Moraes, Mr. Ahmed Hussain, Mr. Alexander Wilsdorf, Mr. Faisal Al Saadi,

Mr. Jakolien van der Meer, Mr. Jiakun Gong, Mr. Amin Fatemi, Mr. Alexander Tang, Mr. Martijn Janssen, Dr. Saskia Roels, Mr. Guanqun Yu, Mr. Chris Boeije, Mr. Christian Kosack, Mr. Mark Khait, Ms. Janice Rossen, Dr. Elisa Battistutta, Mr. Alex Kirichek, Dr. Sian Jones, Mr. Seyed Mojtaba Hosseini Nasab, Mr. Yang Wang, Mr. Anas Dictor, Dr. Roderick Tollenaar Gonzalez, Mr. Ralf Haak, Mr. Rodrigo Salazar, Dr. Negar Khoshnevis Gargar, Dr. Roozbeh Khosrokhavar, Mr. Mohsen Mirzaie Yegane, Mr. Longlong Li, Mr. Daniel Da Silva, Ms. Marlijn Ammerlaan, Ms. Lydia Broekhuijsen-Bentvelzen, and Ms. Hannie Zwiers.

During my project I spent significant time in the Geoscience & Engineering Laboratory at TU Delft. My work was productive and efficient there due to the help of Mr. Wim Verwaal, Mr. Karel Heller, Ms. Jolanda van Haagen, Mr. Jens van den Berg, Ms. Ellen Meijvogel-de Koning, Mr. Joost van Meel, Mr. Marc Friebel, Mr. Jan Etienne, Mr. Arno Mulder, Mr. Armand Middeldorp, Mr. Ben Norder and Mr. Henk van Asten. I am very thankful for their input!

The constant support of my friends, Dr. Rahul Fonseca, Mr.Durgesh Kawale, Dr.Gleb Polevoy, Dr.Rahul Thorat, and Mr.Stephen Green, created an environment which made my time positive and meaningful. This support was especially important at the beginning of my journey when I had just moved to the Netherlands. At that time Rahul Fonseca and Durgesh introduced me to the local traditions in Delft. We have had many fruitful and exciting moments together. Gleb was the person who helped me to remember traditions of my home country while being abroad. Rahul Thorat introduced me to the one of the most enjoyable activities in my life- dancing, which has brought many bright colours into my life. Stephen helped me to extend some of my research skills by bringing critics which is always necessary for me.

Initially I came to the Netherlands to improve my knowledge in the area of reservoir engineering by doing research in the challenging project offered by Shell. Now, I can certainly say that I also have found a new family which has made my spirit richer.

At the end, I am expressing my deep gratitude and admiration to my mother who has always supported me in the difficult times and gave me a basis for professional grow.

*Nikita Lenchenkov, May 2017.*

# Curriculum Vitae

## Nikita Lenchenkov

I started my petroleum engineering degree in 2001 at Ufa State University. During my study there, I got my first experience of conducting scientific research by participating in different projects on the subjects of mathematics, petroleum engineering and fluid mechanics. The results of my work were presented at local and state conferences.

When I was on my third year of study (2003), I joined an oilfield service company "LeL" Ltd were I worked as a part-time field engineer until 2009. During that period, I supported and was directly involved in oil field operations for the application of gel compositions for conformance control in oil fields in Tatarstan and Bashkortostan. That experience honed my engineering skills and gave me relevant experience as a petroleum engineer.

I graduated from the University in 2006 with a diploma with honours (cume laude). My graduate work was about the optimisation of oil production with electro submergible pumps. Results of the same work were presented at the All-Russian conference in Saint-Petersburg where I won a grant to continue my post graduate study at the Saint Petersburg Mining University.

I moved to Saint-Petersburg in 2006 and started my research on the topic of conformance control in heterogeneous reservoirs with inorganic gels. I successfully finished my study in 2009 and joined the Saint-Petersburg Mining University as a researcher. My work was in close collaboration with Gazpromneft on the improvement of chemical methods for enhanced oil recovery. During my work at the Mining University I was also a lecturer of a production engineering course taught for undergraduate students. That helped me to master my teaching skills and get the experience of supervising small student groups.

I joined the Petroleum engineering section of TU Delft: Delft University of Technology as a PhD student in 2013. That project has been done in close collaboration with Shell Global Solutions International. This thesis is the main product of this joint work.

From 2017 I have continued my work at TU Delft: Delft University of Technology as a Postdoctoral researcher on the topic of low salinity polymer interaction with rocks.

# List of publications

1.Nikita S. Lenchenkov, Michiel Slob, Ernst van Dalen, Gerard Glasbergen, Cor van Kruijsdijk.2016. Oil Recovery from Outcrop Cores with Polymeric Nano-Spheres. SPE Improved Oil Recovery Conference, 11-13 April, Tulsa, Oklahoma, USA. 2016. SPE-179641-MS.

2. Nikita S. Lenchenkov, Gerard Glasbergen, Cor van Kruijsdijk. 2017. Flow of a cross-linking polymer in porous media. Submitted to the Transport in Porous Media journal.

3. Nikita S. Lenchenkov, Gerard Glasbergen, Cor van Kruijsdijk. 2017. The characterisation of the size and swelling kinetics of copolymer nano-spheres extracted from an o/w emulsion. Submitted to Colloids and Surfaces A: Physicochemical and Engineering Aspects.

4. Nikita S. Lenchenkov, Gerard Glasbergen, Cor van Kruijsdijk. 2017. Propagation of Polymer Nano-Spheres in Outcrop Cores. Submitted to the SPE journal.